(4)

TIME DOMAIN WAVE PROPAGATION IN MULTILAYERED INTEGRATED CIRCUITS

Department of the Navy
Office of Naval Research
Contract N00014-86-K-0533
OSP 98321

FINAL REPORT

covering the period

August 1, 1986 — September 30, 1988

prepared by

J. A. Kong

Principal Investigator

Massachusetts Institute of Technology
Research Laboratory of Electronics
Cambridge, Massachusetts 02139

UNCLASSIFIED
SECURITY CLASSIFICATION OF THIS PAGE

AD-A202 427

REPORT DOCUMENTATION PAGE

Form Approved
OMB No. 0704-0188

1a. REPORT SECURITY CLASSIFICATION UNCLASSIFIED	1b. RESTRICTIVE MARKINGS
2a. SECURITY CLASSIFICATION AUTHORITY	3. DISTRIBUTION/AVAILABILITY OF REPORT Approved for public release;
2b. DECLASSIFICATION/DOWNGRADING SCHEDULE	distribution unlimited
4. PERFORMING ORGANIZATION REPORT NUMBER(S)	5. MONITORING ORGANIZATION REPORT NUMBER(S)
6a. NAME OF PERFORMING ORGANIZATION Research Laboratory of Electronics Massachusetts Institute of Technology 6b. OFFICE SYMBOL (If applicable)	7a. NAME OF MONITORING ORGANIZATION Office of Naval Research Massachusetts Institute of Technology
6c. ADDRESS (City, State, and ZIP Code) 77 Massachusetts Avenue Cambridge, MA 02139	7b. ADDRESS (City, State, and ZIP Code) E19-628 Cambridge, MA 02139
8a. NAME OF FUNDING/SPONSORING ORGANIZATION Office of Naval Research 8b. OFFICE SYMBOL (If applicable)	9. PROCUREMENT INSTRUMENT IDENTIFICATION NUMBER N00014-86-K-0533
8c. ADDRESS (City, State, and ZIP Code) Attn: Code 1511A:LCM:sw 800 North Quincy Street Arlington, VA 22217	10. SOURCE OF FUNDING NUMBERS PROGRAM ELEMENT NO. / PROJECT NO. 414c002 / TASK NO. / WORK UNIT ACCESSION NO.

11. TITLE (Include Security Classification)
Time Domain Wave Propagation in Multilayered Integrated Circuits

12. PERSONAL AUTHOR(S)
J.A. Kong

13a. TYPE OF REPORT	13b. TIME COVERED	14. DATE OF REPORT (Year, Month, Day)	15. PAGE COUNT
Final Report	FROM 8/1/86 TO 9/30/88	11/1/88	132 pp.

16. SUPPLEMENTARY NOTATION

17. COSATI CODES			18. SUBJECT TERMS (Continue on reverse if necessary and identify by block number)
FIELD	GROUP	SUB-GROUP	

19. ABSTRACT (Continue on reverse if necessary and identify by block number)

Work by J.A. Kong and his collaborators is summarized here.

20. DISTRIBUTION/AVAILABILITY OF ABSTRACT ☒ UNCLASSIFIED/UNLIMITED ☐ SAME AS RPT. ☐ DTIC USERS	21. ABSTRACT SECURITY CLASSIFICATION UNCLASSIFIED
22a. NAME OF RESPONSIBLE INDIVIDUAL Barbara Passero RLE Contract Reports	22b. TELEPHONE (Include Area Code) (617) 253-2566 22c. OFFICE SYMBOL

DD Form 1473, JUN 86 — Previous editions are obsolete. — SECURITY CLASSIFICATION OF THIS PAGE

UNCLASSIFIED

TIME DOMAIN ELECTROMAGNETIC WAVES IN MULTILAYERED MEDIA

Principal Investigator: Jin Au Kong

FINAL REPORT

Under the sponsorship of the ONR Contract N00014-86-K-0533 we have published 15 referenced journal and conference papers on time domain electromagnetic waves in multilayer media.

A rigorous dyadic Green's function formulation in the spectral domain is used to study the dispersion characteristics of signal strip lines in the presence of metallic crossing strips.

A set of coupled vector integral equations for the current distribution on the conductors is derived. Galerkin's method is then applied to derive the matrix eigenvalue equation for the propagation constant. The dispersion properties of the signal lines are studied for both cases of finite and infinite length crossing strips.

The effects of the structure dimensions on the passband and stopband characteristics are investigated. For crossing strips of finite length, the stopband is mainly affected by the period, the crossing strip length, and the separation between the signal and the crossing strips. For crossing strips of infinite length carrying travelling waves, attenuation along the signal line exists over the whole frequency range of operation.

In order to provide shorter interconnects between chips, modern multilayer integrated circuit packages for high-performance mainframe computers employ not only conventional striplines but vertical transmission lines or so-called vias as well. Because vias

may be of comparable length with the striplines, the study of transient electromagnetic wave propagation on the former is equally indispensible to the understanding of how fast the multilayer integrated circuits can operate.

Idealized circuit packages consisting of circular vias going through circular holes in the ground planes that separate different layers of equal thickness are considered. When only one via is present, we show that by treating the layer between two ground planes as a radial waveguide driven by a coaxial feed and making use of symmetry the equivalent network parameters for each layer can be obtained. The multiple layers constitute a periodic structure and presents little difficulty in computing the total transmission matrix. We also study an infinite array of vias and holes with equal spacing along two perpendicular directions. By virtue of the image theory, the problem is reduced to a coaxial transmission line with square outer wall and periodic circular diaphragm discontinuities. Both variational approaches as well as the integral equation method can be applied to the calculation of the characteristic impedance, the junction impedance, and the effective propagation constant. The transient response is then obtained by performing the fast Fourier transform on the frequency domain response or by direct Laplace inversion when the dispersion of junction capacitances is negligible. Our numerical results based on the dimensions of an actual package show that the degree of reflection and signal distortion becomes intolerable when the input rise time is shorter than 500 ps.

The transient fields of a current source on a layered medium are calculated using the double deformation technique, in which complex integrals are deformed in the transverse wavenumber and frequency planes. Singularities from these complex planes correspond to physical modes of the structure, such as guided and leaky waves, and the relative importance of each to the overall response can be discovered. Unlike the Cagniard-deHoop method, double deformation can be applied to dispersive and dissipative media. Also, the causality of the electromagnetic signal can be shown analytically.

A modification to the double deformation technique is presented, which consists of splitting the Fourier transform of the source current into two halves, one for times before the arrival at the observation point, and one after. This greatly increases the range of sources to which the double deformation technique can be applied. Another advantage of the modification, the individual causality and continuity of each mode, will be shown. The relative importance of the different wave modes will be demonstrated, as well as the improvement of this method over more brute-force approaches.

Results will be shown both for line and strip currents on the surface of a coated perfect conductor, for cases where the dielectric coating is both lossless and dissipative. In most cases, only a small number of modes suffices to reproduce the important features of the response, including the arrivals of reflected and lateral rays. The importance of each type of arrival depends on certain features of the time function, especially the initial slope. The response due to a strip current resembles that of a line current, with some smoothing of the sharper features.

An electroquasistatic approach in the spectral domain is derived to analyze a pad-electrode antenna used in the applications of low frequency geophysical probing. An integral equation is derived, which is then solved by the method of moments. A set of unit pulse functions are used to represent the outflowing current distribution on the pad-electrode surface. The potential distribution in the layered medium can be calculated in terms of the outflowing current distribution.

Numerical results for a symmetrical three-layer medium is presented. The effects of layer thickness and conductivity is studied. A more practical measurement environment with four different kinds of conductivity profiles are then investigated. The effects of stand-off thickness, background conductivity, and profile depth are studied. Numerical results reveal that the total electrode current is sensitive to the conductivity of the surrounding

medium, but is insensitive to the standoff thickness. Thus, it can be used to retrieve the background conductivity for different types of conductivity profiles, which is very useful in geophysical probing.

A hybrid method for radar cross section calculation of perfect conductors is discussed. The hybrid method utilizes the electric field integral equation formulation; it combines the method of moments and the physical theory of diffractions. The method of moments is employed to obtain the matrix equation for the problems. The physical theory of diffractions is employed to obtain guess solutions. The conjugate gradient iterative method is applied, with 5 % error criterion and the guess solutions, to obtain accurate solutions. Numerical results indicate that the 5 % error criterion and the guess solution, provided by the physical theory of diffractions, are effective for obtaining accurate solutions and reducing the computation time. For the monostatic radar cross section problems, the physical theory of diffractions is used to provide the guess solution for the first angle, and for all subsequent angles the previous solutions and the physical optics phase corrections are used to generate guess solutions. Based on case studies, it is found that the hybrid method converges and the average number of iterations is insensitive to the number of unknowns and the shape of the targets; it is below 10 in most cases. Therefore, the computation time is proportional to the number of unknowns to the second powers.

Cylindrical microstrip antennas find many applications pertaining to high speed aircrafts and spacecrafts, because of their conformity with the aerodynamical structure of such vehicles. Recently there has been some progress in the theoretical study of such antennas, where the radiation from various cylindrical microstrip elements was computed by assuming an electric surface current distribution on the microstrip patch. The excitation problem of realizing such a current distribution still need to be addressed. Furthermore, the input impedance for the cylindrical microstrip antennas has not been reported.

We address the more realistic problem of the radiation from a cylindrical microstrip antenna excited by a probe. Both the cylindrical-rectangular and the wraparound elements are discussed. The current distribution on the patch is rigorously formulated using a cylindrically stratified medium approach. A set of vector integral equations are derived which governs the current distribution on the patch. This set of equations is then solved using Galerkin's method in which the patch current is expanded in terms of a complete set of basis functions that can take into account the edge singularity condition. The input impedance together with the radiation pattern are derived both exactly and in the small substrate thickness limit where a single mode approximation is employed.

A full-wave analysis is developed to rigorously study the patch current distribution, the radiation fields, and the input impedance for the wraparound and rectangular microstrip antennas excited by a current probe. The analysis is valid for both thick and thin substrates.

For thick substrates, hybrid modes are excited, and only in the case of axially symmetric modes ($n = 0$) the TE_{om} is decoupled from the TM_{om}, and modes of different parity do not couple. In the wraparound patch, all current modes, with no axial variation, radiate weakly, and consequently, they have a narrow bandwidth. The presence of the dielectric substrate widens the bandwidth and broadens the radiation pattern. The radiation pattern is insensitive to the substrate thickness (especially for high dielectrics). The rectangular patch is, generally, slightly less radiating than the wraparound.

A rigorous analysis of the resonant frequency problem of both the cylindrical– rectangular and the wraparound microstrip structures is presented. The problem is formulated in terms of a set of vector integral equations. Using Galerkin's method is solving the integral equations, the complex frequencies are studied with sinusoidal basis functions. The effect of the edge singularity on the convergence is invesgated. A perturbative approach is also used to compute the complex resonant frequencies in the thin substrate limit.

In microelectronic computer packaging, a problem of practical interest is the study of propagation characteristics of a shielded microstrip line in the presence of crossing strips.

The microstrip line and the crossing strips are placed at two different interfaces of a three-layer medium bounded by two parallel conducting plates as shown in Fig. 1. The crossing strips are assumed to be periodic and the three layers to be uniaxially anisotropic.

The network analytical method of electromagnetic fields is applied for the hybrid-mode analysis of the frequency dependent characteristics of the structure. The transverse fields in each region are expressed by their Fourier transform in the x-direction and a Floquet harmonic representation in the y-direction. Using Maxwell's equations and applying boundary conditions, we obtain a set of coupled integral equations for the current distributions $\bar{J}_{s_1}$ and $\bar{J}_{s_2}$ on the microstrip line and the crossing metallic strips, respectively.

The determinantal equation for the dispersion relation can be derived by applying Galerkin's procedure to the derived set of coupled integral equations. The Brillouin diagrams are obtained numerically by seeking the roots of the obtained eigenvalue equation. The stop-band properties are numerically presented as a function of the spacing, length, and width of the crossing metallic strips. The effects of the material and geometrical parameters are also investigated.

We analyze the quasi-electrostatic fields generated by an electrode mounted on a perfectly conducting pad of a finite extent in a planar stratified medium. The axis of stratification is perpendicular to the pad. The electrode is maintained at a prescribed potential relative to the pad. This problem serves as a canonical problem which is useful to model some of the antennas employed in geophysical applications. It is more pertinent to tools which are mounted on a pad and operating at low frequencies.

We derive an integral equation in the spectral domain for the normal current distribution on the pad's surface. A method of moments is then applied to solve the integral equation. A proper set of local basis functions is used to represent the unknown normal current distribution on the pad. The basis functions are chosen to satisfy the edge condition as accurately as possible so that the current distribution can be represented by a reasonable number of basis functions. Both the current distribution on the pad's surface and the current flow pattern in the stratified medium are computed.

The exact image method, previously introduced for problems involving sources in real space with two homogeneous media and a planar interface, is extended to problems involving sources in complex space. The idea seems straightforward because the analytic functions of real space source position can be analytically extended to functions of complex space source position, which has been applied before with success in diffraction problems. The complex source point theory gives a possibility to analyze Gaussian beam problems with a simple source instead of a complicated source in real space. This has been tested by analyzing asymptotic (far field) expressions for a reflecting and a transmitted Gaussian beam resulting in well known Goos-Hänchen and angular shifts for the reflected beam and apparent position for the transmitted beam. The present method suggests itself for more exact calculation of the fields in these beams.

The purpose of this paper is to analyze the transient behavior of nonuniformly coupled and/or frequency dependent transmission line systems terminated with nonlinear loads. In the case of frequency independent line systems, the transient analysis is directly performed in the time domain based on variable transformations and the method of characteristics. When the system is frequency dependent, a new hybrid method of combining the frequency and time domain analysis is presented for dealing with the nonlinear problem.

Theory for quasi-TEM modes propagating in a transversely inhomogeneous (multi-dielectric) longitudinally uniform transmission line, is derived for transient signals. It is

seen that, while the starting point for the theory is completely different, the result is similar to the time-harmonic theory, and previously derived properties for propagating modes also apply in the transient case.

The analysis of resonance, input impedance, and radiation of the elliptic disk microstrip structure is rigorously formulated, using the scalar and vector Mathieu transforms. With the help of these transforms, the resonance frequencies of the structure can be derived exactly using Galerkin's method and approximately using a perturbational approach. Expressions for the input impedance and the radiation pattern are also obtained.

The transient electromagnetic radiation by a vertical electric dipole on a two- layer medium is analysed using the double deformation technique, which is a modal technique based on identification of singularities in the complex frequency and wavenumber planes. Previous application of the double deformation technique to the solution of this problem is incomplete in the early time response. We show that the existence of a pole locus on the negative imaginary frequency axis, which dominates the early time response, proves crucial in obtaining the solution for all times. A variety of combinations response, proves crucial in obtaining the solution for all times. A variety of combinations of parameters are used to illustrate the double deformation technique, and results will be compared with those obtained via explicit inversion, and a single deformation method.

Many integrated circuits contain strip lines at different heights that run parallel or perpendicular to each other. And we have investigated reliable models for these structures. First the capacitances associated with two offset parallel strips at different heights between ground planes are computed using the conformal mapping approach. As an extension, a simplified circuit of parallel-plate lines with transverse ridges is introduced to model two parallel strips with perpendicularly crossing strips on top. We treated it as a distributed circuit consisting of transmission lines segments with periodical capacitive loading. In order to calculate the coupling between two lines, we reduced this structure

to two equivalent single line circuits, viz. the even mode and the odd mode circuits. The Laplace transform approach can be easily applied to find out the transient response. The numerical computation carried out for various environments shows that the crossing strips will cause serious trouble for signals with a rise time of less than 50ps to propagate along a distances of 2cm or longer.

Basically, vias in a multilayered integrated circuits are treated like transmission lines with loadings where they encounter holes in ground planes separating different layers. We have modeled a ground plane with a hole and a circular conductor at the center of the hole as a radial waveguide, which in turn is connected to the via, another section of transmission line. Thus by computing the characteristic impedance of the former, we have derived the equivalent load impedance of the via hole. The load impedance is one important parameter in calculating the transient propagation along vias.

The scattering of electromagnetic waves from a randomly perturbed peridic surface is solved using the Extended Boundary Condition (EBC) method. The scattering from periodic surface is solved exactly using the EBC method and this solution is used in the small perturbation method to solve for the scattered field from a randomly perturbed periodic surface. The random perturbation is modeled as a Gaussian random process and the surface currents and the scattered fields are expanded and solved up to the second order. The theoretical results are illustrated by calculating the bistatic and backscattering coefficients. It is shown that as the correlation length of the random roughness increases, the bistatic scattering pattern of the scattered fields show several beams associated with each Bragg diffraction direction of the periodic surface. When the correlation length becomes smaller, then the shape of the beams become broader. The results obtained using the EBC method is also compared with the results obtained using the Kirchhoff approximation. It is shown that the Kirchhoff approximation results show quite a good agreement with EBC method results for the VV and HH polarized backscattering coefficients for small angles

of incidences. However, the Kirchhoff approximation does not give depolarized returns in the backscattering direction whereas the results obtained using the EBC method give significiant depolarized returns when the incident direction is not perpendicular to the row direction of the periodic surface.

The analysis of resonance, input impedance and radiation of the elliptic disk, microstrip structure is rigorously formulated, using the Scalar and Vector Mathieu Transforms. With the help of these transforms, the resonance frequencies of the structure can be derived exactly using Galerkin's method and approximately using a perturbational approach. Expressions for the input impedance and the radiation pattern are also obtained.

Theory for quasi-TEM modes propagating in a transversely inhomogeneous (multidielectric) longitudinally uniform transmission line, previously derived for time-harmonic waves, is derived for transient signals. It is seen that, while the starting point for the theory is completely different, the result is similar to the time-harmonic theory, and previously derived properties for propagating modes also apply in the transient case. The range of applicability is discussed with a simple example.

Exact image method, recently introduced for the solution of electromagnetic field problems involving sources above a planar interface between two homogeneous media, was originally applied to a restricted pair of medium parameters to obtain a well behaved image located in the 'proper' complex half space. It is demonstrated here with an example that the 'proper' half space limitation can be released to increase the applicability of the exact image theory. However, it is shown that for certain media, numerical difficulties in the field integrals may be encountered, due to crossing of branch cut lines on the complex integration plane. This may occur when the medium where the field is to be calculated is more lossy than the other medium. Methods for the image integration to obtain better convergence for more general media, are discussed.

Simple approximation for diffraction surface currents on a conducting half plane, due to an incoming plane wave, is given in terms of a line current (monofile) in complex space. When compared to the approximation by a current located at the edge, the diffraction pattern is seen to improve by an order of magnitude for a minimal increase in computation effort. Thus, the inconvenient Fresnel integral functions can be avoided in quick calculations of diffracted fields and the accuracy is seen to be good in other directions than along the half plane. The method can be generally applied to problems involving planar metal edges.

We have also proposed a way to account for the effect of complicated geometry from the point of view of continuous transmission line model by letting the coupling between parallel lines in multilayered integrated circuits to be nonuniform. Previously, we devised a scheme that combines the method of characteristics and perturbational series to simplify the computation of the transient response from the coupled transmission line equations. A new transformation for decoupling now enables us to generalize this formulation to calculate the near-end and far-end crosstalks to very high accuracy, given arbitrary positional dependence for both capacitive and inductive coupling coefficients.

The transient response of fundamental sources, such as dipole and line current, was carefully analyzed. With the double-deformation technique, which is a modal technique based on identification of singularities in the complex frequency and wave number planes, we are able to obtain both early and late time response very efficiently. Some results for vertical electric dipole excitation on a two-layer medium have been published. Recently, we have discovered a general scheme of breaking up the integrands so that sources with arbitrary time and space dependence can be incorporated into our formulation without sacrificing convergence.

PUBLICATIONS SUPPORTED BY ONR CONTRACT N00014-86-K-0533 SINCE 1986

Propagation properties of strip lines periodically loaded with crossing strips (J. F. Kiang, S. M. Ali, and J. A. Kong), Submitted to IEEE Transactions on Microwave Theory and Techniques for publication.

Transient electromagnetic wave propagation on vias of multilayer integrated circuit packages" (Y. E. Yang, Q. Gu, and J. A. Kong), *IEEE AP-S International Symposium and URSI Radio Science Meeting,* Syracuse, June 6 – 10, 1988.

Response of layered media to current sources with arbitrary time behavior, (M. J. Tsuk and J. A. Kong), *IEEE AP-S International Symposium and URSI Radio Science Meeting,* Syracuse, June 6 – 10, 1988.

Electrostatic fields due to an electrode mounted on a conducting pad of finite extent in a planar stratified medium (J. F. Kiang, T. M. Habashy, and J. A. Kong), Submitted to IEEE Transactions on Antennas and Propagation for publication.

Radar cross section prediction using a hybrid method (C. F. Lee, R. T. Shin, and J. A. Kong), *IEEE AP-S International Symposium and URSI Radio Science Meeting,* Syracuse, June 6 – 10, 1988.

Impedance parameters and radiation pattern of cylindrical – rectangular and wraparound microstrip antennas, (T. M. Habashy, S. M. Ali, and J. A. Kong), *IEEE AP-S International Symposium and URSI Radio Science Meeting,* Syracuse, June 6 – 10, 1988.

Resonance in cylindrical – rectangular and wraparound microstrip resonators (S. M. Ali, T. M. Habashy, and J. A. Kong), *IEEE AP-S International Symposium and URSI Radio Science Meeting,* Syracuse, June 6 – 10, 1988.

Dispersion characteristics of shielded microstrip lines crossed by periodic metzllic strips in multilayered anisotropic media (S. M. Ali, C. W. Lam, and J. A. Kong), *IEEE AP-S International Symposium and URSI Radio Science Meeting,* Syracuse, June 6 – 10, 1988.

Quasistatic fields due to an electrode mounted on a conducting pad of finite extent in a planar stratified medium (J. F. Kiang, T. M. Habashy, and J. A. Kong), *IEEE AP-S International Symposium and URSI Radio Science Meeting,* Syracuse, June 6 – 10, 1988.

Exact-image method for Gaussian-beam problems involving a planar interface (I. V. Lindell), *J. Opt. Soc. Am. A*, vol.4, no.12, 2185 — 2190, December 1987.

Transient analysis of signal line system in high speed integrated circuits (Q. Gu and J. A. Kong), *1987 International Conference on Communication Technology*, Nanjing, China, November 3 – 5, 1987.

Theory of time-domain quasi-TEM modes in inhomogeneous milticonductor lines (I. V. Lindell and Q. Gu), *IEEE Transactions on Microwave Theory and Techniques*, vol. MTT-35, no. 10, 893-897, October 1987.

Resonance and radiation of the elliptic disk microstrip sturcture Part I: Formulation (T. M. Habashy, J. A. Kong, and W. C. Chew), *IEEE Transactions on Antennas and Propagation*, vol. AP-35, no. 8, 877-886, August 1987.

Transient response of a vertical electric dipole on a two-layer medium (S. Y. Poh and J. A. Kong), *Journal of Electromagnetic Waves and Applications*, vol.1, no.2, 135-158, 1987.

Time domain analysis of nonuniformly coupled lines (Q. Gu, J. A. Kong, and Y. E. Yang), *Journal of Electromagnetic Waves and Applications*, vol.1, no.2, 109-132, 1987.

Electromagnetic Wave Theory (J. A. Kong), Wiley-Interscience, New York, 696 pages, 1986.

Exact-image method for Gaussian-beam problems involving a planar interface

Ismo V. Lindell*

Research Laboratory of Electronics, Department of Electrical Engineering and Computer Science, Massachusetts Institute of Technology, Cambridge, Massachusetts 02139

Received March 16, 1987; accepted August 3, 1987

The exact-image method, recently introduced for the solution of electromagnetic field problems involving sources above a planar interface between two homogeneous media, is shown to be valid also for sources located in complex space, which makes its application possible for Gaussian-beam analysis. It is demonstrated that the Goos–Hänchen shift and the angular shift of a TE-polarized beam are correctly given as asymptotic results by the exact-reflection-image theory. Also, the apparent-image location giving the correct Gaussian beam transmitted through the interface is obtained as another asymptotic check. The theory described here makes it possible to calculate the exact coupling from the Gaussian beam to the reflected and refracted beams as well as to the surface wave.

INTRODUCTION

The Gaussian beam is an important model for radiation from large-aperture antennas and laser sources, from which the energy is sent in a relatively narrow space angle. The introduction by Deschamps[1] of a complex-space dipole to represent mathematically a source for the Gaussian beam made it possible to extend analytical results, derived earlier for real-space sources to Gaussian-beam excitations. The basic Gaussian beam originates from a dipole in complex space, whereas multipoles of higher order can be shown to produce more-complex Hermite–Gaussian and Laguerre–Gaussian beams.[2-4]

The basic problem in Gaussian-beam analysis of a planar interface of two media is that of reflection and refraction of the beam at the interface. This problem has been treated by using a complex-space dipole method[5] and by other methods.[6-8] The general field expressions in the exact formulations are involved, but asymptotic considerations for narrow beams permit a simpler analysis of reflection and transmission problems and lead to the well-known shift phenomena of the reflecting beam. The most famous of these was first demonstrated by Goos and Hänchen[9] in 1947 and analyzed by Artman[10] in 1948 and involved a parallel shift of the beam reflected from an interface in the denser of two lossless dielectric media. Other shifts that can be defined for narrow beams are the angular shift[5,11] and the focal shift.[12] Infinities arising in the idealized theory for the Goos–Hänchen shift can be avoided by using a more-realistic analysis.[6,13,14]

The purpose of the present paper is to give a more-general account of the exact-image theory, which was introduced elsewhere for sources in the air above a planar interface of a homogeneous medium[15,16] (the Sommerfeld problem), and to allow the original source to be in complex space. Thus the theory is applicable to global Gaussian-beam analysis in exact form. In comparison with other exact methods based on Sommerfeld integrals (inverse-Fourier-transform integrals for the fields), the present theory, which deals with equivalent sources and their integration, gives more physical insight and does not resort to special integration procedures that are dependent on the field point. For the application of the exact-image theory, functions characterizing the image sources are needed, and methods for their computation are presented in Refs. 15 and 16. These functions need to be calculated only once in the computer memory, after which the field calculation involves converging well-behaved integrals. The exact image of a point source is a line source, which in general lies in complex space. To check the theory, known asymptotic expressions for the reflected beam shifts and the apparent-transmission-image location are shown to arise as special cases when the exact line image is approximated by a point image.

REFLECTION-IMAGE THEORY

The notation applied here is based on that used in Ref. 15 except that we consider two half-spaces with parameters $\mu_1\mu_0$ and $\epsilon_1\epsilon_0$ for $\hat{u}\cdot\hat{r} > 0$ and parameters $\mu_2\mu_0$ and $\epsilon_2\epsilon_0$ for $\hat{u}\cdot\hat{r} < 0$. In Refs. 15 and 16 the medium $\hat{u}\cdot\hat{r} > 0$ was assumed to be air, but generalization for any medium pair is straightforward if instead of k we write $k_1 = k(\mu_1\epsilon_1)^{1/2}$, where $k = \omega(\mu_0\epsilon_0)^{1/2}$ and we understand that $\mu = \mu_2/\mu_1$ and ϵ_2/ϵ_1 everywhere. To avoid unnecessary, although not excessive, complication, the theory here is limited to dielectric media only with $\mu_1 = \mu_2 = 1$.

As another generalization, the original source is taken to be in complex space. Because the theory in Refs. 15 and 16 was analytically derived and no use of the tacit assumption of a real source location was made, the final expressions can also be applied for complex source locations. The same idea was applied earlier with success when field expressions that were derived for problems with sources in real space were generalized for sources in complex space,[17] resulting in solutions for problems with Gaussian-beam excitation.

Let us consider, for simplicity, the source $\mathcal{J}(\hat{r}) = \hat{v}IL\delta[\hat{r} - (\hat{u}h + j\hat{b})]$, which is a dipole with the direction of the unit vector $\hat{v}$ and the location at the real height h from the interface $\hat{u}\cdot\hat{r} = 0$ and the imaginary depth $j\hat{b}$. In the calculation

0740-3232/87/122185-06$02.00

of the fields in the half-space 1, the half-space 2 can be replaced by the exact-image source, as was shown in Ref. 15:

$$\mathbf{J}_i(\boldsymbol{\rho}, p) = f_1(p)\mathbf{J}_{ct}(\boldsymbol{\rho}) - \left[f_t(p) + \frac{\epsilon - 1}{\epsilon + 1}\delta_+(p)\right]\hat{u}\hat{u}\cdot\mathbf{J}_c(r) - \hat{u}\frac{1}{k_1^2}\frac{\epsilon + 1}{\epsilon}f_t(p)\hat{u}\cdot\nabla[\nabla_t\cdot\mathbf{J}_c(\boldsymbol{\rho})]. \quad (1)$$

Here, p is an integration variable, and the image function $f_t(p)$ can most conveniently be calculated through the following Bessel-function series[16]:

$$f_t(p) = \frac{-8\epsilon}{\epsilon^2 - 1}\sum_{n=1}^{\infty} n\left(\frac{\epsilon - 1}{\epsilon + 1}\right)^n \frac{J_{2n}(p)}{p},$$

$$f_l(p) = \frac{-2J_2(p)}{p}. \quad (2)$$

Further, $\delta_+(p)$ denotes $\delta(p - 0_+)$, t denotes a component transverse to $\hat{u}$, and c denotes the reflection operation

$$\hat{a}_c = \mathbf{C}\cdot\hat{a}, \qquad \mathbf{J}_c(\boldsymbol{\rho}) = \mathbf{C}\cdot\mathbf{J}(\mathbf{C}\cdot\boldsymbol{\rho}), \qquad \mathbf{C} = \mathbf{I} - 2\hat{u}\hat{u}. \quad (3)$$

The field from the image source can be written as a fourfold integral over space and the parameter p:

$$\hat{E}(\boldsymbol{\rho}) = -j\omega\mu_0\int_V\int_0^{\infty}\mathbf{G}_1(D)\cdot\mathbf{J}_i(\boldsymbol{\rho}', p)\,dV'\,dp, \quad (4)$$

with

$$\mathbf{G}_1(D) = \left(\mathbf{I} + \frac{1}{k_1^2}\nabla\nabla\right)\frac{\exp(-jk_1D)}{4\pi D},$$

$$D(\boldsymbol{\rho}, \boldsymbol{\rho}', p) = [(\boldsymbol{\rho} - \boldsymbol{\rho}' + \hat{u}p/jB)\cdot(\boldsymbol{\rho} - \boldsymbol{\rho}' + \hat{u}p/jB)]^{1/2},$$

$$B = k(\epsilon_2 - \epsilon_1)^{1/2}. \quad (5)$$

The image-current expression contains Bessel functions $J_n(p)$, which are convergent only if the integration parameter p is real. For a point source, Eq. (1) can also be written so that the integration parameter p is absent, because in the field integral [Eq. (4)], the coordinate $z = \hat{u}\cdot\boldsymbol{\rho}$ and p are related through the distance function D in the argument of the Green function. The expression [Eq. (1)] can thus be written

$$\mathbf{J}_i(r) = -IL\frac{\epsilon - 1}{\epsilon + 1}\hat{u}(\hat{u}\cdot\hat{v})\delta_+(\boldsymbol{\rho} + \hat{u}h - j\delta_c) - jk_1(\epsilon - 1)^{1/2}IL \times\left\{\hat{v}_c f_1[p(z)]\delta(\hat{p} - j\delta_t) - \hat{u}(\hat{u}\cdot\hat{v})f_t[p(z)]\delta(\hat{p} - j\delta_t) - \hat{u}\frac{1}{k_1^2}\frac{\epsilon + 1}{\epsilon}f_t[p(z)]\hat{u}\cdot\nabla(\hat{v}_c\cdot\nabla)\delta(\boldsymbol{\rho} + \hat{u}h - j\delta_c)\right\}, \quad (6)$$

with

$$p(z) = -jB(z + h + j\hat{u}\cdot\delta). \quad (7)$$

To obtain an exponentially converging Green function, we must select the branch of the distance function D so that $\mathrm{Im}[k_1D] < 0$. Also, to obtain a converging image-current function, the path of z integration must be chosen so that p in Eq. (7) is real and positive, in which case all the Bessel functions in Eqs. (2) converge. This means that the image line must start at the point $\boldsymbol{\rho} = -\hat{u}h + \delta_c$ in complex space and lie parallel to the complex z plane, with

$$\arg(z + h + j\hat{u}\cdot\delta) = \arg(jB). \quad (8)$$

Requiring that the additional condition $\mathrm{Re}[z] \geq 0$ be valid, the complex distance function satisfies $D \neq 0$ for all field points in $\mathrm{Re}[z] > 0$, and the field integrand in Eq. (4) is nonsingular.[15] This condition defines the branch of B, or the square root $(\epsilon_2 - \epsilon_1)^{1/2}$ through

$$\mathrm{Re}[j(\epsilon_2 - \epsilon_1)^{1/2}] = \mathrm{Re}[(\epsilon_1 - \epsilon_2)^{1/2}] \geq 0, \quad (9)$$

implying for example, that if ϵ_1, $\epsilon_2 = \epsilon\epsilon_1 < \epsilon_1$ are real, then $(\epsilon - 1)^{1/2} = -j(1 - \epsilon)^{1/2}$, provided that $(1 - \epsilon)^{1/2} > 0$. For some combination of lossy medium parameters there may be uncertainty in choosing the correct branch of the distance function D to obtain the best convergence.[18] A close study of the integration path on the complex z' plane will reveal that a branch-cut line, starting from the branch points at $z' = z \pm j\rho$, defining the converging branch of the Green function, may be crossed for some combination of parameter values ϵ_1 and ϵ_2 when p moves from 0 to ∞. In this case it is possible to take the image-current line in the wrong half-space with $\mathrm{Re}[z'] > 0$, which makes the integrand converging again. This question is the subject of a forthcoming paper.

REFLECTED GAUSSIAN BEAM

A unique global definition for the Gaussian-beam field does not seem to exist; instead, the term Gaussian beam is understood as an asymptotic property of radiation fields close to the axis of the main radiation. Thus many fields with the *same asymptotic* quadratic exponential behavior are called Gaussian beams. (The present method is not, however, dependent on the definition of the Gaussian beam, since it works for any original sources.) One example is the field from a point source in complex space with the imaginary part of the position vector $\delta = \hat{u}b\cos\theta - \hat{u}_y b\sin\theta$.

The radiation beam of the point source is obtained in the direction of $-\delta$. The reflected beam is obtained from the image source [Eq. (6)], and, for points far enough from the interface, the field can be approximated by a Gaussian beam if the image source can be approximated by a point source. Of course, the correct field is obtained also in space points, where it cannot be described as a Gaussian beam. To demonstrate the validity of the exact-image theory for this problem, we show that the Goos–Hänchen shift and the angular shift of the reflected beam are obtained as asymptotic results from the exact-image field expression. To keep the notation simple, let us consider a two-dimensional problem with the line source $\mathbf{J}(\boldsymbol{\rho}) = \hat{u}_x I\delta(y + jb\sin\theta)\delta(z - h - jb\cos\theta)$, where θ is the angle between $\hat{u}$ and δ. This assumption simplifies the image source [Eq. (1)] into

$$\mathbf{J}_i(\boldsymbol{\rho}, p) = f_1(p)\mathbf{J}_c(\boldsymbol{\rho}) = f_1(p)\hat{u}_x I\delta(y + jb\sin\theta) \times\delta(z + h + jb\cos\theta), \quad (10)$$

where the function $f_1(p)$ is that given in Eqs. (2). The Green function [Eqs. (5)] integrated in the x direction produces the two-dimensional Green function in the medium 1,

$$\mathbf{G}_1(D) = \left(\mathbf{I} + \frac{1}{k_1^2}\nabla\nabla\right)G_1(D), \qquad G_1(D) = \frac{1}{4j}H_0^{(2)}(k_1D), \quad (11)$$

where $H_0^{(2)}(x)$ is the Hankel function.

The field calculated from the exact-image source is valid in any point in the upper half-space, but since we are interested in Gaussian-beam properties, let us consider the far field with $|k_1 D| \gg 1$, in which case the image can be approximated by a point source. Also, the asymptotic expression for the Hankel function can now be used:

$$H_0^{(2)}(k_1 D) \approx \left(\frac{2j}{\pi k_1 D}\right)^{1/2} \exp(-jk_1 D). \tag{12}$$

D here represents the complex distance between the field point $\hat{\rho}$ and the complex integration point $\hat{\rho}' = j\hat{u}p/k_1(\epsilon - 1)^{1/2}$, where $\hat{\rho}' = -\hat{u}h + j\hat{b}_c$, if p integration is done separately. Because the image function $f_1(p)$ is decaying, the effective p-integration range can be regarded as small with respect to $|\hat{\rho} - \hat{\rho}'|$ and we can write

$$D \approx D_0 - \frac{jpq}{k_1}, \qquad D_0 = [(\hat{\rho} - \hat{\rho}') \cdot (\hat{\rho} - \hat{\rho}')]^{1/2},$$

$$q = \frac{\hat{u} \cdot \hat{w}}{(\epsilon - 1)^{1/2}}, \qquad \hat{w} = \frac{\hat{\rho} - \hat{\rho}'}{D_0}. \tag{13}$$

By applying expression (12), we can write the field integral on the plane $x = 0$ as

$$\hat{E}(\hat{\rho}) \approx -j\omega\mu_0 \hat{u}_x I G_1(D_0) \int_0^\infty f_1(p) e^{-pq} dp. \tag{14}$$

If expression (14) can be written in the form

$$\hat{E}(\hat{\rho}) \approx -j\omega\mu_0 \hat{u}_x I G_1(D_0) \exp(jk_1 \hat{u} \cdot \hat{s}) \exp(-jk_1 \hat{w}_0 \cdot s) \times \int_0^\infty f_1(p) \exp(-pq_0) dp, \tag{15}$$

in the vicinity of the radiating direction $\hat{w} \approx \hat{w}_0$, where $\hat{w}_0$ corresponds to a field point $\hat{\rho}_0$ on the axis of the reflected beam, the field can be thought of as arising from the current line shifted by the vector $\hat{s}$ from the mirror-image location $\hat{\rho}'$. Approximation (15) is obviously possible if expression (14) can be expanded as a power series in terms of the small difference vector $\hat{w} - \hat{w}_0$. This is possible only for sufficiently narrow beamwidths. After some steps of Taylor expansion, the expression for $\hat{s}$ can be written in the form

$$\hat{s} = \frac{j\hat{u}}{k_1(\epsilon - 1)^{1/2}} \frac{\int_0^\infty p f_1(p) \exp(-pq_0) dp}{\int_0^\infty f_1(p) \exp(-pq_0) dp}, \tag{16}$$

where $q_0 = \hat{u} \cdot \hat{w}_0/(\epsilon - 1)^{1/2}$. To obtain an expression for $\hat{s}$, the following integral identities are needed:

$$\int_0^\infty f_1(p) e^{-pq} dp = \frac{q - (q^2 + 1)^{1/2}}{q + (q^2 + 1)^{1/2}}, \tag{17}$$

$$\int_0^\infty p f_1(p) e^{-pq} dp = \frac{2}{(q^2 + 1)^{1/2}} \frac{q - (q^2 + 1)^{1/2}}{q + (q^2 + 1)^{1/2}}. \tag{18}$$

Thus we have

$$\hat{s} = \frac{2j\hat{u}}{k_1(\epsilon - 1)^{1/2}(q_0^2 + 1)^{1/2}} = \frac{2j\hat{u}}{k[\epsilon_2 - \epsilon_1 + \epsilon_1(\hat{u} \cdot \hat{w}_0)^2]^{1/2}} = \frac{2j\hat{u}}{k_1(\epsilon - \sin^2\theta)^{1/2}}, \tag{19}$$

with the branch of the square root so defined that $\mathrm{Im}[(\epsilon - \sin^2\theta)^{1/2}] \le 0$.[15] Equation (19) explains the Goos–Hänchen shift and the angular shift when the Taylor-approximation condition is valid. In fact, because $\hat{w}_0 = -\hat{b}_c/b$, we have $q_0 = \cos\theta/(\epsilon - 1)^{1/2}$, and Eq. (17) represents the TE reflection coefficient of a plane wave coming at the angle θ. Let us consider the two possibilities with real ϵ:

(1) $\epsilon < \sin^2\theta$, which can only happen for $\epsilon_1 > \epsilon_2$. In this case, $\hat{s}$ is real, and thus the real part of the location vector is shifted by

$$\hat{s} = \frac{2\hat{u}}{k_1(\sin^2\theta - \epsilon)^{1/2}}, \tag{20}$$

which means a parallel shift of the reflecting beam (Fig. 1). This is the well-known Goos–Hänchen shift. Because $\hat{s}$ is in the $-\hat{u}$ direction, the parallel shift is $s \sin\theta$.

(2) $\epsilon > \sin^2\theta$. In this case the square root is real and the shift $\hat{s}$ is imaginary ($\hat{s} = js\hat{u}$), which means that the image line is shifted an imaginary distance in the $\hat{u}$ direction from the original location. Because the imaginary part of the position vector determines the direction of the beam, the beam is shifted angularly from its mirror-image direction $\hat{w}_0$ to the direction determined by $\hat{b}_c - j\hat{s}$ (Fig. 2). If the shift angle $\Delta\theta$ is small, it satisfies

$$\tan(\Delta\theta) \approx -\frac{s}{b}\cos\theta = \frac{2\cos\theta}{k_1 b(\epsilon - \sin^2\theta)^{1/2}}. \tag{21}$$

The previous expressions are valid only for sufficiently narrow beams, a condition that presumes sufficiently large values for b. They are not valid if the Taylor expansion is not applicable, which happens at and close to the branch point of the square-root function $(q_0^2 + 1)^{1/2}$, i.e., at $\sin^2\theta \approx \sin^2\theta_c = \epsilon$, where Eq. (19) would predict an infinite shift. This is the definition of the critical angle θ_c, for which $(q_0^2 + 1)^{1/2} = 0$. For angles $\theta \approx \theta_c$ we can write, from expression (14) and Eq. (17),

$$\hat{E}(r) \approx -j\omega\mu_0 \hat{u}_x I G_1(D_0) \exp[-2j[2(\cos\theta - \cos\theta_c)/(1 - \epsilon)^{1/2}]^{1/2}], \tag{22}$$

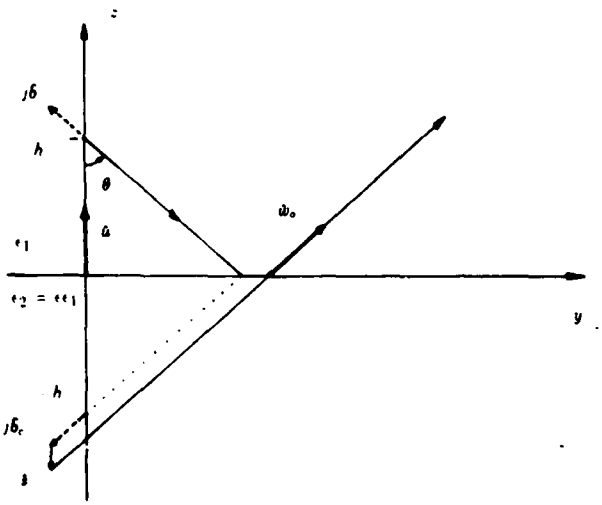

Fig. 1. Goos–Hänchen shift of the Gaussian beam arising from an approximate-image point source with a real shift vector $\hat{s}$ from the mirror-image point $-\hat{u}h + j\hat{b}_c$.

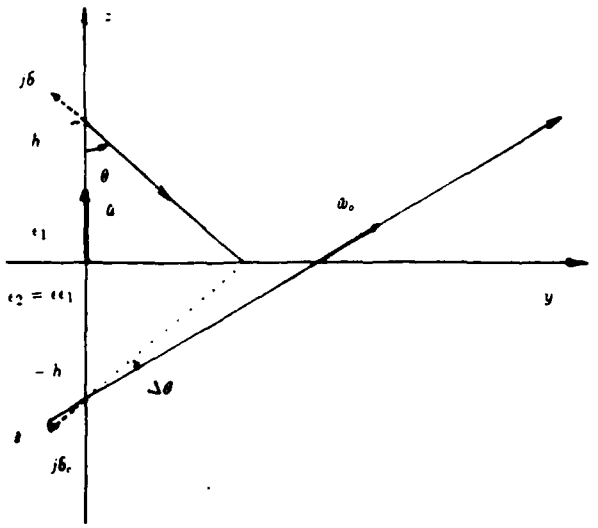

Fig. 2. Angular shift of the Gaussian beam arising from an approximate-image point source with an imaginary shift vector $\hat{s}$ from the mirror-image point $-\hat{u}h + j\delta_\epsilon$.

which cannot be described by a simple shift of the image source because the reflecting beam is distorted and not exactly of Gaussian form. To find out the shift of the maximum of the reflecting beam, some numerical analysis must be made, as in Refs. 6, 13, and 14.

For complex ϵ values, there are both real and imaginary parts for the vector $\hat{s}$, which means a combined Goos–Hänchen and angular shift. In this case, the beam does not enter at the critical angle, because it is now complex. For beams sufficiently narrow the real and imaginary parts of $\hat{s}$ in Eq. (19) determine the Goos–Hänchen and angular shifts, respectively.

This simple test serves as an asymptotic verification of the exact-image theory for the Gaussian-beam reflection analysis. The field of the reflected beam can be calculated at any point from the exact formulation [Eq. (4)] and also at points where it cannot be described as a Gaussian beam and where the asymptotic formulas are not valid. This also includes the coupling to the surface wave, which, however, is small when θ is not ≈ 0.

TRANSMISSION-IMAGE THEORY

The image theory for fields transmitted through a planar interface was developed in Ref. 16, and the generalization discussed for reflection-image theory also applies here. To summarize the result, the upper dielectric half-space is replaced by the transmission-image source:

$$J_t(\hat{\rho}, p) = \hat{u}\hat{u} \cdot J(\hat{\rho})\left[\frac{2\epsilon}{\epsilon+1}\delta_+(p) + F_\epsilon'(Bz, p)\right] + J_t(\hat{\rho})[\delta_+(p) + F_1'(Bz, p)] + \hat{u}[F_\epsilon(Bz, p) - F_1(Bz, p)]H'(z, p)\nabla_t \cdot J(\hat{\rho}). \quad (23)$$

Here, the original source is $J(\hat{\rho})$, and z denotes its coordinate. Further, we have

$$B = k_1(\epsilon - 1)^{1/2} = k(\epsilon_2 - \epsilon_1)^{1/2}, \quad (24)$$

$$H(z, p) = [z^2 + (p/B)^2]^{1/2}, \quad (25)$$

$$F_\epsilon(\tau, p) = \frac{2\epsilon}{\epsilon+1}J_0(p) - \frac{4\epsilon}{\epsilon^2-1} \times \sum_{m=1}^{\infty}\left\{\frac{\epsilon-1}{\epsilon+1}\frac{1-[(p/\tau)^2+1]^{1/2}}{1+[(p/\tau)^2+1]^{1/2}}\right\}^m J_{2m}(p), \quad (26)$$

and the primes in functions H and F denote differentiation with respect to p.

The field is obtained from an integral similar to that in Eq. (4), but the medium is now ϵ_2. Also, the distance function D is here defined to be

$$D(\hat{\rho}, \hat{\rho}', p) = \{[\hat{\rho} - \hat{\rho}' - \hat{u}H(z', p)] \cdot [\hat{\rho} - \hat{\rho}' - \hat{u}H(z', p)]\}^{1/2}. \quad (27)$$

Again, to obtain a converging image function, the parameter p must be real. To obtain a converging Green function, $\mathrm{Im}[k_2 D]$ must be nonpositive, which defines the branch of the D function. Also, in this case, for certain lossy media, the branch cut of the Green function may be crossed if the image is restricted to the half-space $\mathrm{Re}[z'] > 0$, leading to a nonconverging Green function. This problem can be overcome by taking the other branch of the $H(z, p)$ function.

TRANSMITTED GAUSSIAN BEAM

Without delving more into the theory itself, which can be found in Ref. 16, let us apply it to the same line source as in the previous section. The transmission-image source can be written in the form

$$J_t(\hat{\rho}, p) = \hat{u}_x I[\delta_+(p) + F_1'(Bh', p)]\delta(y + jb\sin\theta)\delta(z - h'), \quad (28)$$

where the function F_1' is defined as

$$F_1'(Bh', p) = \frac{-1}{H(H+h')}[(H+h')^2 J_1(p) + (H-h')^2 J_3(p)], \quad (29)$$

and

$$H \equiv H(h', p) = [h'^2 + (p/B)^2]^{1/2}, \qquad h' = h + jb\cos\theta. \quad (30)$$

The convergence condition $\mathrm{Im}[p] = 0$ defines a path $z = H(p)$, which consists of a part of a hyperbolic curve in the complex z plane.[16] To obtain an asymptotic result from the exact-image field solution, let us once again study the far field of the beam. After making use of expression (12), we must now apply the following approximation for large $|\hat{\rho}|$, instead of expressions (13), for $x = 0$, $z < 0$:

$$D \approx D_0 + qH(p), \qquad D_0 = [(y + jb\sin\theta)^2 + z^2]^{1/2}, \qquad q = |z|/D_0 \approx \cos\theta_2. \quad (31)$$

Thus the field in medium 2 can be written in the approximate form

$$\hat{E}(\hat{\rho}) \approx -j\omega\mu_0\hat{u}_x I G_2(D_0)\left\{1 + \int_0^\infty F_1'(Bh', p) \times \exp[-jk_2 qH(p)]dp\right\}. \quad (32)$$

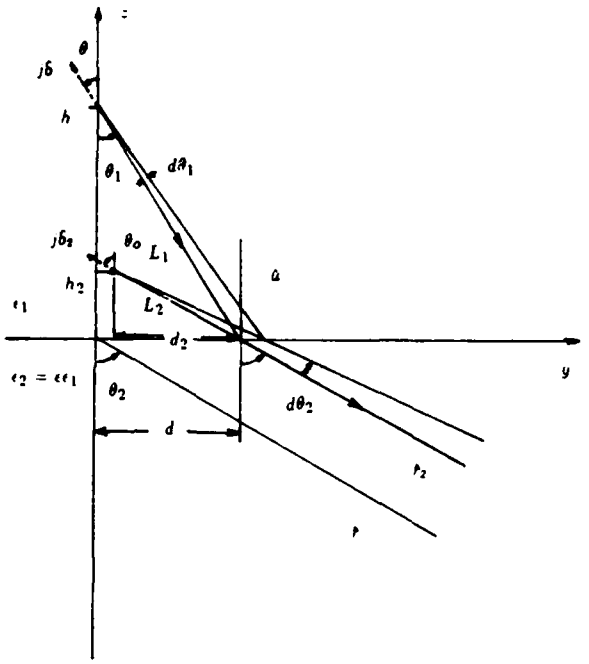

Fig. 3. Gaussian beam transmitted through the interface seen as arising from an approximate point source at point $\hat{u}h_2 + jb_2$.

Here, the Green function is defined as for Eqs. (5), for the medium 2 with k_2 replacing k_1. Applying an integral identity [Ref. 16, Eq. (17)], we can write, for the expression in braces in expression (32),

$$1 + \int_0^\infty F_1'(Bh', p)\exp[-j\gamma H(p)]\mathrm{d}p = \frac{2\gamma}{\gamma + (\gamma^2 - B^2)^{1/2}} \exp[-j(\gamma^2 - B^2h')^{1/2}]. \quad (33)$$

Use of this and (see Fig. 3 for the different parameters)

$$D_0 \approx r + jb\sin\theta\sin\theta_2 \approx r_2 + d'\sin\theta_2, \quad (34)$$

with

$$d' = d + jb\sin\theta, \quad (35)$$

makes it possible to write expression (32) in the following form:

$$\hat{E}(P) \approx -\frac{1}{4}\omega\mu_0\hat{u}_x I\left(\frac{2j}{\pi k_2 r_2}\right)^{1/2}\frac{2k_2\cos\theta_2}{k_1\cos\theta_1 + k_2\cos\theta_2} \times \exp(-jk_2r_2)\exp(-jk_1\sin\theta_1 d')\exp(-jk_1\cos\theta_1 h'). \quad (36)$$

Here, we have made the far-field assumption $r_2 \gg h, d, b$; otherwise the expressions would have been much more complicated. Expression (36) can be interpreted in terms of geometrical-optics rays of the Gaussian beam, with a phase shift in each medium and a transmission coefficient at the interface. From this, an equivalent-source-point location can be defined from the divergence of two adjacent rays close to the beam axis $\theta_1 = \theta$. Taking the combination of the last two exponentials in expression (36), we may require that the corresponding expression for the image case have the same change when the angle θ_1 differs from the axial angle θ. Writing for the exponential expressions

$$\Psi_1 = -jk_1(d'\sin\theta_1 + h'\cos\theta_1) = -j\frac{k_1 h}{\cos\theta_1} + k_1\cos(\theta_1 - \theta), \quad (37)$$

$$\Psi_2 = -jk_2(d_2'\sin\theta_2 + h_2'\cos\theta_2) = -j\frac{k_2 h_2}{\cos\theta_2} + k_2 b_2\cos(\theta_2 - \theta_0), \quad (38)$$

$$k_1\sin\theta = k_2\sin\theta_0, \quad (39)$$

we may require that phase and amplitude changes along the plane $z = 0$ be the same for the original case and the image case. This implies that the differentials of Ψ_1 and Ψ_2 are the same:

$$\mathrm{d}\Psi_1 = \mathrm{d}\Psi_2. \quad (40)$$

When supplemented by the condition between the differentials $\mathrm{d}\theta_1$ and $\mathrm{d}\theta_2$ arising from Snell's law, $k_1\sin\theta_1 = k_2\sin\theta_2$, Eq. (40) gives us the following expression for the unknown h_2:

$$h_2 = h\frac{k_2\cos^3\theta_2}{k_1\cos^3\theta_1} \quad \text{at } \theta_1 = \theta. \quad (41)$$

Because of $L_1 = h/\cos\theta_1$, $L_2 = h_2/\cos\theta_2$, the corresponding result for L_2 is

$$L_2 = L_1\frac{k_2\cos^2\theta_2}{k_1\cos^2\theta_1}, \quad (42)$$

which was also given in Ref. 5. To obtain an expression for b_2, defining the apparent-source location in complex space, we must study the real parts of Eqs. (37) and (38). The direction of the vector is known from the main beam direction in the half-space 2. The magnitude b_2 is not obtained from Eq. (40), since the first differentials vanish identically at $\theta_1 = \theta$. Taking the second differentials of Ψ_1 and Ψ_2 and equating the real parts gives us the result

$$b_2 = b\frac{k_2\cos^2\theta_2}{k_1\cos^2\theta_1} \quad \text{for } \theta_1 = \theta, \quad (43)$$

a condition that was also given in Ref. 5.

Thus the location of the approximate-image source can be obtained through two different approaches: the present exact-image theory and the saddle-point asymptotic analysis of the Fourier-integral representation of the transmitted field in Ref. 5. The present approach has the advantage of working with sources, which gives a more-physical insight for the problem, in addition to being exact.

CONCLUSION

In this paper, the exact-image method, which was previously introduced for problems involving sources in real space with two homogeneous media and a planar interface, is extended to problems involving sources in complex space. This is possible because the analytical functions of real-space source position can be extended to functions of complex-space source position, an idea that has been applied before with success in diffraction problems. The complex-source-point theory makes it possible to analyze Gaussian-beam

problems with a simple source instead of a complicated source in real space. The method has been tested in this paper by analyzing asymptotic (far-field) expressions for a reflected Gaussian beam and a transmitted one, resulting in well-known Goos–Hänchen and angular shifts for the reflected beam and in an apparent position for the transmitted beam. The method described here is recommended for more-exact calculation of the fields in these beams, for example, when the asymptotic approximations will not work.

ACKNOWLEDGMENTS

This work was done while the author was on sabbatical as a visiting scientist at the Research Laboratories of Electronics, Massachusetts Institute of Technology, during the academic year 1986–1987. The author is indebted to J. A. Kong for providing this opportunity and for fruitful discussions on the present topics. This work was funded by the Academy of Finland and, in part, by National Aeronautics and Space Administration grant NAG5-270, by Office of Naval Research contracts N00014-83-K-0528 and N00014-86-K-0533, and by U.S. Army Research Office contract DAAG-29-85-K-0079.

* Permanent address, Electromagnetics Laboratory, Department of Electrical Engineering, Helsinki University of Technology, Otakaari 5A, Espoo 15, 02150 Finland.

REFERENCES

1. G. A. Deschamps, "The Gaussian beam as a bundle of complex rays," Electron. Lett. 7, 684–685 (1971).
2. S. Y. Shin and L. B. Felsen, "Gaussian beam modes by multipoles with complex source point," J. Opt. Soc. Am. 67, 699–700 (1977).
3. M. Hashimoto, "Beam waves with sources at complex location," Electron. Lett. 21, 1096–1097 (1985).
4. K.-M. Luk and P.-K. Yu, "Generation of Hermite-Gaussian beam modes by multipoles with complex source points," J. Opt. Soc. Am. A 2, 1818–1820 (1985).
5. J. W. Ra, H. L. Bertoni, and L. B. Felsen, "Reflection and transmission of beams at a dielectric interface," SIAM J. Appl. Math. 24, 396–413 (1973).
6. B. R. Horowitz and T. Tamir, "Lateral displacement of a light beam at a dielectric interface," J. Opt. Soc. Am. 61, 586–597 (1971).
7. Y. M. Antar and W. M. Boerner, "Gaussian beam interaction with a planar dielectric interface," Can. J. Phys. 52, 962–972 (1974).
8. S. Kozaki and H. Sakurai, "Characteristics of a Gaussian beam at a dielectric interface," J. Opt. Soc. Am. 68, 508–514 (1978).
9. F. Goos and H. Hänchen, "Ein neuer und fundamentaler Versuch zur Totalreflexion," Ann. Physik 1, 333–346 (1947).
10. K. Artmann, "Berechnung der Seitenversetzung des totalreflektierten Strahles," Ann. Physik 2, 87–102 (1948).
11. I. A. White, A. W. Snyder, and C. Pask, "Directional change of beams undergoing partial reflection," J. Opt. Soc. Am. 67, 703–705 (1977).
12. M. McGuirk and C. K. Carniglia, "An angular spectrum representation approach to the Goos–Hänchen shift," J. Opt. Soc. Am. 67, 103–107 (1977).
13. A. Yaghjian, "The Goos–Hänchen shift as an average phase-center shift for an antenna embedded in a dielectric half space," in *Proceedings of the URSI National Convention on Radio Science* (International Union of Radio Science, Albuquerque, N.M., 1982), p. 80.
14. H. M. Lai, F. C. Cheng, and W. K. Tai, "Goos–Hänchen effect around and off the critical angle, J. Opt. Soc. Am. A 3, 550–557 (1986).
15. I. V. Lindell and E. Alanen, "Exact image theory for the Sommerfeld half-space problem, Parts I-III," IEEE Trans. Antennas Propag. AP-32, 126–133, 841–847, 1027–1032 (1984).
16. I. V. Lindell, E. Alanen, and H. von Bagh, "Exact image theory for the calculation of fields transmitted through a planar interface of two media," IEEE Trans. Antennas Propag. AP-34, 129–137 (1986).
17. L. B. Felsen, "Complex source point solutions of the field equations and their relation to the propagation and scattering of Gaussian beams," Symp. Math. Ist. Naz. Alt. Mat. 18, 39–56 (1976).
18. M. Burton, Control Data Canada, Ottawa, Ontario, Canada (personal communication, 1986).

Theory of Time-Domain Quasi-TEM Modes in Inhomogeneous Multiconductor Lines

ISMO V. LINDELL, SENIOR MEMBER, IEEE, AND QIZHENG GU

Abstract—Theory for quasi-TEM modes propagating in a transversely inhomogeneous (multidielectric), longitudinally uniform transmission line, previously derived for time-harmonic waves, is derived for transient signals. It is seen that, while the starting point for the theory is completely different, the result is similar to the time-harmonic theory, and previously derived properties for propagating modes also apply in the transient case. The range of applicability is discussed with a simple example.

I. Introduction

THE INHOMOGENEOUS multiconductor transmission line is interesting because of the wide field of applications of the microstrip structure. In the case of time-harmonic (sinusoidal) fields, the exact TEM modes for this kind of geometry, do not exist. Before the introduction of a theory for the quasi-TEM modes, there were often erroneous assumptions about the nature of fields propagating in such structures. The exact theory for two-conductor lines was first given by dos Santos and Figanier in 1975 [1], generalized to multiconductor lines by Mannersalo in 1977 (not published) and, in a more complete form, by Lindell in 1981 [2]. There also exist other expositions on the subject [3], [4].

As pointed out in [2], the transverse quasi-TEM mode field is a kind of glued-together pair of static electric and static magnetic fields, whose boundary conditions are connected through a pair of consistency equations, which also determine the propagation properties of the quasi-TEM wave. The longitudinal components can be calculated from the transverse components and they are low for small frequencies. This theory was obtained by expanding all unknown quantities in series of ascending powers of the frequency. How this can be generalized to fields of arbitrary time dependence is not evident, because there does not exist a small parameter like ω. However, obviously, a similar theory should apply for transient signals whose spectrum consists of sufficiently low frequencies. A need for a firm foundation for such a theory exists because of the new generation of computers applying microstriplike geometry and rapid pulsed signals, although the important wavelengths of such signals are still large with respect to transverse measures of the line. Calculations of coupling between such signals applying the ideal TEM mode approximation have recently been presented [5], [6].

The theory given here is not based on an asymptotic (perturbational) series approach, but on an iterational consideration, which starts on a quasi-TEM assumption, proceeds to derive properties for such a field, and finally tries to find out conditions of validity for the original assumption.

Manuscript received January 3, 1987; revised May 18, 1987. This work was supported by the Academy of Finland, by the Joint Service Electronics Programs under contract DAAL03-86-K-0002, by the Army Research Office under Contract DAAG29-85-K-0079, and by the Office of Naval Research under Contract N00014-86-K-0533.

I. V. Lindell is with the Department of Electrical Engineering, Helsinki University of Technology, Otakaari 5A, Espoo 15, 02150 Finland.

Q. Gu is with the Research Laboratory of Electronics, Department of Electrical Engineering and Computer Science, Massachusetts Institute of Technology, Cambridge, MA 02139.

IEEE Log Number 8716175.

II. The Iteration Method

The following theory of mode propagation in a transversely inhomogeneous multiconductor waveguide, Fig. 1, is a companion to that given in [2] and uses much of the same notation, the main difference being that the subscripts z are deleted. The electromagnetic field is studied in terms of its transverse and longitudinal components, respectively, transverse and parallel to the guide axis vector $\bar{u}$:

$$\bar{E}(\bar{r},t) = \bar{e}(\bar{r},t) + \bar{u}e(\bar{r},t) \tag{1}$$

$$\bar{H}(\bar{r},t) = \bar{h}(\bar{r},t) + \bar{u}h(\bar{r},t). \tag{2}$$

When the Maxwell equations are written for the decomposed fields and the resulting equations are decomposed into axial and transverse components, we have the set of equations

$$\nabla_\perp \times \bar{e} = -\bar{u}\mu\partial_t h \tag{3}$$

$$\nabla_\perp \times \bar{h} = \bar{u}\epsilon\partial_t e \tag{4}$$

$$\nabla_\perp e = -\partial_z \bar{e} + \partial_t \bar{u} \times (\mu\bar{h}) \tag{5}$$

$$\nabla_\perp h = -\partial_z \bar{h} - \partial_t \bar{u} \times (\epsilon\bar{e}) \tag{6}$$

$$\nabla_\perp \cdot (\epsilon\bar{e}) = -\epsilon\partial_z e \tag{7}$$

$$\nabla_\perp \cdot (\mu\bar{h}) = -\mu\partial_z h. \tag{8}$$

Here, $\nabla_\perp$ denotes the transverse component of ∇; μ and ϵ are functions of the transverse vector $\bar{\rho}$, and the partial derivatives $\partial F/\partial\xi$ are denoted in short by $\partial_\xi F$.

Equations (3)–(8) are exact. As a starting point to the iteration method leading to the quasi-TEM theory, we assume that the right-hand sides of (3), (4), (7), and (8) are small and approximate them by zeros. This assumption will be studied more closely later on. After solving for the transverse fields on the left-hand side, the longitudinal

0018-9480/87/1000-0893$01.00

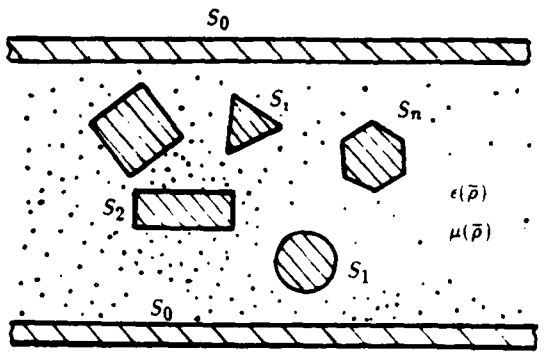

Fig. 1. Cross section of the transversely inhomogeneous multiconductor line with N conductors S_i and a conducting sheath S_0. The unit vector $\bar{u}$ and z coordinate are perpendicular to the plane.

fields are solved from (5) and (6). The iteration could be continued by substituting these on the right-hand sides of (3), (4), (7), and (8), and solving for the next approximations for the transverse fields. The process will evidently converge if the longitudinal fields are small enough. Here, we are only concerned with the first round of iteration, which gives us static approximation of the transverse fields and quasi-static approximation of longitudinal fields.

III. Static Approximation

Setting $e = 0$ and $h = 0$ in the four equations (3), (4), (7), and (8) gives us equations for the first approximation of the transverse fields $\bar{e}_0, \bar{h}_0$:

$$\nabla_\perp \times \bar{e}_0(\bar{r}, t) = 0 \tag{9}$$

$$\nabla_\perp \cdot (\epsilon \bar{e}_0) = 0 \tag{10}$$

$$\nabla_\perp \times \bar{h}_0(\bar{r}, t) = 0 \tag{11}$$

$$\nabla_\perp \cdot (\mu \bar{h}_0) = 0. \tag{12}$$

Equations (9) and (10) constitute an electrostatic problem in two dimensions, and as the boundary conditions on the conductors we have

$$\bar{n} \times \bar{e}_0 = 0. \tag{13}$$

Correspondingly, (11) and (12) define a magnetostatic problem with the boundary conditions

$$\bar{n} \cdot \bar{h}_0 = 0. \tag{14}$$

Here, $\bar{n}$ denotes the unit vector normal to the conductor boundaries. The static problems can be treated with potential quantities. In fact, defining the electric field in terms of a scalar potential ϕ:

$$\bar{e}_0(\bar{r}, t) = -\nabla_\perp \phi(\bar{r}, t) \tag{15}$$

(9) will be automatically satisfied, whence the equations for ϕ, from (10) and (13), are

$$\nabla_\perp \cdot (\epsilon \nabla_\perp \phi) = 0 \tag{16}$$

$$\phi(\bar{r}, t) = U_i(z, t) \qquad \text{for } \bar{\rho} \in S_i. \tag{17}$$

Here, S_i denotes the surface of the ith conductor, $i = 0, 1, \cdots, N$. For simplicity, we assume that there is a sheath conductor denoted by $i = 0$ and define $U_0 = 0$ so that U_i means the voltage between the ith conductor and the sheath. The present theory is not limited to closed geometries. If the correct behavior of potential functions in the infinity is taken into account, the analysis can be written in very much the same fashion. However, instead of defining voltages with respect to the sheath, another reference potential ("ground") must be assumed.

The solution of (16) and (17) obviously depends on the set of boundary values $U_i(z, t)$, which can be represented as an N-vector $\boldsymbol{U}(z, t)$. To be able to write the solution for any boundary values, we must solve N different normalized problems for functions $\phi_i(\bar{\rho})$, making up an N-vector function $\boldsymbol{\phi}(\bar{\rho})$, satisfying the boundary conditions $\phi_j = 1$ on S_j and $\phi_j = 0$ on all the other conductors ($i \neq j$). The solution corresponding to the boundary value vector $\boldsymbol{U}(z, t)$ can then be written as

$$\phi(\bar{r}, t) = \sum_{i=1}^{N} U_i(z, t)\phi_i(\bar{\rho}) = \boldsymbol{U}(z, t) \circ \boldsymbol{\phi}(\bar{\rho}). \tag{18}$$

Here, we have adopted the notation $\circ$ for the inner product of two N-vectors to distinguish it from the "dot" product of two vectors in the physical three-space.

In the same manner, the magnetostatic problem can be formulated in terms of an axial vector potential $\bar{A} = \bar{u}A$:

$$\mu(\bar{\rho})\bar{h}_0(\bar{r}, t) = \nabla_\perp A(\bar{r}, t) \times \bar{u}. \tag{19}$$

Equation (12) is automatically satisfied through (19). Out of (11) and (14) comes

$$\nabla_\perp \cdot \left(\frac{1}{\mu} \nabla_\perp A \right) = 0 \tag{20}$$

$$A(\bar{r}, t) = \Psi_i(z, t) \qquad \text{for } \bar{\rho} \in S_i. \tag{21}$$

Here, Ψ_i denotes the magnetic flux/unit length between the conductor i and the sheath. In terms of a general solution N-vector $\boldsymbol{A}(\bar{\rho})$ and a set of boundary values $\boldsymbol{\Psi}(z, t)$ the solution can be written as

$$A(\bar{r}, t) = \boldsymbol{\Psi}(z, t) \circ \boldsymbol{A}(\bar{\rho}). \tag{22}$$

In the electrostatic problem (16), (17), the boundary-value voltage N-vector uniquely defines the quantities Q_i, i.e., the charge/unit length on each conductor through

$$Q_i(z, t) = \oint_{C_i} \epsilon \bar{e}_0 \cdot \bar{n} dl = -\oint_{C_i} \epsilon \frac{\partial \phi}{\partial n} dl \tag{23}$$

where C_i denotes the circumference of the ith conductor. The linear relation between the voltage and charge N-vectors can be written in terms of a static capacitance/unit length matrix $\underline{C}$

$$\boldsymbol{Q}(z, t) = \underline{C} \circ \boldsymbol{U}(z, t). \tag{24}$$

For the magnetostatic problem, there is also a linear relation between the magnetic fluxes and the currents I_i on the conductors, defined by

$$I_i(z, t) = \oint_{C_i} \bar{h}_0 \cdot d\bar{l} = -\oint_{C_i, \mu} \frac{1}{\mu} \frac{\partial A}{\partial n} dl \tag{25}$$

$$\boldsymbol{\Psi}(z, t) = \underline{L} \circ \boldsymbol{I}(z, t) \tag{26}$$

where $\underline{L}$ is the inductance/unit length matrix.

IV. The Quasi-TEM Field

Until now, the two static problems have no connection. The boundary value N-vectors are, however, coupled through (5) and (6). From (5), we can solve the approximate longitudinal component e_1:

$$e_1(\bar{r},t) = \partial_z\phi(\bar{r},t) + \partial_t A(\bar{r},t). \tag{27}$$

The corresponding approximation for the longitudinal magnetic field h_1 cannot be obtained from (6) explicitly:

$$\nabla_\perp h_1(\bar{r},t) = -\partial_z \bar{h}_0(\bar{r},t) - \bar{u}\times\epsilon\partial_t\bar{e}_0(\bar{r},t)$$
$$= \bar{u}\times\left[\frac{1}{\mu}\nabla_\perp\partial_z A(\bar{r},t) + \epsilon\nabla_\perp\partial_t\phi(\bar{r},t)\right]. \tag{28}$$

Because the right-hand side of (28) is curl free, as can easily be checked, h_1 can be obtained through integration from a reference point $\bar{\rho}_0$ to the general point $\bar{\rho}$. Integrating round the conductor i, the integral should vanish since h_1 is a unique physical quantity. To obtain unique values for h_1 from (28) by integration, one more condition for h_1 is needed, because the reference value $h_1(\bar{\rho}_0)$ is not known. The missing condition is obtained by integrating (3) over the waveguide cross section, which gives us zero if Stokes' theorem is invoked, because the line integral of the electric field around the perimeter vanishes. Thus, $\partial_t \int h dS = 0$, or the integral is constant in time. If the fields are switched on at some finite time, the constant is zero and we have for the additional condition for h_1

$$\int_S h_1(\bar{r},t)\,dS = 0 \tag{29}$$

where S is the total cross section surface of the waveguide.

Because of the boundary condition $e_1 = 0$ on the conductors, (27) defines a relation between the boundary values of the potentials ϕ and A:

$$\partial_z U(z,t) + \partial_t \Psi(z,t) = 0. \tag{30}$$

This is, in fact, one form of writing the Faraday law, in which a moving magnetic flux produces an induced voltage. The other equation, (28), gives rise to another relation between integrated quantities of the potentials ϕ and A, in the form of a continuity equation:

$$\partial_z I(z,t) + \partial_t Q(z,t) = 0. \tag{31}$$

Substituting from (24) and (26), we have

$$\partial_z U(z,t) = -\underline{\underline{L}}\circ\partial_t I(z,t) \tag{32}$$

$$\partial_z I(z,t) = -\underline{\underline{C}}\circ\partial_t U(z,t). \tag{33}$$

These are recognized as transmission-line equations for a multiconductor line. Eliminating I, we have the wave equation

$$\left(\partial_z^2\underline{\underline{I}} - \underline{\underline{L}}\circ\underline{\underline{C}}\partial_t^2\right)\circ U(z,t) = 0. \tag{34}$$

Here, $\underline{\underline{I}}$ denotes the $N\times N$ unit matrix. Limiting ourselves to the solution traveling in the positive z direction, the operator in (34) can be halved to produce the equation

$$\left(\partial_z\underline{\underline{I}} + \left(\underline{\underline{L}}\circ\underline{\underline{C}}\right)^{1/2}\partial_t\right)\circ U(z,t) = 0. \tag{35}$$

Because $\underline{\underline{C}}$ and $\underline{\underline{L}}$ are positive definite and symmetric matrices, there exists a square-root matrix $(\underline{\underline{L}}\circ\underline{\underline{C}})^{1/2}$ which is positive definite. Hence, it possesses a complete set of eigenvectors and positive eigenvalues, and the solution of (35) can be written in terms of the solutions of

$$\left(\underline{\underline{L}}\circ\underline{\underline{C}}\right)^{1/2}\circ V^j = \frac{1}{v_j}V^j. \tag{36}$$

Corresponding to each eigenvector V^j there exists a mode of the original problem, whose voltage vector can be written as

$$U^j(z,t) = V^j f_j(z - v_j t) \tag{37}$$

with an arbitrary function f_j. Thus, the eigenvalues of the algebraic equation (36) define the velocities of the N quasi-TEM modes on the inhomogeneous waveguide. The current distribution vector corresponding to the jth mode, I^j, satisfies similar equations but with $\underline{\underline{L}}$ and $\underline{\underline{C}}$ interchanged. As in [2], this leads to an eigenvector different from U^j, in general, which means that there does not exist a simple scalar impedance, but the impedance is a matrix quantity, denoted here by $\underline{\underline{Z}}$.

V. Traveling Wave Solutions

The practical multiconductor line problem, with possible small deviation from axial uniformity, can be treated with traveling wave quantities with less effort than with current/voltage quantities. In fact, we can define the voltage wave vectors [7] by

$$U_\pm = U \pm \underline{\underline{Z}}\circ I \tag{38}$$

where the impedance matrix is defined in any of the following equivalent forms [2]:

$$\underline{\underline{Z}} = \left(\underline{\underline{L}}\circ\underline{\underline{C}}\right)^{1/2}\circ\underline{\underline{C}}^{-1} = \underline{\underline{C}}^{-1}\circ\left(\underline{\underline{C}}\circ\underline{\underline{L}}\right)^{1/2}$$
$$= \left(\underline{\underline{L}}\circ\underline{\underline{C}}\right)^{-1/2}\circ\underline{\underline{L}} = \underline{\underline{L}}\circ\left(\underline{\underline{C}}\circ\underline{\underline{L}}\right)^{-1/2}. \tag{39}$$

It must be noted that since in the general case the matrices $\underline{\underline{C}}$ and $\underline{\underline{L}}$ do not commute, the square root of their product is dependent on the order of the product. Solving the voltage and current vectors from (38) in terms of voltage waves and substituting in (32) give us the two equations

$$\partial_z U_\pm(z,t) \pm \left(\underline{\underline{L}}\circ\underline{\underline{C}}\right)^{1/2}\circ\partial_t U_\pm(z,t) = 0. \tag{40}$$

It is seen that equations (40) are uncoupled for both traveling voltage vectors. Thus, they possess solutions of the type

$$U^j_\pm(z,t) = V^j f_j(z \mp v_j t). \tag{41}$$

For a line with slight nonuniformity along its axis, equations (40) can be generalized to possess a perturbational coupling term on the right-hand side [5], [6].

It is also easy to show that the integral of the Poynting vector $\frac{1}{2}\bar{e}_0\times\bar{h}_0^*$ over the cross section equals the sum of $\frac{1}{2}U\circ I^*$, or the propagating power in the quasi-TEM mode can be expressed in terms of fields or boundary values.

VI. On the Validity of the Quasi-TEM Concept

After having calculated the approximate longitudinal field components in terms of the approximate transverse components, we can substitute them on the right-hand sides of (3), (4), (7), and (8) and calculate a better approximation for the transverse fields, $\bar{e}_2, \bar{h}_2$. For these fields not to differ from the original approximations $\bar{e}_0, \bar{h}_0$ significantly, the right-hand sides should be small. What does this mean? Obviously, in order to be able to approximate the transverse curl operations in (3) and (4) by zero, the right-hand sides should be small with respect to other derivatives than curl of the vector functions on the left-hand sides. In this case, the iteration would converge and the terms already calculated would present a reasonable approximation to the fields.

Let us study the question in terms of simple consideration of order. If, for example, the following inequality is valid:

$$\|\nabla_\perp \bar{e}_0\| \gg |\mu \partial_t h_1| \tag{42}$$

then obviously from (3), $\nabla \times \bar{e}_0$ is small when compared to other transverse derivatives of $\bar{e}_0$ and it can be approximated by zero. Thus, when solving the next iterational step, the transverse field $\bar{e}_2$ in terms of h_1 from (3), the solution $\bar{e}_2$ does not differ from $\bar{e}_0$ very much. Now the order of $\nabla_\perp$ is $1/D$, where D is the transverse dimension of the guide. If the dimension of the axial variation of the fields is L, we have $f'(z - v_p t)$ of the order $f(z - v_p t)/L$, where v_p is the phase velocity of the mode and from (28) and (42) we may write

$$|\bar{e}_0| \gg \mu v_p \left(\frac{D}{L}\right) |-\bar{h}_0 + v_p \bar{u} \times \epsilon \bar{e}_0|. \tag{43}$$

This inequality is obviously valid if D/L is small enough, i.e., if the transverse dimension of the guide is small enough with respect to field variations in the z direction. In other words, the variation of the signal should be so slow that the propagating field does not change much at the distance of the transverse dimension in z direction. But this is not all, because the vector term on the right-hand side may also be small. This happens if the inhomogeneity of the guide is small. In fact, if the guide becomes homogeneous, the solution of (20) becomes a multiple of the solution of (16) and the relation obtained from (30) is $\phi = v_p A$, or from (15) and (19) $\bar{h}_0 = \bar{u} \times \bar{e}_0/\eta$, with $\eta = \mu v_p = 1/\epsilon v_p$, which makes the right-hand side of (43) vanish. If the inhomogeneity is small, the term need not vanish, but it is small and (43) is valid for larger values of the ratio D/L.

There does not seem to be an easy way to express the condition of validity in more exact terms. A simpler condition is obtained if the ratios $|e_1|/|\bar{e}_0|, |h_1|/|\bar{h}_0|$ are considered. This not only shows us that the basic approximation of the field is quasi TEM, but also gives an idea on the convergence. In fact, writing

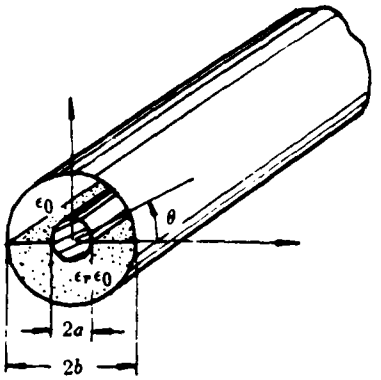

Fig. 2. The inhomogeneous coaxial cable. Basic wave is a TE wave, which is quasi-TEM for sufficiently slowly varying transient signals and/or small inhomogeneity (small $\epsilon_r - 1$).

$$\frac{|e_1|}{|\bar{e}_0|} = \left|\frac{f'(z - v_p t)}{f(z - v_p t)}\right| \frac{|\phi - v_p A|}{|\nabla_\perp \phi|} = \left|\frac{f'}{f}\right| \frac{|(\phi - A) \circ V|}{|\nabla_\perp \phi \circ V|} \tag{44}$$

we may require this to satisfy the condition $\ll 1$. The last factor is zero for homogeneous line and small for small inhomogeneity. Because the maximum values of ϕ and A are their boundary value 1, it is obviously bounded by the value $2D$, which shows us that the quasi-TEM mode is always possible if the signal is varying slowly enough.

VII. Example

Let us elucidate the problem of convergence through a simple example of inhomogeneous coaxial cable with $\mu = \mu_0$ and $\epsilon_r = 1$ for $\theta = \theta \cdots \pi$ and $\epsilon_r \neq 1$ for $\theta = 0 \cdots -\pi$, Fig. 2. Because of the special symmetry, the potential fields ϕ and A are multiples of the same function $g(\rho)$:

$$g(\rho) = \frac{\ln\left(\frac{b}{\rho}\right)}{\ln\left(\frac{b}{a}\right)}. \tag{45}$$

The inductance is the same as for the homogeneous coaxial line:

$$L = L_0 = \frac{\mu_0}{2\pi} \ln\left(\frac{b}{a}\right) \tag{46}$$

and the capacitance equals

$$C = \left(\frac{1 + \epsilon_r}{2}\right) C_0 = \frac{\pi(1 + \epsilon_r)\epsilon_0}{\ln\left(\frac{b}{a}\right)}. \tag{47}$$

The phase velocity of the quasi-TEM wave is

$$v_p = \frac{1}{\sqrt{L_0 C}} = c\sqrt{\frac{2}{1 + \epsilon_r}}. \tag{48}$$

The potentials are

$$\phi(\bar{r},t) = Vg(\rho)f(z-v_p t) \quad (49)$$

$$A(\bar{r},t) = \Psi g(\rho)f(z-v_p t) = \frac{V}{v_p}g(\rho)f(z-v_p t). \quad (50)$$

From (27) we have

$$e_1 = Vg(\rho)f'(z-v_p t) - v_p\frac{V}{v_p}g(\rho)f'(z-v_p t) = 0 \quad (51)$$

or the longitudinal electric field vanishes in this approximation. Thus, the quasi-TEM is in fact a TE field in this approximation, which is due to the special symmetry of the structure. From (28) we have

$$h_1(\bar{r},t) = \frac{V}{\eta}f'(z-v_p t)\int_{\bar{r}_0}^{\bar{r}}\left(\frac{c}{v_p}-\epsilon_r(\bar{\rho})\frac{v_p}{c}\right)\cdot(\bar{m}\cdot\nabla_\perp g)\,dC + h_1(\bar{r}_0). \quad (52)$$

The unit vector $\bar{m}$ is normal to the integration path. Because $\bar{m}\cdot\nabla_\perp g(\rho) = 0$ on each radial lin , it is clear that h_1 is a function of θ only. Thus, the integration path can be taken along any circle of radius ρ. If the constant $h_1(\bar{r}_0)$ is determined through the condition (29), the result is

$$h_1(\bar{r},t) = \frac{V}{\eta\ln(b/a)}f'(z-v_p t)\frac{\epsilon_r-1}{\sqrt{2(\epsilon_r+1)}}\left(|\theta|-\frac{\pi}{2}\right) \quad \text{for } -\pi \le \theta \le \pi. \quad (53)$$

This expression is seen to vanish for $\epsilon_r = 1$, in which case the guide is homogeneous. The null field is obtained for $\theta = \pm\pi/2$ and maxima at $\theta = 0, \pi$. To check the quasi-TEM character of the wave, we compare the magnitudes of h_1 and $\bar{h}_0$:

$$\frac{|h_1|}{|\bar{h}_0|} = \left(\frac{\epsilon_r-1}{\epsilon_r+1}\right)\left|\frac{f'(z-v_p t)}{f(z-v_p t)}\right|\left|\left(|\theta|-\frac{\pi}{2}\right)\rho\right|. \quad (54)$$

The maximum value of the last factor is $\pi b/2$. Thus, the right-hand side of (54) gives us the relative rate of change of the signal in the axial direction over the distance $(\epsilon_r-1)\pi b/2(\epsilon_r+1)$. Obviously, the convergence of the iteration is good and the quasi-TEM concept valid if this rate is small.

VIII. Conclusions

The quasi-TEM mode theory of inhomogeneous multiconductor waveguides, previously presented for time-harmonic fields, was generalized for fields with arbitrary time dependence. The theory is based upon an iterative approach, and the condition for its convergence was outlined and elucidated with a simple example. It was seen that the resulting theory, basically similar to that given for the time-harmonic case, can be applied for transient signals, provided the variation of the signal is slow enough or the inhomogeneity is not too large.

Acknowledgment

This work was done while the first author was on sabbatical leave at the MIT Research Laboratory of Electronics, during the academic year 1986–87. The authors wish to express their gratitude to professor J. A. Kong for this possibility and for fruitful discussions upon the present topic.

References

[1] A. F. dos Santos, and J. P. Figanier, "The method of series expansion in the frequency domain applied to multidielectric transmission lines," *IEEE Trans. Microwave Theory Tech.*, vol. MTT-23, pp. 753–756, Sept. 1975.

[2] I. V. Lindell, "On the quasi-TEM modes in inhomogeneous multiconductor transmission lines," *IEEE Trans. Microwave Theory Tech.*, vol. MTT-29, pp. 812–817, Aug. 1981.

[3] M. Aubourg, "Onde quasi-TEM des guides cylindriques blindés," *Annales de Télécommunication*, vol. 34, nos. 1–2, pp. 45–51, 1979.

[4] C. Vassallo, *Théorie des Guides d'Ondes Électromagnétiques*. Paris: Eyrolles, 1985.

[5] Y-C. E. Yang, J. A. Kong, and Q. Gu, "Time-domain perturbational analysis of nonuniformly coupled transmission lines," *IEEE Trans. Microwave Theory Tech.*, vol. MTT-33, pp. 1120–1130, Nov. 1985.

[6] Q. Gu, J. A. Kong, and Y-C. E. Yang, "Time domain analysis of nonuniformly coupled line systems," *JEWA*, vol. 1, no. 2, pp. 109–132, 1987.

[7] P. E. Adair and G. I. Haddad, "Coupled-mode analysis of nonuniform coupled transmission lines," *IEEE Trans. on Microwave Theory Tech.*, vol. MTT-17, pp. 746–752, Oct. 1969.

Ismo V. Lindell (S'68–M'69–SM'83) was born in Viipuri, Finland, on November 23, 1939. He received the degrees of Dipl. Eng., Lic. Tech., and Dr. Tech. in 1963, 1967, and 1971, respectively, all in electrical engineering, from the Helsinki University of Technology (HUT), Espoo, Finland.

He was a Research and Teaching Assistant from 1963 to 1970, Acting Associate Professor or Acting Professor from 1970 to 1975 and 1983–84, and Associate Professor since 1975, in Radio Engineering, with the HUT. Since 1984, he has been Head of the Electromagnetics Laboratory. During the academic year 1972–73, he was a Visiting Associate Professor at the University of Illinois, Urbana, and in 1986-87 he was a Visiting Scientist at M.I.T., Cambridge, MA. In 1985–86 he was Chairman of the IEEE Finland Section, and since 1977 he has been the Commission B official member of Finland in URSI.

Dr. Lindell has authored scientific papers and two books: *Radio Wave Propagation* and *Antenna Theory* (both in Finnish). He is the recipient of the 1987 S. A. Schelkunoff award of the Antennas and Propagation Society. His main interest is electromagnetic theory.

Qizheng Gu was born in Jiangsu, China. He graduated from Fudan University, Shanghai, China, in 1960.

From 1960 to 1962, he worked on the design and analysis of automatic control systems at the Shanghai Design Institute of Machinery and Electrical Engineering. In 1962, he joined the Department for Research and Development at the Shanghai Xinhua Radio Factory, where he was engaged in research on microwave passive and active devices, receiver systems, PLL and AFC systems, and microwave integrated circuits. Since October 1982, he has been a senior engineer and Deputy Director of the Department for Research and Development. In June 1983, he came to the United States as a Visiting Scientist at the Research Laboratory of Electronics, Massachusetts Institute of Technology. His research is on electromagnetic transmission and interference in high-speed microelectronic integrated circuits.

Mr. Gu is a member of the Shanghai Electronics Association Council and the Microwave Committee of the Chinese Institute of Electronics.

Resonance and Radiation of the Elliptic Disk Microstrip Structure, Part I: Formulation

T.M. Habashy
J.A. Kong
W.C. Chew

Reprinted from
IEEE TRANSACTIONS ON ANTENNAS AND PROPAGATION
Vol. AP-35, No. 8, August 1987

Resonance and Radiation of the Elliptic Disk Microstrip Structure, Part I: Formulation

TAREK M. HABASHY, MEMBER, IEEE, JIN AU KONG, FELLOW, IEEE, AND WENG CHO CHEW, SENIOR MEMBER, IEEE

Abstract—**The analysis of resonance, input impedance, and radiation of the elliptic disk microstrip structure is rigorously formulated, using the scalar and vector Mathieu transforms. With the help of these transforms, the resonance frequencies of the structure can be derived exactly using Galerkin's method and approximately using a perturbational approach. Expressions for the input impedance and the radiation pattern are also obtained.**

I. Introduction

IT IS KNOWN that circular or rectangular disk microstrip antennas usually radiate waves which are linearly polarized [1]–[3]. However, in such structures circular polarization can be obtained using a complicated feed setup comprising more than one feed.

From experimental measurements [1], [2] and recent analytical work [3], it is shown that by using a slightly elliptical shaped disk, circular polarization can be achieved while retaining a single, simple feed. Also, for applications in harmonic multipliers and parametric amplifiers, the circular microstrip disk resonator is unsuitable due to a harmonious relationship of mode frequencies. However, suitable modes for both applications can be found in the resonances of an elliptic structure where a further degree of freedom, the eccentricity, enables the desired frequency relationships to be achieved [4]–[6]. Thus, the eccentricity as a design parameter provides an additional flexibility and enhances the usefulness of the elliptic disk structure. An added advantage of the use of the elliptic structure over the circular one is that the former can be designed to have a wider frequency band of operation than the latter. A broad-band structure can be realized out of the circular structure only through the use of more than one element [7]–[9].

In past studies of the elliptic disk microstrip structure, more work was devoted to the analysis of the structure as a resonator [4]–[6] than as an antenna [1]–[3]. In [5], the analysis of the elliptic resonator is carried out by employing the magnetic wall cavity model, whereas in [6], the analysis is carried out using a quasistatic approximation where an equivalent capacitance of the elliptic structure is derived. In both analyses, the resonant frequencies obtained are pure real and therefore do not account for the radiation losses, thus rendering the obtained results very limited. Also, using the equivalent capacitance to calculate the resonant frequencies is proven to be incorrect [10]–[12].

In the analysis of the elliptic structure as a radiator and in calculating the radiation pattern [3], the fringing effects of the electric field are taken into account by superficially imposing an impedance boundary condition at the opening of the cavity. This surface impedance is approximated by the one obtained from solving the circular disk antenna, thus limiting the obtained results for small eccentricity.

In this paper, a rigorous analysis of the elliptic microstrip structure is carried out using the scalar and vector Mathieu transforms [13]. These transforms allow an exact formulation of the elliptic disk structure which has long been thought almost impossible to formulate rigorously [6]. It is shown that the current distribution on the disk is rigorously derived using these transforms and that it is governed by a set of vector integral equations. These equations are then solved using the Galerkin's method, in which the current is expanded in terms of the orthogonal set of the transverse magnetic (TM) and transverse electric (TE) modes of the magnetic wall cavity, since they form a complete set of basis functions, to obtain linear algebraic equations in the expansion coefficients. The eigenvalue equation is then obtained by setting the determinant of the coefficients of these algebraic equations to zero. In the limit of a thin substrate, a perturbative approach is used to get a simple expression for the resonant frequencies. Finally, the input impedance and the radiation pattern are derived both exactly and in the limit of a thin substrate.

II. Field Expressions Due to the Current Distribution on the Disk

Fig. 1 shows the geometrical configuration of the problem. A perfectly conducting elliptical disk is placed on top of a dielectric substrate backed by a perfectly conducting ground plane. The disk has a semimajor axis a and a semiminor axis b and of a focal length $2c_0$. The dielectric substrate has a permittivity of ϵ_1 and thickness d. An elliptical coordinate system (u, v, z) is used to express points in space. These are related to the Cartesian coordinates as follows:

$$x = c_0 \cosh(u) \cos(v), \quad y = c_0 \sinh(u) \sin(v).$$

The disk is fed by a probe P situated at (u_0, v_0). Using the

Manuscript received August 25, 1986; revised March 15, 1987.

T. M. Habashy is with Schlumberger-Doll Research, Old Quarry Road, Ridgefield, CT 06877.

J. A. Kong is with the Department of Electrical Engineering and Computer Science, Research Laboratory of Electronics, Massachusetts Institute of Technology, Cambridge, MA 02139.

W. C. Chew is with the Department of Electrical and Computer Engineering, University of Illinois, 1406 West Green street, Urbana, IL 61801.

IEEE Log Number 8715345.

stratified medium formulation [10]–[12], [14], the z-component of the electric and magnetic fields in the free space region due to the current distribution on the disk can be shown to be given by

$$E_z = \sum_{n,\alpha} \int_0^\infty dk_\rho k_\rho \, e\alpha_n(k_\rho)[\pm e^{\pm ik_z z} - R^{TM} e^{ik_z(2H+z)}]\psi\alpha_n(c_0 k_\rho, u, v) \quad (1)$$

$$H_z = \sum_{n,\alpha} \int_0^\infty dk_\rho k_\rho \, h\alpha_n(k_\rho)[e^{\pm ik_z z} + R^{TE} e^{ik_z(2H+z)}]\psi\alpha_n(c_0 k_\rho, u, v) \quad (2)$$

where the positive sign is for $z > 0$ and the negative sign is for $z < 0$. $\psi\alpha_n(c_0 k_\rho, u, v)$ is an elliptic harmonic given by the product of a radial and an angular Mathieu function and is defined in [13, appendix A]. H is the height of the disk above the substrate which will be later set equal to zero and is introduced to avoid the ambiguity in applying the boundary conditions at the plane of the disk. The transverse components of the electric and magnetic fields can be readily obtained from E_z and H_z using the following formulas [14]:

$$\tilde{\mathbf{E}}_s(k_\rho, u, v, z) = \frac{1}{k_\rho^2}\left[\nabla_T\left(\frac{\partial \tilde{E}_z}{\partial z}(k_\rho, u, v, z)\right) + i\omega\mu_0 \nabla_T \times (\hat{\mathbf{z}}\tilde{H}_z(k_\rho, u, v, z))\right]$$

$$\tilde{\mathbf{H}}_s(k_\rho, u, v, z) = \frac{1}{k_\rho^2}\left[\nabla_T\left(\frac{\partial \tilde{H}_z}{\partial z}(k_\rho, u, v, z)\right) - i\omega\epsilon \nabla_T \times (\hat{\mathbf{z}}\tilde{E}_z(k_\rho, u, v, z))\right]$$

where

$$\nabla_T = \frac{1}{h}\left(\hat{\mathbf{u}}\frac{\partial}{\partial u} + \hat{\mathbf{v}}\frac{\partial}{\partial v}\right)$$

and $\tilde{E}_z(k_\rho, u, v, z)$, $\tilde{H}_z(k_\rho, u, v, z)$, $\tilde{\mathbf{E}}_s(k_\rho, u, v, z)$ and $\tilde{\mathbf{H}}_s(k_\rho, u, v, z)$ are the integrands of $E_z(u, v, z)$, $H_z(u, v, z)$, $\mathbf{E}_s(u, v, z)$ and $\mathbf{H}_s(u, v, z)$, respectively. $e\alpha_n(k_\rho)$ and $h\alpha_n(k_\rho)$ are the spectral amplitudes of the electric and magnetic fields, respectively, and are obtained by equating the currents on the disk to the discontinuity in the tangential magnetic field at the disk. Thus, we get the following relationship:

$$\mathbf{K}(u, v) = \begin{bmatrix} K_u(u, v) \\ K_v(u, v) \end{bmatrix} = -\sum_{n,\alpha} \int_0^\infty dk_\rho \tilde{\mathbf{M}}\alpha_n(c_0 k_\rho, u, v) \cdot \mathbf{K}\alpha_n(k_\rho), \qquad \text{for } (u, v) \in D \quad (3)$$

where

$$\mathbf{K}\alpha_n(k_\rho) = \begin{bmatrix} 2i\omega\epsilon \, e\alpha_n(k_\rho)/k_\rho \\ 2ik_z \, h\alpha_n(k_\rho)/k_\rho \end{bmatrix} \quad (4)$$

and $\tilde{\mathbf{M}}\alpha_n(c_0 k_\rho, u, v)$ is given by [13]

$$\tilde{\mathbf{M}}\alpha_n(c_0 k_\rho, u, v) = \frac{1}{h}\begin{bmatrix} \frac{\partial}{\partial u}\psi\alpha_n(c_0 k_\rho, u, v) & \frac{\partial}{\partial v}\psi\alpha_n(c_0 k_\rho, u, v) \\ \frac{\partial}{\partial v}\psi\alpha_n(c_0 k_\rho, u, v) & -\frac{\partial}{\partial u}\psi\alpha_n(c_0 k_\rho, u, v) \end{bmatrix}.$$

The transverse electric field due to the current distribution on the disk D is thus given, for $z = 0$ and $H = 0$, by

$$\mathbf{E}_s(u, v) = \begin{bmatrix} E_u(u, v) \\ E_v(u, v) \end{bmatrix} = \sum_{n,\alpha} \int_0^\infty dk_\rho \tilde{\mathbf{M}}\alpha_n(c_0 k_\rho, u, v) \cdot \tilde{\mathbf{G}}(k_\rho) \cdot \mathbf{K}\alpha_n(k_\rho) \quad (5)$$

where $\tilde{\mathbf{G}}(k_\rho)$ is given by [11], [12]

$$\tilde{\mathbf{G}}(k_\rho) = \begin{bmatrix} \frac{k_z}{2\omega\epsilon}(1 - R^{TM}) & 0 \\ 0 & \frac{\omega\mu_0}{2k_z}(1 + R^{TE}) \end{bmatrix}$$

and the reflection coefficients for the TM and TE polarizations are given by

$$R^{TM} = \frac{i\epsilon_1 k_z - \epsilon k_{1z} \tan(k_{1z} d)}{i\epsilon_1 k_z + \epsilon k_{1z} \tan(k_{1z} d)}$$

$$R^{TE} = \frac{ik_z \tan(k_{1z} d) + k_{1z}}{ik_z \tan(k_{1z} d) - k_{1z}}$$

where

$$\omega^2\mu_0\epsilon - k_z^2 = k_\rho^2 = \omega^2\mu_0\epsilon_1 - k_{1z}^2.$$

III. The Vector Integral Equations Governing the Current Distribution on the Disk

The current distribution on the disk is governed by the condition that the current has to vanish outside the disk, together with the boundary condition on the tangential component of the electric field on the disk. These two conditions give rise to two dual vector integral equations which can then be solved using Galerkin's method. From the condition on the current we have

$$\mathbf{K}(u, v) = 0, \qquad \text{for } u > u_s. \quad (6)$$

From the condition on the tangential electric field, we have

$$\mathbf{E}_s(u, v) + \mathbf{E}_s^p(u, v) = 0, \qquad \text{for } u < u_s \quad (7)$$

where $\mathbf{E}_s(u, v)$ is given by (1), $\mathbf{E}_s^p(u, v)$ is given in Appendix I and $u = u_s$ corresponds to the points on the outer edge of the elliptic disk. Expressing these two conditions explicitly in

terms of the current spectral amplitudes $\mathbf{K}\alpha_n(k_\rho)$, we get

$$-\sum_{n,\alpha}\int_0^\infty dk_\rho \tilde{\mathbf{M}}\alpha_n(c_0k_\rho, u, v) \cdot \mathbf{K}\alpha_n(k_\rho) = 0, \quad \text{for } u > u_s \tag{8}$$

$$\sum_{n,\alpha}\int_0^\infty dk_\rho \tilde{\mathbf{M}}\alpha_n(c_0k_\rho, u, v) \cdot \tilde{\mathbf{G}}(k_\rho) \cdot \mathbf{K}\alpha_n(k_\rho) = -\sum_{n,\alpha}\int_0^\infty dk_\rho \tilde{\mathbf{M}}\alpha_n(c_0k_\rho, u, v) \cdot \mathbf{T}\alpha_n(k_\rho), \quad \text{for } u < u_s \tag{9}$$

which are two dual vector integral equations governing the unknown current spectral amplitudes $\mathbf{K}\alpha_n(k_\rho)$. $\mathbf{T}\alpha_n(k_\rho)$ is the source spectral amplitude given in Appendix I. To solve these equations using Galerkin's approach, the current distribution on the disk is expanded in terms of the orthogonal set of the TM and TE modes of the magnetic wall cavity since they form a complete set of basis functions.

$$\mathbf{K}(u, v) = \sum_{n,\alpha,m} \hat{\mathbf{S}}\alpha_{nm}(u, v) \cdot \mathbf{a}\alpha_{nm}, \qquad u < u_s \tag{10}$$

where $\mathbf{a}\alpha_{nm}$ is a two-component vector whose components are the unknown coefficients of expansion, and $\hat{\mathbf{S}}\alpha_{nm}(u, v)$ is given by

$$\hat{\mathbf{S}}\alpha_{nm}(u, v) = \frac{1}{h}\begin{bmatrix} \frac{\partial}{\partial u}\psi\alpha_n(c_0k\overset{e}{\alpha}_{nm}, u, v) & \frac{\partial}{\partial v}\psi\alpha_n(c_0k\overset{h}{\alpha}_{nm}, u, v) \\ \frac{\partial}{\partial v}\psi\alpha_n(c_0k\overset{e}{\alpha}_{nm}, u, v) & -\frac{\partial}{\partial u}\psi\alpha_n(c_0k\overset{h}{\alpha}_{nm}, u, v) \end{bmatrix} \tag{11}$$

where

$$J\acute{\alpha}_n(c_0k\overset{e}{\alpha}_{nm}, u_s) = 0 \tag{12}$$

and

$$J\alpha_n(c_0k\overset{h}{\alpha}_{nm}, u_s) = 0. \tag{13}$$

The first column of $\hat{\mathbf{S}}\alpha_{nm}(u, v)$ represents the TM current modes of the magnetic wall elliptical cavity whereas the second column represents those of the TE polarization. Upon substituting the expansion in (10) into (6), we get

$$\sum_{r,\beta}\int_0^\infty dk_\rho' \tilde{\mathbf{M}}\beta_r(c_0k_\rho', u, v) \cdot \mathbf{K}\beta_r(k_\rho') = -\sum_{n,\alpha,m} \hat{\mathbf{S}}\alpha_{nm}(u, v) \cdot \mathbf{a}\alpha_{nm}, \qquad u < u_s$$
$$= 0, \qquad u > u_s.$$

Applying the orthogonality property (14) developed in [13], we get

$$\mathbf{K}\beta_r(k_\rho) = -c\beta_r(\mathbf{k}_\rho) \sum_{n,\alpha,m} \hat{S}_{nm,r}(\alpha, \beta, c_0k_\rho) \cdot \mathbf{a}\alpha_{nm} \tag{14}$$

where

$$\hat{S}_{nm,r}(\alpha, \beta, c_0k_\rho) = \int_0^{u_s} du \int_0^{2\pi} dv \cdot h^2 \tilde{\mathbf{M}}\beta_r(c_0k_\rho, u, v) \cdot \hat{\mathbf{S}}\alpha_{nm}(u, v). \tag{15}$$

Equation (14) supplies a relationship between the current spectral amplitude $\mathbf{K}\beta_r(k_\rho)$ and the coefficients of the current modal expansion $\mathbf{a}\alpha_{nm}$. The various components of $\hat{S}_{nm,r}(\alpha, \beta, c_0k_\rho)$ are given by integrals I_2 and I_3 evaluated in Appendix II and $c\beta_r(\mathbf{k}_\rho)$ is given in [13, sec. 6].

The next step is to find the modal expansion coefficients $\mathbf{a}\alpha_{nm}$. This is done by substituting the expansion of $\mathbf{K}\beta_r(k_\rho)$ given by (14) into the second boundary condition given by (9), multiplying the resulting equation by $h^2\hat{\mathbf{S}}\gamma_{js}^t(u,v)$ and integrating over the area of the elliptic disk, one finally gets the following set of equations:

$$\sum_{n,\alpha,m} \tilde{\mathbf{A}}_{nm,js}(\alpha, \gamma) \cdot \mathbf{a}\alpha_{nm} = \mathbf{b}_{js}(\gamma) \tag{16}$$

where

$$\tilde{\mathbf{A}}_{nm,js}(\alpha, \gamma) = \sum_{r,\beta}\int_0^\infty dk_\rho\, c\beta_r(k_\rho) \cdot \hat{S}_{js,r}^t(\gamma, \beta, c_0k_\rho) \cdot \tilde{\mathbf{G}}(k_\rho) \cdot \hat{S}_{nm,r}(\alpha, \beta, c_0k_\rho)$$

$$\mathbf{b}_{js}(\gamma) = \sum_{t,\beta}\int_0^\infty dk_\rho \hat{S}_{js,r}^t(\gamma, \beta, c_0k_\rho) \cdot \mathbf{T}\beta_r(k_\rho)$$

where the superscript t denotes transposing the matrix. For these equations to be of practical use, the modal series expansion has to be truncated and these equations can then be recast in the following matrix form:

$$\tilde{\mathbf{A}} \cdot \mathbf{a} = \mathbf{b}. \tag{17}$$

$\tilde{\mathbf{A}}$ is a matrix whose elements are the matrices $\tilde{\mathbf{A}}_{nm,js}(\alpha, \gamma)$, whereas $\mathbf{a}$ and $\mathbf{b}$ are vectors whose elements are the vectors $\mathbf{a}\alpha_{nm}$ and $\mathbf{b}_{nm}(\alpha)$, respectively. The matrix equation (17) can thus be easily solved for the unknown coefficients $\mathbf{a}$.

In the case of a thin substrate, the structure approaches that of the magnetic wall cavity model and in the limit when $d \to 0$, the vector integral equations give a solution similar to the magnetic wall model. Thus in the case of a thin substrate structure, the dominant modes are the TM modes. Furthermore, if the operating frequency is around $\omega_{\alpha nm}^e$, which is the unperturbed resonant frequency of the magnetic wall cavity for the TM polarization (E-polarization), we will find that only modes which have a resonant frequency of $\omega_{\alpha nm}^e$ in the unperturbed state, will have a dominant contribution to the currents on the disk and all other modes will be relatively negligible. Thus, in the case of a thin substrate and for operating frequencies around $\omega_{\alpha nm}^e$, a single mode approxima-

tion can be employed in which the $TM_{\alpha nm}$ is the only mode to be considered.

IV. Perturbation Formula for the Resonant Frequencies

The exact resonant frequency of the structure, acting as a resonator, can be obtained by setting the determinant of the coefficient of (17) to zero, to get

$$\det [\tilde{\mathbf{A}}] = 0.$$

As is clear from this equation, the calculation of the resonant frequencies using this equation is not a simple task. However, in the limit of a thin substrate, a perturbational approach can be used to calculate the resonant frequencies in a much simpler way. In this limit, the elliptic microstrip structure can be viewed as a perturbation of an elliptic resonator with a perfectly magnetic side wall. The resonant frequency shift of this perturbed magnetic wall cavity is given by [10], [11], [15]

$$\Delta\omega = \omega_f - \omega_i \approx \frac{L}{4\langle W_T \rangle_i} \tag{18}$$

where

$$L = -i \iint_{\Delta S} dS\, \hat{\mathbf{n}} \cdot (\mathbf{E}_i^* \times \mathbf{H}_f)$$

and

$$\langle W_T \rangle_i = \frac{1}{2} \epsilon_1 \iiint_V dV |\mathbf{E}_i|^2$$

where $\mathbf{E}_i$ and ω_i are the electric field and the resonant frequency of the unperturbed cavity, $\mathbf{H}_f$ and ω_f are the magnetic field and the resonant frequency of the perturbed cavity (i.e., the open cavity), $\langle W_T \rangle_i$ is the unperturbed time average total energy stored in the cavity and ΔS is the surface area of the magnetic wall.

In the unperturbed case and because the substrate thickness is assumed to be small, the field components are independent of z. Thus, the only existing modes are the $TM_{\alpha nm}$ modes for which E_z is the only nonvanishing electric field component. Let us consider the perturbation of a specific $TM_{\alpha nm}$ mode whose unperturbed resonant frequency of the magnetic wall cavity is $\omega_{\alpha nm}$ given as the solution of the equation

$$J'_{\alpha_n}(c_0 k^e_{\alpha nm}, u_s) = 0$$

where

$$k^e_{\alpha nm} = \omega^e_{\alpha nm} \sqrt{\mu_0 \epsilon_1}.$$

For this mode, the unperturbed electric field and resonant frequency are given by

$$\mathbf{E}_i = \hat{\mathbf{z}}\, A\, \psi_{\alpha_n}(c_0 k_i, u, v), \qquad k_i = k^e_{\alpha nm} \tag{19a}$$

and

$$\omega_i = \omega_{\alpha nm} \tag{19b}$$

and therefore

$$L = i \int_{-d}^{0} dz \int_0^{2\pi} dv\, h\, E^*_{iz} H_{fv}, \qquad \text{evaluated at } u = u_s.$$

From (1) and (2), and by applying the boundary conditions, it can be shown that

$$E_{fz} = -\frac{\epsilon}{\epsilon_1} \sum_{r,\gamma} \int_0^\infty dk_\rho k_\rho\, e\gamma_r(k_\rho)(1 + R^{TM}) \cdot \frac{\cos\{k_{1z}(z+d)\}}{\cos(k_{1z}d)} \psi\gamma_r(c_0 k_\rho, u, v)$$

$$H_{fz} = \sum_{r,\gamma} \int_0^\infty dk_\rho k_\rho\, h\gamma_r(k_\rho)(1 + R^{TE}) \cdot \frac{\sin\{k_{1z}(z+d)\}}{\sin(k_{1z}d)} \psi\gamma_r(c_0 k_\rho, u, v)$$

and, therefore, the v-component of H_f is given by

$$H_{fv} = \frac{1}{h} \sum_{r,\gamma} \left[\int_0^\infty dk_\rho \frac{k_{1z}}{k_\rho} h\gamma_r(k_\rho)(1 + R^{TE}) \cdot \frac{\cos\{k_{1z}(z+d)\}}{\sin(k_{1z}d)} \frac{\partial}{\partial v} \psi\gamma_r(c_0 k_\rho, u, v) - i\omega\epsilon \int_0^\infty dk_\rho \frac{1}{k_\rho} e\gamma_r(k_\rho)(1 + R^{TM}) \cdot \frac{\cos\{k_{1z}(z+d)\}}{\cos(k_{1z}d)} \frac{\partial}{\partial u} \psi\gamma_r(c_0 k_\rho, u, v) \right]$$

and hence

$$L = \pi A^* J\alpha_n(c_0 k_i, u_s) \sum_r \left[\int_0^\infty dk_\rho \frac{1}{k_\rho} h\tilde{\alpha}_r(k_\rho) \cdot (1 + R^{TE}) J\tilde{\alpha}_r(c_0 k_\rho, u_s) Q\tilde{\alpha}_{rn}(c_0 k_\rho c_0 k_i) + \omega\epsilon \int_0^\infty dk_\rho \frac{1}{k_\rho} e\gamma_r(k_\rho)(1 + R^{TM}) \cdot \frac{\tan(k_{1z}d)}{k_{1z}} J'\alpha_r(c_0 k_\rho, u_s) N\alpha_{nr}(c_0 k_i, c_0 k_\rho) \right] \tag{20}$$

where $Q\tilde{\alpha}_{rn}(c_0 k_\rho, c_0 k_i)$ and $N\alpha_{nr}(c_0 k_i, c_0 k_\rho)$ are defined and given in Appendix II and by $\tilde{\alpha}$ we mean the parity opposite to α.

In the limit when $d/a \to 0$, and from (10), (19), (4), (14), and the results of Appendix II, $a\alpha_{nm}$, $h\tilde{\alpha}_r(k_\rho)$ and $e\alpha_r(k_\rho)$ can be approximated as

$$a\alpha_{nm} \approx \frac{i\omega_i \epsilon_1}{k_i^2} A$$

$$e\alpha_r(k_\rho) = \frac{\pi A}{2} k_\rho\, c\alpha_r(k_\rho) \frac{\omega_i \epsilon_1}{\omega\epsilon} \frac{1}{k_\rho^2 - k_i^2} \cdot J\alpha_n(c_0 k_i, u_s) J'\alpha_r(c_0 k_\rho, u_s) N\alpha_{nr}(c_0 k_i, c_0 k_\rho) \tag{21}$$

$$h\bar{\alpha}_r(k_\rho) = \frac{\pi A}{2}\, c\bar{\alpha}_r(k_\rho)\, \frac{k_\rho}{k_z}\, \frac{1}{\omega_i \mu_0} \cdot J\bar{\alpha}_r(c_0 k_\rho, u_s)\, J\alpha_n(c_0 k_i, u_s)\, Q\alpha_{nr}(c_0 k_i, c_0 k_\rho). \quad (22)$$

Finally, the unperturbed time average total energy stored in the cavity is given by

$$\langle W_T \rangle_i = \frac{1}{2}\epsilon_1 |A|^2 d \int_0^{2\pi} dv \int_0^{u_s} du\, h^2 [\psi\alpha_n(c_0 k_i, u, v)]^2$$

and from Appendix II, we obtain

$$\langle W_T \rangle_i = -\frac{1}{4}\pi\epsilon_1 d \frac{|A|^2}{k_i} J\alpha_n(c_0 k_i, u_s) \cdot \left[\frac{\partial}{\partial k_\rho} J'\alpha_n(c_0 k_\rho, u_s)\right]_{k_\rho = k_i} R\alpha_n(c_0 k_i). \quad (23)$$

Substituting (20), (21), (22), and (23) into (18) we finally get the required perturbational formula for the resonant frequency shift of the $TM_{\alpha nm}$ mode.

V. Calculation of the Input Impedance

The input impedance across the terminals of the probe P is given by [12], [16]

$$Z_{in} = -\frac{1}{I^2}\int dV\, \mathbf{E}_1 \cdot \mathbf{J}$$

where $\mathbf{E}_1$ is the total electric field in the substrate region due to the current on the disk D as well as the current on the probe P. The volume integration in the expression of the input impedance is carried out over the volume of the probe. $\mathbf{J}$ is the current distribution on the probe. To simplify the analysis, the current distribution on the probe is modeled as a uniform cylindrical current sheet of radius a and hence $\mathbf{J}$ is given by

$$\mathbf{J} = \hat{\mathbf{z}}\, \frac{I}{2\pi}\, \frac{\delta[|\rho - \rho_0| - a]}{|\rho - \rho_0|}, \qquad -d < z < 0$$

where ρ_0 is the vector connecting the origin of the coordinate system to the center of the probe. The input impedance is hence given by

$$Z_{in} = -\frac{1}{I^2}\int dV (E^p_{1z} + E^i_{1z}) J_z$$

where E^p_{1z} is the electric field due to the current on the probe. E^i_{1z} is the electric field due to the currents induced on the disk and can be shown to be given by

$$E^i_{1z} = -\frac{1}{2i\omega\epsilon_1}\sum_{p,\gamma}\int_0^\infty dk_\rho k_\rho^2 [\mathbb{K}\gamma_p(k_\rho)]_u \cdot \frac{\cos\{k_{1z}(z+d)\}}{\cos(k_{1z}d)}(1 + R^{TM})\psi\gamma_p(c_0 k_\rho, u, v)$$

thus, the input impedance is given by [12]

$$Z_{in} = \frac{1}{4\pi\omega\epsilon_1}\int_0^\infty dk_\rho \frac{k_\rho}{k_{1z}} J_0^2(k_\rho a) \cdot \left[\frac{2}{ik_{1z}}\left\{\frac{2k_\rho^2 e^{ik_{1z}d/2}\sin(k_{1z}d/2)}{k_{1z}} - k_1^2 d\right\} + i\frac{k_\rho^2}{k_{1z}^2} \cdot (1 - R^{TM})\tan(k_{1z}d/2)\, e^{-ik_{1z}d/2} \cdot \left\{1 + 2\frac{R^{TM}_{10}}{X^{TM}_{10}} e^{ik_{1z}d}\right\}\right] + \frac{1}{2i\omega\epsilon_1 I} \cdot \sum_{p,\gamma}\int_0^\infty dk_\rho \frac{k_\rho^2}{k_{1z}} J_0(k_\rho a)[\mathbb{K}\gamma_p(k_\rho)]_u \cdot (1 + R^{TM})\tan(k_{1z}d)\psi\gamma_p(c_0 k_\rho, u_0, v_0)$$

where

$$R^{TM}_{10} = \frac{\epsilon k_{1z} - \epsilon_1 k_z}{\epsilon k_{1z} + \epsilon_1 k_z}$$

$$X^{TM}_{10} = 1 + R^{TM}_{10}.$$

$[\mathbb{K}\gamma_p(k_\rho)]_u$ is the u-component of $\mathbb{K}\gamma_p(k_\rho)$ and is given by (14) and (16). In the limit of a thin substrate, and since the dominant modes are those of the TM polarization, the u-component of the current on the disk can thus be shown, from (14), (15) and the results of Appendix II, to be given approximately by

$$[\mathbb{K}\gamma_p(k_\rho)]_u = \pi\, c\gamma_p(k_\rho) J'\gamma_p(c_0 k_\rho, u_s) \cdot \sum_{r,s} a\gamma^{TM}_{rs} \frac{(k\bar{\gamma}^\epsilon_{rs})^2}{k_\rho^2 - (k\bar{\gamma}^\epsilon_{rs})^2} J\gamma_r(c_0 k\bar{\gamma}^\epsilon_{rs}, u_s) \cdot N\gamma_{rp}(c_0 k\bar{\gamma}^\epsilon_{rs}, c_0 k_\rho) \quad (24)$$

where $a\gamma^{TM}_{rs}$ are the TM current expansion coefficients. Under the single mode approximation (corresponding to the $TM_{\alpha nm}$ mode), we thus obtain

$$[\mathbb{K}\alpha_p(k_\rho)]_u = \pi\, c\alpha_p(k_\rho) J'\alpha_p(c_0 k_\rho, u_s) \cdot a\alpha^{TM}_{nm} \frac{(k\bar{\alpha}^\epsilon_{nm})^2}{k_\rho^2 - (k\bar{\alpha}^\epsilon_{nm})^2} J\alpha_n(c_0 k\bar{\alpha}^\epsilon_{nm}, u_s) \cdot N\alpha_{np}(c_0 k\bar{\alpha}^\epsilon_{nm}, c_0 k_\rho) \quad (25)$$

and hence the input impedance is given approximately by

$$Z_{in} = \frac{1}{4\pi\omega\epsilon_1}\int_0^\infty dk_\rho \frac{k_\rho}{k_{1z}} J_0^2(k_\rho a) \cdot \left[\frac{2}{ik_{1z}}\left\{\frac{2k_\rho^2 e^{ik_{1z}d/2}\sin(k_{1z}d/2)}{k_{1z}} - k_1^2 d\right\}\right. + i\frac{k_\rho^2}{k_{1z}^2}(1 - R^{TM})\tan(k_{1z}d/2)e^{ik_{1z}d/2}$$

$$\cdot \left\{1+2\frac{R_{10}^{TM}}{X_{10}^{TM}}e^{ik_{1z}d}\right\}\Bigg] + \frac{\pi}{2i\omega\epsilon_1 I}$$

$$\cdot a\alpha_{nm}^{TM} J\alpha_n(c_0 k\hat{\alpha}_{nm}^{\epsilon}, u_s)\int_0^{\infty} dk_\rho \frac{k_\rho^2}{k_{1z}} J_0(k_\rho a)(1+R^{TM})$$

$$\cdot \tan(k_{1z}d)\cdot \frac{(k\hat{\alpha}_{nm}^{\epsilon})^2}{k_\rho^2-(k\hat{\alpha}_{nm}^{\epsilon})^2}\sum_p c\alpha_p(k_\rho) J'\alpha_p(c_0 k_\rho, u_s)$$

$$\cdot N\alpha_{np}(c_0 k\hat{\alpha}_{nm}^{\epsilon}, c_0 k_\rho)\psi\alpha_p(c_0 k_\rho, u_0, v_0).$$

VI. Radiation Pattern

In this section, the far-field expression for the electric field in the thin substrate limit will be developed. In this case and because the structure approaches the magnetic wall cavity model (where the probe becomes almost shielded from the outside region), the contribution of the current on the probe to the radiation field is negligible compared to that of the currents induced on the disk.

From (1) and (4), the z-component of the electric field due to the current on the disk in the upper half-space is given by

$$E_z = \frac{1}{2i\omega\epsilon}\sum_{p,\gamma}\int_0^{\infty} dk_\rho k_\rho^2 [\mathbf{K}\gamma_p(k_\rho)]_u \cdot \psi\gamma_p(c_0 k_\rho, u, v)(1-R^{TM})e^{ik_z z}.$$

Under the single mode approximation (for the $TM_{\alpha nm}$ mode), $[\mathbf{K}\alpha_p(k_\rho)]_u$ is given by (25) and hence E_z is given by

$$E_z = \frac{\pi}{2i\omega\epsilon} a\alpha_{nm} J\alpha_n(c_0 k\hat{\alpha}_{nm}^{\epsilon}, u_s)\int_0^{\infty} dk_\rho k_\rho^2 \cdot \frac{(k\hat{\alpha}_{nm}^{\epsilon})^2}{k_\rho^2-(k\hat{\alpha}_{nm}^{\epsilon})^2}(1-R^{TM})e^{ik_z z} \cdot \sum_p c\alpha_p(k_\rho) N\alpha_{np}(c_0 k\hat{\alpha}_{nm}^{\epsilon}, c_0 k_\rho) \cdot J'\alpha_p(c_0 k_\rho, u_s) S\alpha_p(c_0 k_\rho, v) J\alpha_p(c_0 k_\rho, u).$$

It can be shown that the characteristic value b_n together with the expansion coefficients $D_m^n(c_0 k_\rho)$ and $F_m^n(c_0 k_\rho)$ of the Mathieu functions, defined in [13, appendix I], are even functions of k_ρ. Thus

$$J'\alpha_p(-c_0 k_\rho, u_s) = (-1)^p J'\alpha_p(c_0 k_\rho, u_s)$$

$$H\alpha_p^{(1)}(c_0 k_\rho e^{i\pi}, u) = -(-1)^p H\alpha_p^{(2)}(c_0 k_\rho, u)$$

and $N\alpha_{nm}(c_0 k\hat{\alpha}_{nm}^{\epsilon}, c_0 k_\rho)$, $S\alpha_p(c_0 k_\rho, v)$ are even in k_ρ, whereas $c\alpha_p(k_\rho)$ is odd in k_ρ. Hence, the integral along the positive real axis in the expression of E_z can be extended to an integral over the whole real axis, to get

$$E_z = \frac{\pi}{4i\omega\epsilon} a\alpha_{nm} J\alpha_n(c_0 k\hat{\alpha}_{nm}^{\epsilon}, u_s) \cdot \int_{-\infty}^{\infty} dk_\rho k_\rho^2 \frac{(k\hat{\alpha}_{nm}^{\epsilon})^2}{k_\rho^2-(k\hat{\alpha}_{nm}^{\epsilon})^2}(1-R^{TM})e^{ik_z z} \cdot \sum_p c\alpha_p(k_\rho) N\alpha_{np}(c_0 k\hat{\alpha}_{nm}^{\epsilon}, c_0 k_\rho) \cdot J'\alpha_p(c_0 k_\rho, u_s) S\alpha_p(c_0 k_\rho, v) H\alpha_p^{(1)}(c_0 k_\rho, u).$$

In the far field, it can be shown that $c_0 \cosh(u) \to \rho$ and that the asymptotic expansion of $H\alpha_p^{(1)}(c_0 k_\rho, u)$ is thus given by

$$H\alpha_p^{(1)}(c_0 k_\rho, u) \sim L\alpha_p(c_0 k_\rho)\frac{1}{\sqrt{k_\rho \rho}} \cdot \exp\left\{i\left(k_\rho \rho - \frac{2p+1}{4}\pi\right)\right\} \sim \sqrt{\frac{\pi}{2}}(-1)^p L\alpha_p(c_0 k_\rho) H_0^{(1)}(k_\rho \rho)$$

where

$$Le_p(c_0 k_\rho) = Se_p(c_0 k_\rho, 0)$$

and

$$Lo_p(c_0 k_\rho) = S'o_p(c_0 k_\rho, 0).$$

Thus, in the far field, i.e., for large values of ρ and z, the integrand is rapidly oscillating and the integral can hence be evaluated using the method of stationary phase. A stationary point exists at $k_\rho = k \sin(\theta)$, where $\theta = \tan^{-1}(\rho/z)$. Thus, we get

$$E_z \sim -\frac{\pi}{4i\omega\epsilon}\sqrt{\frac{\pi}{2}} a\alpha_{nm}^{TM} k^2 \sin(\theta)\cos(\theta) \cdot \frac{(k\hat{\alpha}_{nm}^{\epsilon})^2}{(k\hat{\alpha}_{nm}^{\epsilon})^2 - k^2\sin^2(\theta)} J\alpha_n(c_0 k\hat{\alpha}_{nm}^{\epsilon}, u_s) \cdot [1-R^{TM}(k_\rho = k\sin\theta)] \sum_p (-1)^p c\alpha_p(k\sin\theta) \cdot L\alpha_p(c_0 k\sin\theta) N\alpha_{np}(c_0 k\hat{\alpha}_{nm}^{\epsilon}, c_0 k\sin\theta) \cdot J'\alpha_p(c_0 k\sin\theta, u_s) S\alpha_p(c_0 k\sin\theta, \phi) \cdot \int_{-\infty}^{\infty} dk_\rho \frac{k_\rho}{k_z} e^{ik_z z} H_0^{(1)}(k_\rho \rho).$$

Using Sommerfeld's identity [14], we finally obtain

$$E_z \sim \frac{\pi}{2\omega\epsilon}\sqrt{\frac{\pi}{2}} a\alpha_{nm}^{TM} k^2 \sin(\theta)\cos(\theta) \cdot \frac{(k\hat{\alpha}_{nm}^{\epsilon})^2}{(k\hat{\alpha}_{nm}^{\epsilon})^2 - k^2\sin^2(\theta)} J\alpha_n(c_0 k\hat{\alpha}_{nm}^{\epsilon}, u_s) \cdot [1-R^{TM}(k_\rho = k\sin\theta)]\frac{e^{ikr}}{r}\sum_p (-1)^p c\alpha_p(k\sin\theta) \cdot L\alpha_p(c_0 k\sin\theta) N\alpha_{np}(c_0 k\hat{\alpha}_{nm}^{\epsilon}, c_0 k\sin\theta) \cdot J'\alpha_p(c_0 k\sin\theta, u_s) S\alpha_p(c_0 k\sin\theta, \phi)$$

where

$$r = \sqrt{\rho^2 + z^2}$$

and in the far field $v \sim \phi$. Similarly, the expression for H_z in the far field is given by

$$H_z \sim -\frac{\pi}{2}\sqrt{\frac{\pi}{2}}\, a\alpha_{nm}^{TM} k \sin(\theta) J\alpha_n(c_0 k\hat{\alpha}_{nm}, u_s) \cdot [1 + R^{TE}(k_\rho = k\sin\theta)]\frac{e^{ikr}}{r} \cdot \sum_p (-1)^p c\bar{\alpha}_p(k\sin\theta) \cdot L\bar{\alpha}_p(c_0 k\sin\theta) Q\alpha_{np}(c_0 k\hat{\alpha}_{nm}, c_0 k\sin\theta) \cdot J\bar{\alpha}_p(c_0 k\sin\theta, u_s) S\bar{\alpha}_p(c_0 k\sin\theta, \phi)$$

where $\bar{\alpha} = e$ (even) if $\alpha = o$ (odd) and $\bar{\alpha} = o$ (odd) if $\alpha = e$ (even). Finally, the θ- and ϕ-components of the electric field are given by

$$E_\theta = -E_z/\sin(\theta), \text{ and } E_\phi = -\sqrt{\mu_0/\epsilon}\, H_z/\sin(\theta).$$

VII. Conclusion

The scalar and vector Mathieu transforms, developed in [13], allow the rigorous formulation of the elliptic disk microstrip antenna which has long been thought almost impossible to formulate exactly [6].

It is shown that the current distribution on the disk is rigorously derived using these transforms and that it is governed by vector integral equations. These vector integral equations are then solved using Galerkin's method in which the current distribution on the disk is expanded in terms of the TM and TE current modes of the magnetic wall cavity model, which form a complete set of basis functions. The limit of small substrate thickness is then applied to these equations to get simple approximate expressions for the current amplitudes.

The resonance in the elliptic disk structure is then analyzed using two different approaches: Galerkin's method and a perturbative approach. The input impedance together with the radiation pattern are derived both exactly and in the small substrate thickness limit.

Appendix I

Field Expressions Due to Probe Excitation

First, we will develop field expressions due to the probe excitation in the unbounded medium. In the next part of the appendix, we will then generalize the expressions to include the effect of stratification. The electric field $\mathbf{E}$ is governed by the following differential equation

$$\nabla\times\nabla\times\mathbf{E}(u, v, z) - k^2\mathbf{E}(u, v, z) = i\omega\mu_0\mathbf{J}(u, v, z)$$

where $\mathbf{J}(u, v, z)$ is the current distribution on the probe. We will represent the solution of this equation in terms of the dyadic Green's function in the elliptic coordinate system, which has the following form

$$\bar{\mathbf{G}}(\mathbf{r}, \mathbf{r}') = \left(\bar{\mathbf{I}} + \frac{1}{k^2}\nabla\nabla\right) g(\mathbf{r}, \mathbf{r}')$$

and $g(\mathbf{r}, \mathbf{r}')$ is the solution of the following differential equation

$$(\nabla^2 + k^2) g(\mathbf{r}, \mathbf{r}') = -\frac{1}{h^2}\delta(u-u')\delta(v-v')\delta(z-z').$$

From the results of [13], $g(\mathbf{r}, \mathbf{r}')$ can be expanded in terms of the scalar elliptic harmonics as follows:

$$g(\mathbf{r}, \mathbf{r}') = \frac{i}{2}\sum_{n,\alpha}\int_0^\infty dk_\rho \frac{k_\rho}{k_z} w\alpha_n(k_\rho)\psi\alpha_n(c_0 k_\rho, u', v') \cdot \psi\alpha_n(c_0 k_\rho, u, v) e^{ik_z|z-z'|}$$

and hence the electric field is given by

$$\mathbf{E}(u, v, z) = -\frac{1}{2\omega\epsilon}\sum_{n,\alpha}(\bar{\mathbf{I}}k^2 + \nabla\nabla)\int_{V_p} dr'\mathbf{J}(\mathbf{r}')\int_0^\infty dk_\rho \cdot \frac{k_\rho}{k_z} w\alpha_n(k_\rho)\psi\alpha_n(c_0 k_\rho, u', v')\psi\alpha_n(c_0 k_\rho, u, v) e^{ik_z|z-z'|}$$

where V_p is the volume of the probe. Thus,

$$\mathbf{E}(u, v, z) = -\frac{1}{2\omega\epsilon}\sum_{n,\alpha}\left(\hat{z}k^2 + \nabla\frac{\partial}{\partial z}\right)\int_0^\infty dk_\rho \frac{k_\rho}{k_z} J_0(k_\rho a) \cdot w\alpha_n(k_\rho)\psi\alpha_n(c_0 k_\rho, u_0, v_0))\psi\alpha_n(c_0 k_\rho, u, v) f(k_\rho, z)$$

where $f(k_\rho, z)$ is given by [12]

$$f(k_\rho, z) = \int_{-d}^{0} dz' e^{ik_z|z-z'|} = \begin{cases} \dfrac{2}{ik_z}\left[e^{ik_z d/2}\cos\{k_z(z+d/2)\} - 1\right], & -d < z < 0 \\ \dfrac{2}{k_z} e^{ik_z|z+d/2|}\sin(k_z d/2), & 0 < z < -d. \end{cases}$$

Thus, in the case of the structure considered in Fig. 1 and by applying the stratified medium formulation [14], the z-component of the electric field in the air region and the substrate is given as follows [12].

In the air region ($z > 0$):

$$E_z^P(u, v, z) = -\frac{iI}{2\omega\epsilon}\sum_{n,\alpha}\int_0^\infty dk_\rho \frac{k_\rho^3}{k_{1z}^2} J_0(k_\rho a) w\alpha_n(k_\rho) \cdot (1 - R^{TM})\psi\alpha_n(c_0 k_\rho, u_0, v_0)\psi\alpha_n(c_0 k_\rho, u, v) e^{ik_z z}. \quad (26a)$$

In the substrate ($-d < z < 0$):

$$E_{1z}^P(u, v, z) = \frac{iI}{\omega\epsilon_1}\sum_{n,\alpha}\int_0^\infty dk_\rho \frac{k_\rho}{k_{1z}^2} J_0(k_\rho a) w\alpha_n(k_\rho) \cdot \psi\alpha_n(c_0 k_\rho, u_0, v_0)\psi\alpha_n(c_0 k_\rho, u, v)$$

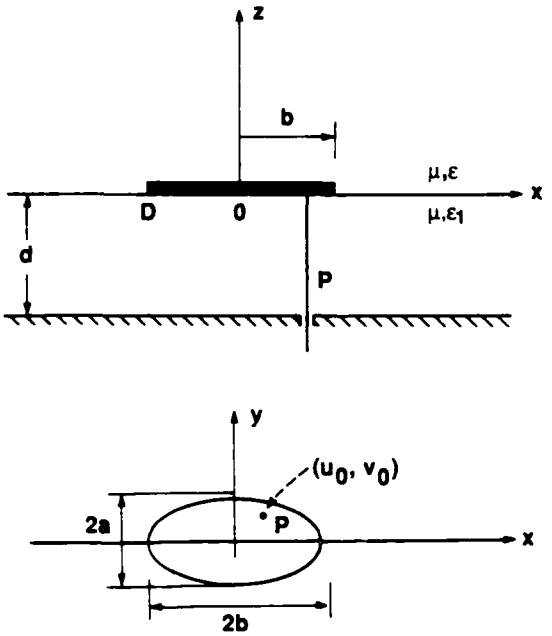

Fig. 1. Geometrical configuration of the elliptic disk excited by a probe.

$$\cdot \left\{ k_\rho^2 e^{ik_{1z}d/2} \cos\{k_{1z}(z+d/2)\} - k_1^2 + \frac{ik_\rho^2 \sin(k_{1z}d/2) e^{ik_{1z}d/2}}{(1 - R_{10}^{TM} e^{i2k_{1z}d})} \cdot [(1 + R_{10}^{TM} e^{ik_{1z}d}) \cdot e^{ik_{1z}(z+d/2)} + (1 + e^{ik_{1z}d}) R_{10}^{TM} e^{-ik_{1z}(z+d/2)}] \right\} \quad (26b)$$

where R^{TM} and R_{10}^{TM} are given in Sections II and V, respectively. At $z = 0$, the transverse component of the electric field is given by

$$\mathbf{E}_s^P(u, v) = \begin{bmatrix} E_u^P(u, v) \\ E_v^P(u, v) \end{bmatrix} = \sum_{n,\alpha} \int_0^\infty dk_\rho \tilde{\mathbf{M}}\alpha_n(c_0 k_\rho, u, v) \cdot \mathbf{T}\alpha_n(k_\rho) \quad (27)$$

where

$$\mathbf{T}\alpha_n(k_\rho) = \begin{bmatrix} P\alpha_n(k_\rho) \\ 0 \end{bmatrix}$$

and

$$P\alpha_n(k_\rho) = \frac{I}{2\omega\epsilon} \frac{k_z}{k_{1z}^2} k_\rho J_0(k_\rho a) w\alpha_n(k_\rho) \cdot (1 - R^{TM}) \psi\alpha_n(c_0 k_\rho, u_0, v_0).$$

Appendix II

Evaluation of $I_1 = \int_0^{2\pi} dv' \int_0^u du' h^2 \psi\alpha_n(c_0 k_\rho, u', v') \cdot \psi\beta_r(c_0 k_\rho', u', v')$: $\psi\alpha_n(c_0 k_\rho, u', v')$ and $\psi\beta_r(c_0 k_\rho', u', v')$ are governed by the following:

$$\frac{\partial^2}{\partial u'^2} \psi\alpha_n + \frac{\partial^2}{\partial v'^2} \psi\alpha_n + h^2 k_\rho^2 \psi\alpha_n = 0 \quad (28)$$

$$\frac{\partial^2}{\partial u'^2} \psi\beta_r + \frac{\partial^2}{\partial v'^2} \psi\beta_r + h^2 k_\rho'^2 \psi\beta_r = 0. \quad (29)$$

Multiplying (28) by $\psi\beta_r$ and (29) by $\psi\alpha_n$ and subtracting, we get

$$\frac{\partial}{\partial u'} \left[\psi\alpha_n \frac{\partial}{\partial u'} \psi\beta_r - \psi\beta_r \frac{\partial}{\partial u'} \psi\alpha_n \right] + \frac{\partial}{\partial v'} \left[\psi\alpha_n \frac{\partial}{\partial v'} \psi\beta_r - \psi\beta_r \frac{\partial}{\partial v'} \psi\alpha_n \right] + h^2 (k_\rho'^2 - k_\rho^2) \psi\alpha_n \psi\beta_r = 0.$$

Integrating over u' from 0 to u and over v' from 2 to 2π. Using the periodicity property of the angular functions together with the fact that $J'\gamma_m(c_0 k_\rho, 0) = 0$ and finally employing the orthogonality relationship of the sine and cosine functions, we get

$$I_1 = \frac{\pi}{k_\rho^2 - k_\rho'^2} [J\alpha_n(c_0 k_\rho, u) J'\alpha_r(c_0 k_\rho', u) - J'_{\alpha_n}(c_0 k_\rho, u) J\alpha_r(c_0 k_\rho', u)] N\alpha_{nr}(c_0 k_\rho, c_0 k_\rho') \delta_{\alpha\beta}$$

provided that $k_\rho \neq k_\rho'$ and both n and r have to be even or odd (I_1 vanishes if n and r are of different parity). $N\alpha_{nr}(c_0 k_\rho, c_0 k_\rho')$ is defined as follows:

$$N\alpha_{nr}(c_0 k_\rho, c_0 k_\rho') = \frac{1}{\pi} \int_0^{2\pi} dv\, S\alpha_n(c_0 k_\rho, v) S\alpha_r(c_0 k_\rho', v)$$

hence,

$$Ne_{nr}(c_0k_\rho, c_0k'_\rho) = \sum_m{}' (1+\delta_{m0}) D^n_m(c_0k_\rho) D'^r_m(c_0k'_\rho)$$

$$No_{nr}(c_0k_\rho, c_0k'_\rho) = \sum_m{}' F^n_m(c_0k_\rho) F'^r_m(c_0k'_\rho).$$

If $k'_\rho \to k_\rho$, the following two cases have to be considered.

Case (i): $r \neq n$: In this case and as $k'_\rho \to k_\rho$, the quantity between the square brackets in the expression for I_1 has a nonvanishing value whereas $N\alpha_{nr}(c_0k_\rho, c_0k'_\rho)$ vanishes (see [13, eq. (4)]). Applying L'Hopital's rule, we obtain

$$I_1 = -\frac{\pi}{2k_\rho}\left[J\alpha_n(c_0k_\rho, u) J'\alpha_r(c_0k_\rho, u) - J'\alpha_n(c_0k_\rho, u) J\alpha_r(c_0k_\rho, u)\right] \cdot \left[\frac{\partial}{\partial k'_\rho} N\alpha_{nr}(c_0k_\rho, c_0k'_\rho)\right]_{k'_\rho = k_\rho} \delta_{\alpha\beta}.$$

Case (ii): $r = n$: In this case and in the limit when $k'_\rho \to k_\rho$, $N\alpha_{nn}(c_0k_\rho, c_0k'_\rho) \to R\alpha_n(c_0k_\rho)$ (see [13, eq. (3)]) whereas the quantity between the square brackets vanishes and hence, we get

$$I_1 = -\frac{\pi}{2k_\rho}\left\{J\alpha_n(c_0k_\rho, u)\left[\frac{\partial}{\partial k'_\rho} J'\alpha_n(c_0k'_\rho, u)\right]_{k'_\rho = k_\rho} - J'\alpha_n(c_0k_\rho, u)\left[\frac{\partial}{\partial k'_\rho} J\alpha_n(c_0k'_\rho, u)\right]_{k'_\rho = k_\rho}\right\} \cdot R\alpha_n(c_0k_\rho)\delta_{\alpha\beta}.$$

Evaluation of $I_2 = \int_0^u du' \int_0^{2\pi} dv' [\partial/\partial u' \psi\alpha_n(c_0k_\rho, u', v') \partial/\partial u' \psi\beta_r(c_0k'_\rho, u', v') - \partial/\partial v' \psi\alpha_n(c_0k_\rho, u', v') \partial/\partial v' \psi\beta_r(c_0k'_\rho, u', v')]$. Using integration by parts, two alternative forms for I_2 can be obtained. The first is

$$I_2 = \pi J'\alpha_n(c_0k_\rho, u) J\alpha_r(c_0k'_\rho, u) \cdot N\alpha_{nr}(c_0k_\rho, c_0k'_\rho)\delta_{\alpha\beta} + k_\rho^2 I_1$$

and the second is

$$I_2 = \pi J\alpha_n(c_0k_\rho, u) J'\alpha_r(c_0k'_\rho, u) \cdot N\alpha_{nr}(c_0k_\rho, c_0k'_\rho)\delta_{\alpha\beta} + k_\rho'^2 I_1.$$

n and r have to be of the same parity (I_2 vanishes if they are of opposite parity).

Evaluation of $I_3 = \int_0^u du' \int_0^{2\pi} dv' [\partial/\partial u' \psi\alpha_n(c_0k_\rho, u', v') \partial/\partial v' \psi\beta_r(c_0k'_\rho, u', v') + \partial/\partial v' \psi\alpha_n(c_0k_\rho, u', v') \partial/\partial u' \psi\beta_r(c_0k'_\rho, u', v')]$. Using integration by parts, it can be shown that I_3 is given by

$$I_3 = -\pi J\alpha_n(c_0k_\rho, u) J\tilde{\alpha}_r(c_0k'_\rho, u) Q\alpha_{nr}(c_0k_\rho, c_0k'_\rho)\delta_{\alpha\beta}$$

where $\tilde{\beta} = e$ (even), if $\beta = o$ (odd) and $\tilde{\beta} = o$ (odd), if $\beta = e$ (even), and

$$Q\alpha_{nr}(c_0k_\rho, c_0k'_\rho) = \frac{1}{\pi}\int_0^{2\pi} dv S'\alpha_n(c_0k_\rho, v) S\tilde{\alpha}_r(c_0k'_\rho, v)$$

hence,

$$Qe_{nr}(c_0k_\rho, c_0k'_\rho) = -\sum_m m D^n_m(c_0k_\rho) F'^r_m(c_0k'_\rho)$$

$$Qo_{nr}(c_0k_\rho, c_0k'_\rho) = \sum_m{}' m F^n_m(c_0k_\rho) D'^r_m(c_0k'_\rho)$$

with n and r of the same parity (i.e., both n and r have to be either even or odd).

References

[1] S. A. Long, L. C. Shen, D. H. Schaubert, and F. G. Farrar, "An experimental study of the circular-polarized elliptical printed-circuit antenna," *IEEE Trans. Antennas Propagat.*, vol. AP-29, pp. 95–99, 1981.

[2] S. A. Long and M. W. McAllister, "The impedance of an elliptical printed-circuit antenna," *IEEE Trans. Antennas Propagat.*, vol. AP-30, pp. 1197–1200, 1982.

[3] L. C. Shen, "The elliptical microstrip antenna with circular polarization," *IEEE Trans. Antennas Propagat.*, vol. AP-29, pp. 90–94, 1981.

[4] A. K. Sharma and B. Bhat, "Spectral domain analysis of elliptic microstrip disk resonators," *IEEE Trans. Microwave Theory Tech.*, vol. MTT-28, pp. 573–576, 1980.

[5] R. T. Irish, "Elliptic resonator and its use in microstrip systems," *Electron. Lett.*, vol. 7, no. 7, pp. 149–150, 1971.

[6] J. G. Kretzschmar, "Theoretical results for the elliptic microstrip resonator," *IEEE Trans. Microwave Theory Tech.*, vol. MTT-20, pp. 342–343, 1972.

[7] T. M. Habashy, S. M. Ali, and J. A. Kong, "Impedance parameters and radiation pattern of two coupled circular microstrip disk antennas," *J. Appl. Phys.*, vol. 54, pp. 493–506, 1983.

[8] S. M. Ali, T. M. Habashy, and J. A. Kong, "Resonance in two coupled circular microstrip disk resonators," *J. Appl. Phys.*, vol. 53, pp. 6418–6429, 1982.

[9] T. M. Habashy and J. A. Kong, "Coupling between two circular microstrip disk resonators," *Electromagn.*, vol. 3, pp. 347–370, 1983.

[10] W. C. Chew and J. A. Kong, "Resonance of the axial-symmetric modes in microstrip disk resonators," *J. Math. Phys.*, vol. 21, pp. 582–591, 1980.

[11] ——, "Resonance of nonaxial symmetric modes in circular microstrip disk antenna," *J. Math. Phys.*, vol. 21, pp. 2590–2598, 1980.

[12] ——, "Analysis of a circular microstrip disk antenna with a thick dielectric substrate," *IEEE Trans. Antennas Propagat.*, vol. AP-29, pp. 68–76, 1981.

[13] T. M. Habashy, J. A. Kong, and W. C. Chew, "Scalar and vector Mathieu transform pairs," *J. Appl. Phys.*, vol. 60, pp. 3395–3400, 1986.

[14] J. A. Kong, *Electromagnetic Wave Theory*. New York: Wiley, 1985.

[15] R. F. Harrington, *Time-Harmonic Electromagnetic Fields*. New York: McGraw-Hill, 1961, pp. 319.

[16] M. L. Weeks, *Antenna Engineering*. New York: McGraw-Hill, 1968, pp. 153–155.

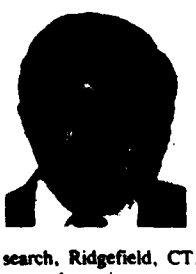

Tarek M. Habashy (S'79–M'83) was born in Cairo, Egypt. He received the B.Sc. degree with honors from Cairo University, Cairo, Egypt, and the M.Sc. and Ph.D. degrees from Massachusetts Institute of Technology, Cambridge, in 1976, 1980, and 1983, respectively, all in electrical engineering.

During the academic year 1982–1983, he had a postdoctoral appointment in the Department of Electrical Engineering and Computer Science, Massachusetts Institute of Technology. Since September 1983, he has been with Schlumberger-Doll Research, Ridgefield, CT, as a member of the professional staff conducting research on inverse scattering problems and electromagnetic well-logging techniques. He is currently the program leader of the Dielectric Logging Program.

Dr. Habashy received the Carlton E. Tucker award of the Massachusetts Institute of Technology in 1982 for outstanding teaching performance by graduate students in the Department of Electrical Engineering and Computer Science. He is currently serving as a member of the international editorial advisory board of the new *Journal of Electromagnetic Waves and Applications* (JEWA). He is a member of AGU, AAAS, Sigma Xi, the New York Academy of Sciences and U.S. Commission B of the International Union of Radio Science.

Jin Au Kong (S'65-M'69-SM'74-F'85) is Professor of Electrical Engineering and Chairman of Area IV on Energy and Electromagnetic Systems in the Department of Electrical Engineering and Computer Science at the Massachusetts Institute of Technology, Cambridge. In 1977-1980 he served the United Nations as a high-level Consultant to the Undersecretary-General on science and technology, and as an Interregional Advisor on remote sensing technology for the Department of Technical Cooperation for Development. His research interest is in the area of electromagnetic wave theory and applications. He has published five books and over 200 refereed journal articles and conference papers. He is the Editor-in-Chief of the *Journal of Electromagnetic Waves and Applications*, and the Editor of the Wiley Series in Remote Sensing.

Weng Cho Chew (S'79-M'80-SM'86) was born in Malaysia. He received the B.S. degree in 1976, the M.S. and Engineer's degrees in 1978, and the Ph.D. degree in 1980, all in electrical engineering from the Massuchusetts Institute of Technology, Cambridge.

His research interest has been in the area of wave propagation and interaction with heterogeneous media for geophysical subsurface sensing, microwave and millimeter wave applications, mixed boundary value problems for microwave integrated circuits and microstrip antenna applications. He has also studied electrochemical and dielectric properties of rocks. From 1981 to 1985, he was with Schlumberger-Doll Research in Ridgefield, CT. While he was there, he was a program leader and department manager. Currently, he is an Associate Professor with the Department of Electrical and Computer Engineering, University of Illinois.

Dr. Chew is a member of Eta Kappa Nu, Tau Beta Pi, the International Union of Radio Science, and an active member of the Society of Exploration Geophysics. He is an NSF Presidential Young Investigator for 1986. He is an Associate Editor and AdCom member of the IEEE Geoscience and Remote Sensing Society, and was a Guest Editor of *Radio Science*.

Journal of Electromagnetic Waves and Applications, Vol. 1, No. 2, 133–158, 1987

Transient Response of a Vertical Electric Dipole (VED) On a Two-Layer Medium

S. Y. Poh and J. A. Kong

Research Laboratory of Electronics
Department of Electrical Engineering and Computer Science
Massachusetts Institute of Technology
Cambridge, MA 02139, USA

Abstract– The transient electromagnetic radiation by a vertical electric dipole on a two-layer medium is analysed using the double deformation technique, which is a modal technique based on identification of singularities in the complex frequency and wavenumber planes. Previous application of the double deformation technique to the solution of this problem is incomplete in the early time response. In this paper we show that the existence of a pole locus on the negative imaginary frequency axis, which dominates the early time response, proves crucial in obtaining the solution for all times. A variety of combinations of parameters are used to illustrate the double deformation technique, and results will be compared with those obtained via explicit inversion, and a single deformation method.

I. INTRODUCTION

The time response of a VED over a two-layer nondispersive dielectric was analyzed by Ezzeddine *et al.* [1] employing the geometrical optics approach for early arrivals, together with an explicit inversion scheme, analogous to the Cagniard-de Hoop method [2,3], that is valid for all times. The solution is expressible as single integrals. As the latter technique is inapplicable for problems involving dispersive media, Ezzeddine *et al.* [4] further analyzed the pulse response of a VED over a two-layer medium by applying the *double deformation technique* [5] which involves complex plane deformation in both the wavenumber and frequency planes. The resulting solution, although numerical in nature, does not require excessive computation, and may be readily extended to consider dispersive media. The results as presented in [4], however, lacked completeness insofar as the early time solutions for both lossless and dissipative media are concerned.

In this paper, we seek to *resolve* the problem encountered by Ezzeddine *et al.* [4] in the early time response for the radiation of a VED on a two-layer medium. The existence of an additional pole locus on the negative imaginary frequency axis proves crucial in improving the early time response. The analysis presented is valid for both non-dispersive and dispersive media. However, the emphasis in the presented results is on non-dispersive media since much of the effort and motivation is to *complete* an initial picture regarding the double deformation approach. Some variety in the choice of parameters is used to illustrate the double defor-

mation technique, and results will be compared with those obtained via explicit inversion, and a single, wavenumber plane, deformation approach.

II. FORMULATION

The geometrical configuration to be considered [Fig. 1] comprises a vertical electric dipole (VED) located at the origin on the surface of a two-layer medium and the observation point a distance ρ away, on the same horizontal plane. The dipole is assumed to be excited by a current pulse which is zero for $t < 0$ and a damped sinusoid for $t > 0$, e.g.

$$i(t) = I_o t^n \sin\omega_0 t\, e^{-\alpha_0 t}\, u_{-1}(t) \qquad \text{for } n = 0, 1, 2, \ldots \tag{1}$$

where $u_{-1}(t)$ is the unit step function. This choice of function allows us to simulate a variety of waveforms by varying the values of ω_0 and α_0. The corresponding Fourier transform is given by

$$I(k_o) = \frac{i^n}{2n!} I_o \left[\frac{1}{\left(k_o + \frac{\omega_0}{c} + i\frac{\alpha_0}{c}\right)^{n+1}} - \frac{1}{\left(k_o - \frac{\omega_0}{c} + i\frac{\alpha_0}{c}\right)^{n+1}} \right] \tag{2}$$

where $k_o = \omega/c$ and c is the speed of light in free space.

The upper half-space medium is assumed to be free space with permittivity ϵ_o and permeability μ_o. Using cylindrical coordinates ρ, ϕ, and z, the time-harmonic response for the magnetic field at a point, (ρ, ϕ, z), in the upper half space is given by [6]

$$\overline{H} = \hat{\phi} H_\phi(\omega) = \frac{iI(\omega)l}{8\pi} \int_{\text{SIP}} dk_\rho \frac{k_\rho^2}{k_{oz}} H_1^{(1)}(k_\rho \rho) \left[1 + R^{\text{TM}}\right] e^{ik_{oz}z} \tag{3}$$

where

$$R^{\text{TM}} = \frac{R_{01} + R_{12} e^{i2k_{1z}d}}{1 + R_{01} R_{12} e^{i2k_{1z}d}} \tag{4}$$

$$R_{01} = \frac{\underline{\epsilon}_{r1} k_{oz} - k_{1z}}{\underline{\epsilon}_{r1} k_{oz} + k_{1z}}$$

$$R_{12} = \frac{\underline{\epsilon}_{r2} k_{1z} - \underline{\epsilon}_{r1} k_{2z}}{\underline{\epsilon}_{r2} k_{1z} + \underline{\epsilon}_{r1} k_{2z}}$$

$$k_{oz}^2 + k_\rho^2 = k_o^2 = \omega^2 \mu_o \epsilon_o$$

$$k_{1z}^2 + k_\rho^2 = \underline{k}_1^2 = \omega^2 \mu_o \underline{\epsilon}_{r1} \epsilon_o = \underline{\epsilon}_{r1} k_o^2$$

$$k_{2z}^2 + k_\rho^2 = \underline{k}_2^2 = \omega^2 \mu_o \underline{\epsilon}_{r2} \epsilon_o = \underline{\epsilon}_{r2} k_o^2$$

and SIP is the Sommerfeld integration path. For the configuration of interest [Fig. 1], $z = 0$.

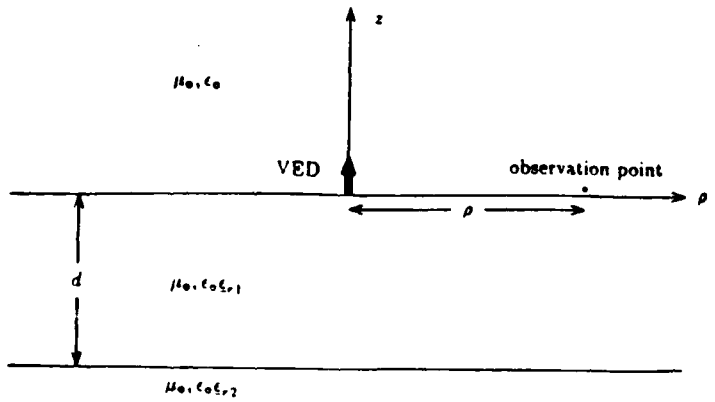

Figure 1. Geometrical configuration of the problem.

In the time domain, the magnetic field may be expressed as the inverse Fourier transform

$$H_\phi(t) = \frac{1}{\pi} Re \left\{ \int_0^\infty d\omega \, e^{-i\omega t} H_\phi(\omega) \right\}$$

The evaluation of the resulting double integral is difficult both analytically and numerically [7–8]. In the double deformation method [5], the paths of integration are deformed to the steepest descent paths (SDPs) in both the k_ρ and ω planes. The double integral corresponding to the transient magnetic field is then reduced to single integrals associated with the contributions of singularities enclosed in the path deformations and double integrals along the steepest descent paths in the k_ρ and ω planes.

III. DEFORMATION IN THE k_ρ PLANE

For the integrand in the k_ρ plane, we find two branch points at $k_\rho = k_o$ and $k_\rho = \underline{k}_2$. There is no branch point at $k_\rho = \underline{k}_1$, corresponding to $k_{1z} = 0$, since the integrand in (3) is even in k_{1z}. We first deform the original, Sommerfeld path of integration (SIP) in the k_ρ plane to the vertical steepest descent paths, SDP1 and SDP2 [Fig. 2] about the branch points at k_o and $\underline{k}_2$ respectively. The branch cuts as shown in Fig. 2 are chosen such that k_{oz} and k_{2z} have positive real parts on their respective upper Riemann sheets, on which SIP is defined, and negative real parts on their lower sheets. In the process of deformation, we find that the deformed path traverses *three*, namely the sheets corresponding to upper sheet for both k_{oz} and k_{2z} (UU), lower sheet for k_{oz} and upper for k_{2z} (LU) and lower sheet for both k_{oz} and k_{2z} (LL), of the *four possible* sheets. In our analysis, we choose to fix the real part of k_{oz} and of k_{2z} as positive regardless of Riemann sheet but apply the appropriate signs explicitly in the integrand instead.

In other words, from (4), on the Riemann sheet denoted by (UU),

$$R_{UU}^{\mathrm{TM}} = \frac{R_{01} + R_{12}e^{i2k_{1z}d}}{1 + R_{01}R_{12}e^{i2k_{1z}d}} = R^{\mathrm{TM}} \qquad Re(k_{oz}),\ Re(k_{2z}) \geq 0 \qquad (5)$$

while on the sheet (LU),

$$R_{LU}^{\mathrm{TM}} = \frac{1 - R_{01}R_{12}e^{i2k_{1z}d}}{R_{01} - R_{12}e^{i2k_{1z}d}} = 1/R^{\mathrm{TM}} \qquad Re(k_{oz}),\ Re(k_{2z}) \geq 0 \qquad (6)$$

since

$$R_{01}\Big|_{k_{oz}=-k_{oz}} = 1/R_{01}$$

On the sheet (LL),

$$R_{LL}^{\mathrm{TM}} = \frac{R_{12} - R_{01}e^{i2k_{1z}d}}{R_{01}R_{12} - e^{i2k_{1z}d}} \qquad Re(k_{oz}),\ Re(k_{2z}) \geq 0 \qquad (7)$$

because

$$R_{12}\Big|_{k_{2z}=-k_{2z}} = 1/R_{12}$$

In the k_ρ plane, pole singularities may also be present, on the traversed Riemann sheets, as zeros of the denominators of the reflection coefficients in (5)–(7). The positions of these poles vary as a function of frequency ω.

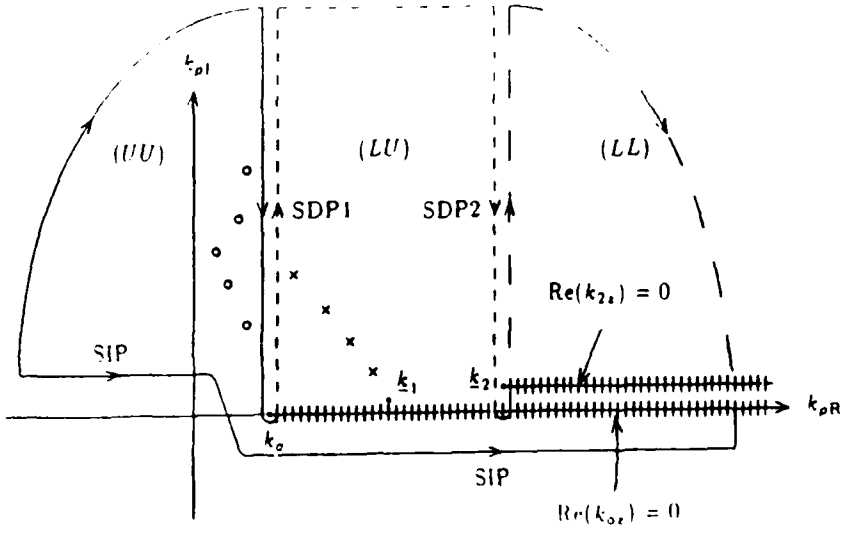

Figure 2. Original and deformed integration paths in k_ρ plane with enclosed poles.
o : pole intercepted on the sheet $Re(k_{oz}) \geq 0$, $Re(k_{2z}) \geq 0$.
$\times$: pole intercepted on the sheet $Re(k_{oz}) < 0$, $Re(k_{2z}) \geq 0$.
No poles intercepted on the sheet $Re(k_{oz}) < 0$, $Re(k_{2z}) < 0$.

At this point, the original k_ρ integral is replaced by contributions from any intercepted singularities, the integration over the semi-circular arc and the integrations along the vertical paths SDP1 and SDP2.

By Jordan's lemma, the integration over the semi-circular path evaluates to zero. We note that along SDP1, $k_\rho = k_o + iq$, where $q \geq 0$ and the contribution to the time-domain magnetic field is given by

$$H_{\phi SDP1}(\tau) = \frac{I_o l}{8\pi^2} Re \left\{ \int_0^\infty dk_o\, e^{-ik_o\tau} I(k_o) \int_0^\infty dq\, \frac{(k_o+iq)^2}{\sqrt{k_o^2-(k_o+iq)^2}} \cdot H_1^{(1)}((k_o+iq)\rho) \left[2 + R_{UU}^{\mathrm{TM}} + R_{LU}^{\mathrm{TM}}\right]_{k_\rho = k_o+iq} \right\} \tag{8}$$

and along SDP2, $k_\rho = \underline{k}_2 + iq$, $q \geq 0$,

$$H_{\phi SDP2}(\tau) = \frac{I_o l}{8\pi^2} Re \left\{ \int_0^\infty dk_o\, e^{-ik_o\tau} I(k_o) \int_0^\infty dq\, \frac{(\underline{k}_2+iq)^2}{\sqrt{k_o^2-(\underline{k}_2+iq)^2}} \cdot H_1^{(1)}((\underline{k}_2+iq)\rho) \left[-R_{LU}^{\mathrm{TM}} + R_{LL}^{\mathrm{TM}}\right]_{k_\rho = \underline{k}_2+iq} \right\} \tag{9}$$

where we have performed the normalization $k_o = \omega/c$, $\tau = ct$ and $I(\omega) = I_o I(k_o)/c$, and where the square roots are defined as having positive real parts.

Therefore after deformation in the k_ρ plane the total magnetic field $H_\phi(\tau)$ is given by

$$H_\phi(\tau) = H_{\phi SDP1}(\tau) + H_{\phi SDP2}(\tau) + \sum_M H_{\phi MUU}(\tau) + \sum_M H_{\phi MLU}(\tau) + \sum_M H_{\phi MLL}(\tau) \tag{10}$$

where $H_{\phi SDP1}(\tau)$ and $H_{\phi SDP2}(\tau)$ are the contributions from the steepest descent path integrals and $H_{\phi MUU}(\tau)$, $H_{\phi MLU}(\tau)$ and $H_{\phi MLL}(\tau)$ are the contributions from the intercepted poles in the deformation through the three Riemann surfaces.

To obtain the contributions from the intercepted poles, we have to first determine their positions in the complex k_ρ plane as a function of frequency k_o. We first write

$$R_{UU}^{\mathrm{TM}} = \frac{f_t^{\mathrm{M}}(k_\rho, k_o)}{g_t^{\mathrm{M}}(k_\rho, k_o)} \tag{11a}$$

$$R_{LU}^{\mathrm{TM}} = \frac{g_t^{\mathrm{M}}(k_\rho, k_o)}{f_t^{\mathrm{M}}(k_\rho, k_o)} \tag{11b}$$

$$R_{LL}^{\mathrm{TM}} = \frac{s_t^{\mathrm{M}}(k_\rho, k_o)}{r_t^{\mathrm{M}}(k_\rho, k_o)} \tag{11c}$$

where

$$g_t^{\mathrm{M}}(k_\rho, k_o) = 1 + R_{01}R_{12}e^{i2k_{1z}d}$$
$$f_t^{\mathrm{M}}(k_\rho, k_o) = R_{01} + R_{12}e^{i2k_{1z}d}$$

$$r_t^{\mathrm{M}}(k_\rho, k_o) = R_{01}R_{12} + e^{i2k_{1z}d}$$
$$s_t^{\mathrm{M}}(k_\rho, k_o) = R_{12} + R_{01}e^{i2k_{1z}d}$$

To determine the existence and positions of the poles, we have to solve for the *zeros* of $g_t^{\mathrm{M}}(k_\rho, k_o)$, $f_t^{\mathrm{M}}(k_\rho, k_o)$ and $r_t^{\mathrm{M}}(k_\rho, k_o)$ in the complex k_ρ plane. The residues of these singularities contribute to the field solution only if they lie in the respective regions of interest. For instance, for the zeros of $g_t^{\mathrm{M}}(k_\rho, k_o)$ to contribute, they have to lie in the (UU) region of the k_ρ plane [Fig. 2].

Denoting the zeros of $g_t^{\mathrm{M}}(k_\rho, k_o)$ by K_{MUU}, the zeros of $f_t^{\mathrm{M}}(k_\rho, k_o)$ by K_{MLU}, and those of $r_t^{\mathrm{M}}(k_\rho, k_o)$ by K_{MLL}, we have that $k_\rho = K_{MUU}$ satisfies

$$\ln(R_{01}R_{12}) + i2k_{1z}d = i(2M+1)\pi \qquad M = \text{ integer} \tag{12}$$

while $k_\rho = K_{MLU}$ satisfies

$$\ln\left(\frac{R_{12}}{R_{01}}\right) + i2k_{1z}d = i(2M+1)\pi \qquad M = \text{ integer} \tag{13}$$

and $k_\rho = K_{MLL}$ satisfies

$$-\ln(R_{01}R_{12}) + i2k_{1z}d = i(2M+1)\pi \qquad M = \text{ integer} \tag{14}$$

where all $Re(\sqrt{\bullet}) \geq 0$. The pole loci for K_{MUU} and K_{MLU}, normalised to layer thickness d, for varying M are shown in Fig. 3 for $\epsilon_1 = 3.2$ (ice), and $\epsilon_2 = 80$ (water). Details on the determination of these loci are presented in [9]. Although there are two sets of poles for each M owing to the modal equations being even in k_ρ, we have shown only the set that lies in our domain of interest. As noted in Fig. 2, we find no solution for K_{MLL} corresponding to (14) in the region of interest which is designated (LL). This will be the case whenever $\epsilon_2 > \epsilon_1$, and is explained later in this section.

Both K_{MUU} and K_{MLU} converge towards $k_\rho = \underline{k}_1$ for $k_o d \to \infty$ but $k_\rho = \underline{k}_1$ is not a pole singularity of the reflection coefficients. Mathematically this is due to the fact that R_{UU}^{TM} and R_{LU}^{TM} remain finite for this value of k_ρ.

From the deformation process illustrated in Fig. 2, we find that the singularities of importance to the left of the $Re(k_\rho) = k_o$ line are those (K_{MUU}) due to R_{UU}^{TM} since the path remains on the top Riemann sheet intercepting only the corresponding poles. On the other hand, to the right of the $Re(k_\rho) = k_o$ line and to the left of the $Re(k_\rho) = Re(\underline{k}_2)$ line, the deformed path crosses the branch cut into the lower Riemann sheet of k_{oz} but remains on the top Riemann sheet for k_{2z} and therefore intercepts poles (K_{MLU}) attributed to R_{LU}^{TM}. Furthermore we find that, for varying k_o, the pole loci for K_{MU} intersects the $Re(k_\rho) = k_o$ line at two points corresponding to $k_o = k_{M1}$ and $k_o = k_{M2}$. This explains why we need only integrate over the range k_{M1} to k_{M2} for k_o when we consider the field contribution of K_{MUU}. For the K_{MLU} loci, the intersection with the $Re(k_\rho) = k_o$ line occurs only at one frequency corresponding to $k_o = k_{M3}$, and there is no intersection with the $Re(k_\rho) = Re(\underline{k}_2)$ line.

Physically, k_{M3} corresponds to the cutoff frequency of the M th transverse magnetic (TM) mode *guided* in the bounded layer. The integration from k_{M3} to

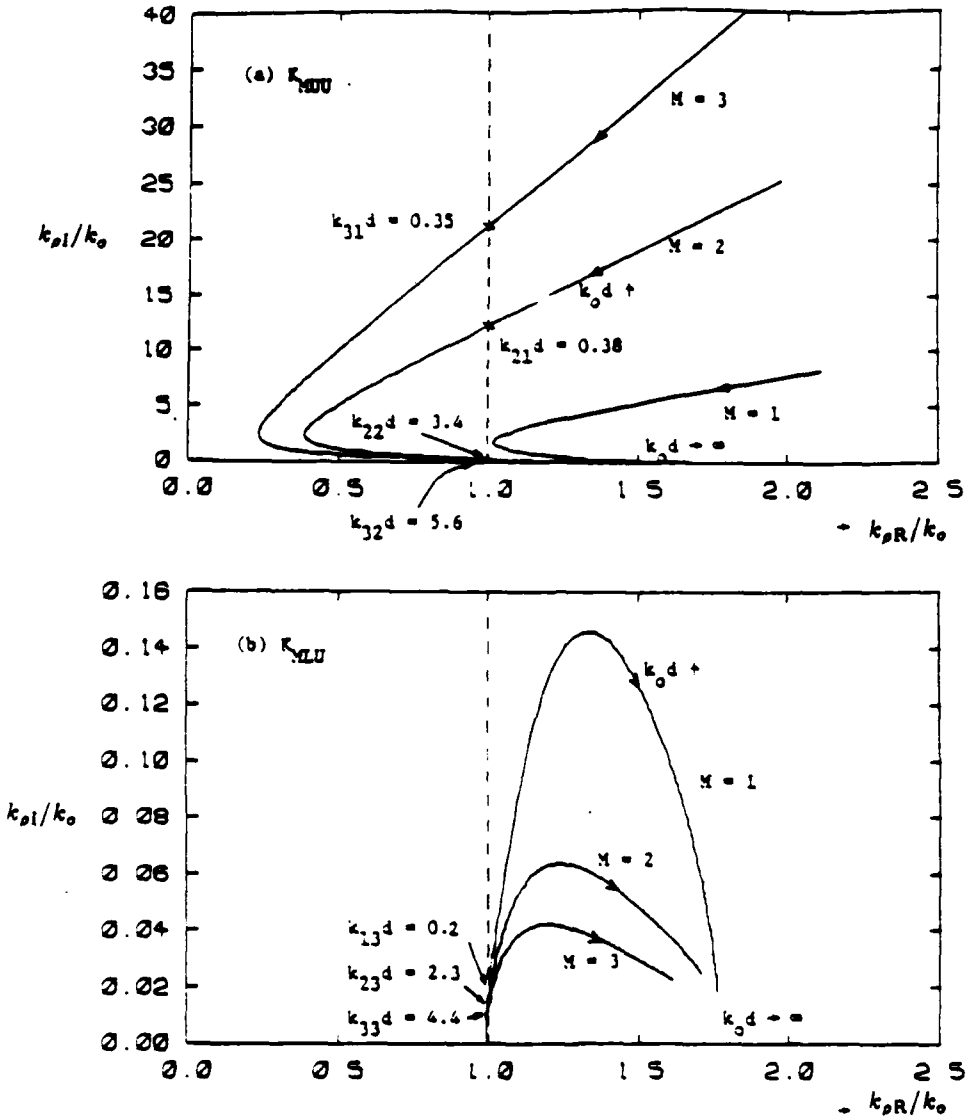

Figure 3. Pole loci on k_ρ/k_o plane for $\epsilon_1 = 3.2$, $\epsilon_2 = 80$, and positive k_o. (a) Pole loci (K_{MUU}), $M = 1, 2, 3$. Region of interest is *left* of $Re(k_\rho) = k_o$. (b) Pole loci (K_{MLU}), $M = 1, 2, 3$. Region of interest is *right* of $Re(k_\rho) = k_o$ and *left* of $Re(k_\rho) = Re(\underline{k}_2)$ (not shown).

∞ sums the contribution of the M th guided mode over all frequencies of propagation. We find that the excited K_{MUU} poles correspond to *leaky* wave modes in both the upper and lower half-spaces having $k_o > Re(k_\rho) > 0$, $Im(k_\rho) > 0$; $Re(k_{oz}) > 0$, $Im(k_{oz}) < 0$, and $Re(k_{2z}) > 0$, $Im(k_{2z}) < 0$, while the excited K_{MLU} poles correspond to *surface* wave modes having $Re(k_{oz}) < 0$ and $Im(k_{oz}) > 0$, in the *upper* half-space and *leaky* waves in the *lower* half-space. We comment that any K_{MLL} pole singularities would correspond to modes comprising surface

waves in both the lower and upper half-spaces. However, for $\epsilon_2 > \epsilon_1$, as considered here, such wave modes cannot be supported and, consistently so, K_{MLL} singularities are not intercepted in the deformation of the SIP.

The expressions pertaining to the pole contributions discussed above are

$$H_{\phi MUU}(\tau) = Re\left\{ -\frac{I_o l}{4\pi}\int_{k_{M1}}^{k_{M2}} dk_o\, e^{-ik_o\tau} I(k_o) \frac{K_{MUU}^2}{\sqrt{k_o^2 - K_{MUU}^2}} H_1^{(1)}(K_{MUU}\rho) \cdot \frac{f_t^M(K_{MUU}, k_o)}{\left.\frac{\partial}{\partial k_\rho} g_t^M(k_\rho, k_o)\right|_{k_\rho = K_{MUU}}} \right\} \qquad M = \text{integer} \qquad (15)$$

$$H_{\phi MLU}(\tau) = Re\left\{ \frac{I_o l}{4\pi}\int_{k_{M3}}^{\infty} dk_o\, e^{-ik_o\tau} I(k_o) \frac{K_{MLU}^2}{\sqrt{k_o^2 - K_{MLU}^2}} H_1^{(1)}(K_{MLU}\rho) \cdot \frac{g_t^M(K_{MLU}, k_o)}{\left.\frac{\partial}{\partial k_\rho} f_t^M(k_\rho, k_o)\right|_{k_\rho = K_{MLU}}} \right\} \qquad M = \text{integer} \qquad (16)$$

The total magnetic field may then be evaluated from (10) using (8)-(9) and (15)-(16). This is what we shall refer to as the *single deformation* approach. However, the double integrals in (8) and (9) are not easily evaluated due to the oscillatory nature of the integrand as a function of real k_o. The *double deformation* method seeks to alleviate this problem by deforming the real k_o path of integration to the positive or negative imaginary k_o axis. At the same time we are potentially able to infer physical processes, that may be occurring, from the intermediate results obtainable through the deformation. We reiterate that the deformation in the k_o plane is performed only on the steepest descent path integrals in the k_ρ plane and not the entire original field expression. As such, contributions derived from various singularities in the k_o plane should be interpreted as contributing to the time-response of these integrals which, for time-harmonic excitation, correspond to both the direct (from saddle-point), lateral (from branch cuts) waves. This is so when both the dipole and the observation point are on the upper boundary in which case the saddle point coincides with the branch point at $k_\rho = k_o$ [6].

IV. DEFORMATION IN THE k_o PLANE

Interchanging the order of integration in (8) and (9), we have

$$H_{\phi SDP1}(\tau) = \frac{I_o l}{8\pi^2} Re \left\{ \int_0^\infty dq \int_0^\infty dk_o\, e^{-ik_o\tau} I(k_o) \frac{(k_o+iq)^2}{\sqrt{k_o^2-(k_o+iq)^2}} \cdot H_1^{(1)}((k_o+iq)\rho) \left[2 + \frac{f_t^M(k_o+iq,k_o)}{g_t^M(k_o+iq,k_o)} + \frac{g_t^M(k_o+iq,k_o)}{f_t^M(k_o+iq,k_o)} \right] \right\} \tag{17}$$

and

$$H_{\phi SDP2}(\tau) = \frac{I_o l}{8\pi^2} Re \left\{ \int_0^\infty dq \int_0^\infty dk_o\, e^{-ik_o\tau} I(k_o) \frac{(\underline{k}_2+iq)^2}{\sqrt{k_o^2-(\underline{k}_2+iq)^2}} \cdot H_1^{(1)}((\underline{k}_2+iq)\rho) \left[-\frac{g_t^M(\underline{k}_2+iq,k_o)}{f_t^M(\underline{k}_2+iq,k_o)} + \frac{s_t^M(\underline{k}_2+iq,k_o)}{r_t^M(\underline{k}_2+iq,k_o)} \right] \right\} \tag{18}$$

The deformation of the original k_o integration path to the positive or negative imaginary axes is determined by the value of τ relative to ρ and also to $\rho\sqrt{\epsilon_2}$ which then determines the convergence of the resulting deformed integral.

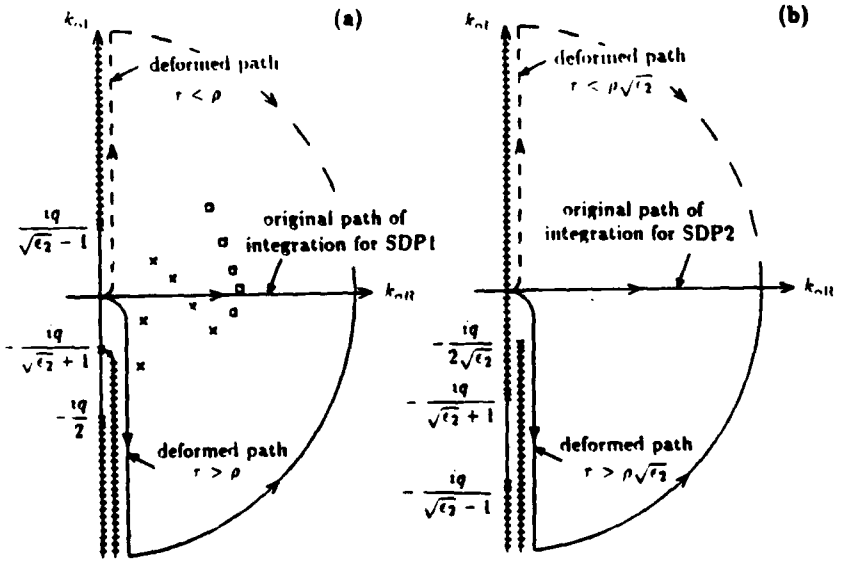

Figure 4. Original and deformed paths for k_o integration for (a) SDP1 and (b) SDP2.

We find that [Fig. 4]:

(i) For $\tau < \rho$, the k_o integrals for both SDP1 and SDP2 are deformed to the positive imaginary axis ($k_o = iu$, $u > 0$).

(ii) For $\rho\sqrt{\epsilon_2} > \tau > \rho$, the k_o integral is deformed to the negative imaginary axis ($k_o = -iu$, $u > 0$) for SDP1 and to the positive imaginary axis for SDP2.

(iii) For $\tau > \rho\sqrt{\epsilon_2}$, the k_o integrals for both SDP1 and SDP2 are deformed to the negative imaginary axis ($k_o = -iu$, $u > 0$).

Corresponding to (i), (ii) and (iii), each deformation results in the original, real k_o axis, integration path being replaced by the positive *or* negative imaginary axis and an arc of infinite radius subtending either the first *or* fourth quadrant. Consistent with each deformation, the integrations over the arcs result in zero contribution by Jordan's lemma. The contributions to $H_{\phi SDP1}(\tau)$ and $H_{\phi SDP2}(\tau)$ are to be found in the resulting double integral over q and u and the residues of any singularities, in the first or fourth quadrants, intercepted in the deformations. These singularities are characterized by the zeros of $g_t^M(k_o - iq, k_o)$ and $f_t^M(k_o + iq, k_o)$ for SDP1 and the zeros of $f_t^M(\underline{k}_2 + iq, k_o)$ and $r_t^M(\underline{k}_2 - iq, k_o)$ for SDP2. We must also consider the singularities associated with $I(k_o)$. For SDP1, there are branch points, corresponding to the transformed k_{oz} and k_{2z}, at $k_o = -iq/2$, and at $k_o = -iq/(\sqrt{\epsilon_2} + 1)$ and $iq/(\sqrt{\epsilon_2} - 1)$ respectively. The branch cuts chosen are shown in Fig. 4(a). The sign of the square roots associated with the transformed k_{oz} and k_{2z}, evaluated anywhere in the complex k_o plane, should be determined with reference to the fact that their real parts are *positive* on the original, real-axis, integration path. On the other hand, for SDP2, the branch points are located at $k_o = -iq/(2\sqrt{\epsilon_2})$, corresponding to the transformed k_{2z}, and at $k_o = -iq/(\sqrt{\epsilon_2} + 1)$ and $-iq/(\sqrt{\epsilon_2} - 1)$ corresponding to the transformed k_{oz}. The branch cuts are shown in Fig. 4(b). The signs of the square roots associated with the transformed k_{oz} and k_{2z}, evaluated anywhere in the complex k_o plane, are again determined with reference to the fact that their real parts are *positive* on the real-axis.

The singularities in the k_o plane, determined from the zeros of $g_t^M(k_o + iq, k_o)$ and denoted by P_{Mg}, are the solutions of

$$\ln [R_{01}R_{12}]_{k_\rho = k_o - iq} + i2d\sqrt{\underline{\epsilon}_{r1}k_o^2 - (k_o + iq)^2} = i(2M+1)\pi \qquad M = \text{integer} \tag{19}$$

The zeros of $f_t^M(k_o - iq, k_o)$, denoted by P_{Mf1} satisfy

$$\ln\left[\frac{R_{12}}{R_{01}}\right]_{k_\rho = k_o - iq} - i2d\sqrt{\underline{\epsilon}_{r1}k_o^2 - (k_o + iq)^2} = i(2M+1)\pi \qquad M = \text{integer} \tag{20}$$

In addition, for SDP2, the zeros $f_t^M(\underline{k}_2 + iq, k_o)$, denoted by P_{Mf2} satisfy

$$\ln\left[\frac{R_{12}}{R_{01}}\right]_{k_\rho = \underline{k}_2 - iq} - i2d\sqrt{\underline{\epsilon}_{r1}k_o^2 - (\underline{k}_2 + iq)^2} = i(2M+1)\pi \qquad M = \text{integer} \tag{21}$$

and the zeros $r_t^M(\underline{k}_2 + iq, k_o)$, denoted by P_{Mr} satisfy

$$-\ln [R_{01}R_{12}]_{k_\rho = \underline{k}_2 + iq} + i2d\sqrt{\underline{\epsilon}_{r1}k_o^2 - (\underline{k}_2 - iq)^2} = i(2M+1)\pi \qquad M = \text{integer} \tag{22}$$

where all square roots in (19)-(22) are defined to have positive real components. The details of solving (19)-(22) are examined in [9].

The loci of P_{Mg} and P_{Mf1} as functions of qd are illustrated in Figs. 5(a)-(b) for $\epsilon_1 = 3.2$ and $\epsilon_2 = 80$. From Fig. 5(a), we find that, for each M, the locus for P_{Mg} intersects, if at all, the k_o axis at two frequencies corresponding to k_{M1}

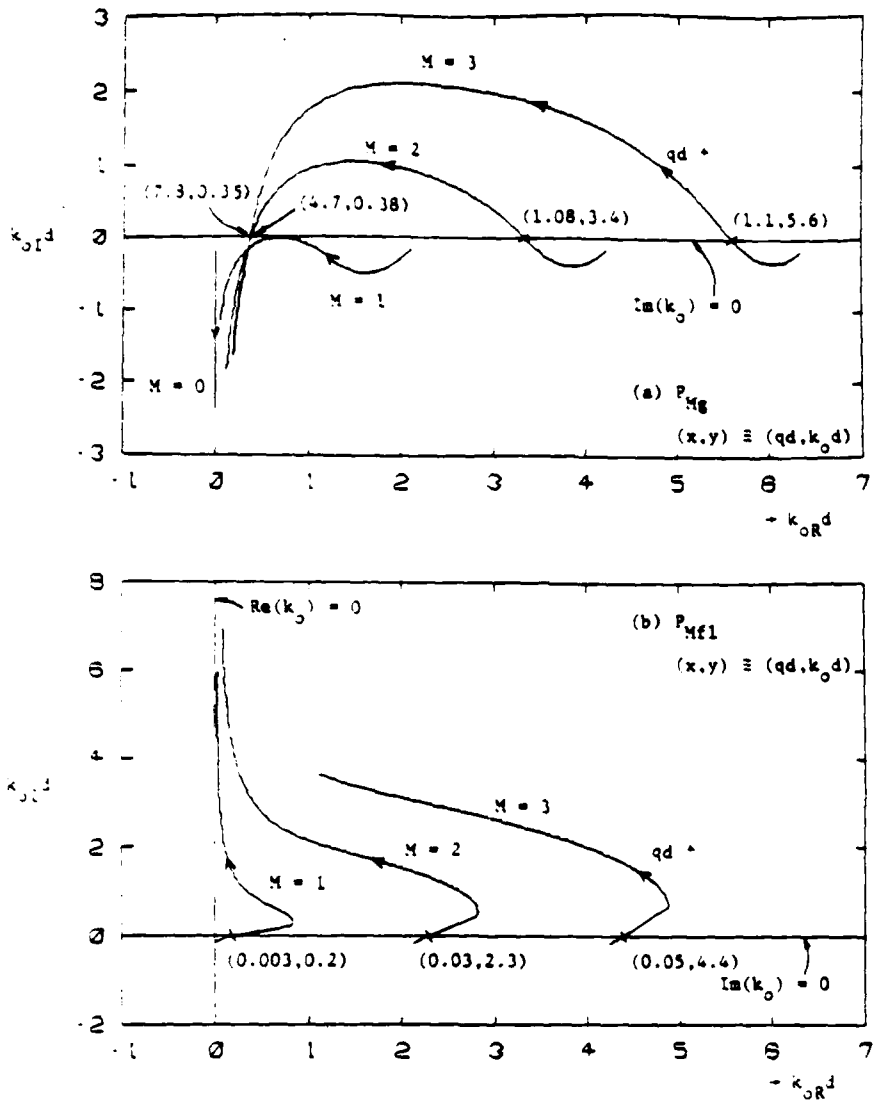

Figure 5. Pole loci as function of qd in $k_o d$ plane. No pole loci are enclosed for P_{Mf2} and $P_{M\tau}$ in the deformation. $\epsilon_1 = 3.2$, $\epsilon_2 = 80$. (a) Poles P_{Mg} for $M = 0, 1, 2, 3$. (b) Poles P_{Mf1} for $M = 1, 2, 3$.

and k_{M2}. The locus for P_{Mf1}, on the other hand, intersects the k_o axis at k_{M3}. We denote the corresponding q values by q_{M1}, q_{M2} and q_{M3}. These *critical* frequencies are identical in value to the k_{M1}, k_{M2} and k_{M3} in (15) and (16) and are crucial to the determination of causality.

Neither of the loci for P_{Mf2} and $P_{M\tau}$ exists in the domain of deformation for the cases we consider with $\epsilon_2 > \epsilon_1 > 1$. As such they do not contribute for $\tau < \rho\sqrt{\epsilon_2}$ and do not pose any problems in terms of satisfying causality.

We find in particular a pole locus designated by $M = 0$ for P_{Mg} with no correspondence to any locus intercepted in the k_ρ plane since it never intersects the real k_o axis and lies entirely on the negative imaginary axis. The Appendix discusses the details associated with the existence and search of this elusive pole locus and its contribution to the magnetic field. Its location on the negative imaginary k_o axis implies a response which decays exponentially with time and hence is essentially important only for the early-time response. The corresponding results and implications will be discussed in Section VI.

Causality requires that the total field solution be zero before the time it takes the electromagnetic wave to travel the separation distance at its speed in the intervening medium, which in this case is the less dense of the two interfacing media, has elapsed. The waves excited as modes and attributed to the k_ρ plane singularities are time-harmonic modes, each of which is valid for all times at a single frequency and are therefore non-causal. The summation of poles on the k_ρ plane in any manner also does not result in a causal solution. In [4,9], one finds how the contributions due to singularities in the first quadrant of the k_o plane (intercepted by deformation for $\tau < \rho$) will combine with these non-causal modes to give a zero contribution for $\tau < \rho$. The fact that the double integrals over q and u for the corresponding deformation combine to give a zero contribution to the magnetic field over this period is also illustrated.

IV.1 $H_\phi(\tau)$ for $\rho\sqrt{\epsilon_2} > \tau > \rho$

With causality accounted for, we next consider the time interval $\rho\sqrt{\epsilon_2} > \tau > \rho$. Only SDP1 is deformed downwards while SDP2 is deformed upwards. The contributions to $H_{\phi SDP1}(\tau)$ will come from: $H_{\phi Mg}$ and $H_{\phi Mf1}$ — due to P_{Mg} and P_{Mf1}; $H_{\phi 1DP}$ — from the singularities due to the source function $I(k_o)$; H_{SDP1^d} — the remaining double integral over q and u. The *upward* deformation of SDP2 results in H_{SDP2^u} — the remaining double integral over q and u, i.e.

$$H_{\phi SDP1}(\tau) = \sum_M H_{\phi Mg} + \sum_M H_{\phi Mf1} + H_{\phi 1DP} + H_{\phi SDP1^d} \tag{23}$$

$$H_{\phi SDP2}(\tau) = H_{\phi SDP2^u} \tag{24}$$

where

$$H_{\phi Mg}(\tau) = -\frac{I_o l}{4\pi} Re \left\{ i \left[\int_0^{q_{M2}} + \int_{q_{M1}}^{\infty} \right] dq\, e^{-iP_{Mg}\tau} I(P_{Mg}) \frac{(P_{Mg}+iq)^2}{\sqrt{P_{Mg}^2 - (P_{Mg}+iq)^2}} \right.$$

$$\left. \cdot H_1^{(1)}((P_{Mg}+iq)\rho) \frac{f_i^M(P_{Mg}+iq,\, P_{Mg})}{\dfrac{\partial}{\partial k_o} g_i^M(k_o+iq,\, k_o)\Big|_{k_o=P_{Mg}}} \right\} \tag{25}$$

$$H_{\phi Mf1}(\tau) = -\frac{I_o l}{4\pi} Re \left\{ i \int_0^{q_{M3}} dq\, e^{-iP_{Mf1}\tau} I(P_{Mf1}) \frac{(P_{Mf1}+iq)^2}{\sqrt{P_{Mf1}^2 - (P_{Mf1}+iq)^2}} \right.$$

$$\left. \cdot H_1^{(1)}((P_{Mf1}+iq)\rho) \frac{g_t^M(P_{Mf1}+iq,\, P_{Mf1})}{\dfrac{\partial}{\partial k_o} f_t^M(k_o+iq,\, k_o)\Big|_{k_o=P_{Mf1}}} \right\} \quad (26)$$

In accordance with the choice of source function (1), $I(k_o)$ has a pole of $(n+1)$th order in the fourth quadrant at $k_o = k_p$, then

$$H_{\phi 1DP}(\tau) = -\frac{I_o l}{4\pi n!} Re \left\{ i \lim_{k_o \to k_p} \left[\frac{d^n}{dk_o^n}(k_o - k_p)^{n+1} e^{-ik_o\tau} I(k_o) \right.\right.$$

$$\cdot \int_0^\infty dq \frac{(k_o+iq)^2}{\sqrt{k_o^2 - (k_o+iq)^2}} H_1^{(1)}((k_o+iq)\rho)$$

$$\left.\left. \cdot \left[2 + \frac{f_t^M(k_o+iq,\, k_o)}{g_t^M(k_o+iq,\, k_o)} + \frac{g_t^M(k_o+iq,\, k_o)}{f_t^M(k_o+iq,\, k_o)} \right] \right] \right\} \quad (27)$$

The expressions for the remaining double integrals take the form

$$H_{\phi SDP1^d}(\tau) = \frac{I_o l}{8\pi^2} Re \left\{ i \int_0^\infty dq \int_0^\infty du\, e^{-u\tau} I(-iu) \right.$$

$$\cdot \frac{(q-u)^2}{\sqrt{(q-u)^2 - u^2}} H_1^{(1)}(i(q-u)\rho) \quad (28)$$

$$\left. \cdot \left[2 + \frac{f_t^M(k_\rho, -iu)}{g_t^M(k_\rho, -iu)} + \frac{g_t^M(k_\rho, -iu)}{f_t^M(k_\rho, -iu)} \right]_{k_\rho = i(q-u)} \right\}$$

and

$$H_{\phi SDP2^u}(\tau) = -\frac{I_o l}{8\pi^2} Re \left\{ i \int_0^\infty dq \int_0^\infty du\, e^{u\tau} I(iu) \right.$$

$$\cdot \frac{(q+u\sqrt{\varepsilon_{r2}})^2}{\sqrt{(q+u\sqrt{\varepsilon_{r2}})^2 - u^2}} H_1^{(1)}(i(q+u\sqrt{\varepsilon_{r2}})\rho) \quad (29)$$

$$\left. \cdot \left[-\frac{g_t^M(k_\rho, iu)}{f_t^M(k_\rho, iu)} + \frac{s_t^M(k_\rho, iu)}{r_t^M(k_\rho, iu)} \right]_{k_\rho = i(q+u\sqrt{\varepsilon_{r2}})} \right\}$$

The presence of the $M = 0$ loci for P_{Mg}, which are the zeros of $g_t^M(i(q-u), -iu)$, on the negative imaginary axis $k_o = -iu$, modifies the corresponding

u integration in (28) to be a principal value integral. In addition, the term '2' in square brackets in (28) may be dropped in the computation as the corresponding solution is purely imaginary. This can be readily shown by interchanging the order of integration and performing the variable transformation, $Q = q - u$.

To summarize, the total time-domain solution of (5) for $\rho\sqrt{\epsilon_2} > \tau > \rho$ is expressible in terms of (15)-(16) and (23)-(29), i.e.

$$\begin{aligned} H_\phi(\rho < \tau < \rho\sqrt{\epsilon_2}) = &\sum_M H_{\phi MUU}(\tau) + \sum_M H_{\phi MLU}(\tau) \\ &+ \sum_M H_{\phi Mg}(\tau) + \sum_M H_{\phi Mf1}(\tau) \\ &+ H_{\phi 1DP}(\tau) + H_{\phi SDP1^d}(\tau) + H_{\phi SDP2^u}(\tau) \end{aligned}$$

where all components, except for $H_{\phi SDP1^d}$ and $H_{\phi SDP2^u}$, comprise single integrals while $H_{\phi SDP1^d}$ and $H_{\phi SDP2^u}$ are double integrals of rapid convergence by construction.

IV.2 $H_\phi(\tau)$ for $\tau > \rho\sqrt{\epsilon_2}$

We now consider the remaining time interval $\tau > \rho\sqrt{\epsilon_2}$. Both SDP1 and SDP2 are now deformed downwards. The contributions to $H_{\phi SDP1}(\tau)$ will come from: $H_{\phi Mg}$ and $H_{\phi Mf1}$ — due to P_{Mg} and P_{Mf1}; $H_{\phi 1DP}$ — from the singularities due to the transformed source function $I(k_o)$; and H_{SDP1^d} — the remaining double integral over q and u. The expressions for these contributions are identical to those in (25)-(28).

The *downward* deformation of SDP2 results in contributions from the poles of P_{Mf2} and P_{Mr}, the source pole at $k_o = k_p$, and the contribution from H_{SDP2^d} — the remaining double integral over q and u, i.e.

$$H_{\phi SDP1}(\tau) = \sum_M H_{\phi Mg} + \sum_M H_{\phi Mf1} + H_{\phi 1DP} + H_{\phi SDP1^d} \tag{30}$$

$$H_{\phi SDP2}(\tau) = \sum_M H_{\phi Mf2} + \sum_M H_{\phi Mr} + H_{\phi 2DP} + H_{\phi SDP2^d} \tag{31}$$

where

$$H_{\phi Mf2}(\tau) = \frac{I_o l}{4\pi} Re \left\{ i \int_0^\infty dq\, e^{-iP_{Mf2}\tau} I(P_{Mf2}) \frac{(P_{Mf2}\sqrt{\epsilon_{r2}} + iq)^2}{\sqrt{P_{Mf2}^2 - (P_{Mf2}\sqrt{\epsilon_{r2}} + iq)^2}} \right.$$

$$\left. \cdot H_1^{(1)}((P_{Mf2} + iq)\rho) \frac{g_t^M(P_{Mf2}\sqrt{\epsilon_{r2}} + iq,\, P_{Mf2})}{\dfrac{\partial}{\partial k_o} f_t^M(k_o\sqrt{\epsilon_{r2}} + iq,\, k_o)\Big|_{k_o = P_{Mf2}}} \right\} \tag{32}$$

$$H_{\phi M\tau}(\tau) = -\frac{I_o l}{4\pi} Re \left\{ i \int_0^\infty dq\, e^{-iP_{M\tau}\tau} I(P_{M\tau}) \frac{(P_{M\tau}\sqrt{\epsilon_{r2}} + iq)^2}{\sqrt{P_{M\tau}^2 - (P_{M\tau}\sqrt{\epsilon_{r2}} + iq)^2}} \right.$$

$$\left. \cdot H_1^{(1)}((P_{M\tau}\sqrt{\epsilon_{r2}} + iq)\rho) \frac{s_t^M(P_{M\tau}\sqrt{\epsilon_{r2}} + iq,\, P_{M\tau})}{\dfrac{\partial}{\partial k_o} r_t^M(k_o\sqrt{\epsilon_{r2}} + iq,\, k_o)\Big|_{k_o = P_{M\tau}}} \right\} \quad (33)$$

We have stated that for the cases under study, P_{Mf2} and $P_{M\tau}$ are not intercepted. Equations (32)–(33) are shown here for the sake of completeness and are applicable in cases where they are enclosed in the deformation.

For the source-pole contribution, we have

$$H_{\phi 2DP}(\tau) = -\frac{I_o l}{4\pi n!} Re \left\{ i \lim_{k_o \to k_p} \left[\frac{d^n}{dk_o^n} (k_o - k_p)^{n+1} e^{-ik_o\tau} I(k_o) \right.\right.$$

$$\cdot \int_0^\infty dq\, H_1^{(1)}((k_o\sqrt{\epsilon_{r2}} + iq)\rho) \frac{(k_o\sqrt{\epsilon_{r2}} + iq)^2}{\sqrt{k_o^2 - (k_o\sqrt{\epsilon_{r2}} + iq)^2}} \quad (34)$$

$$\left.\left. \cdot \left(-\frac{g_t^M(k_o\sqrt{\epsilon_{r2}} + iq,\, k_o)}{f_t^M(k_o\sqrt{\epsilon_{r2}} + iq,\, k_o)} + \frac{s_t^M(k_o\sqrt{\epsilon_{r2}} + iq,\, k_o)}{r_t^M(k_o\sqrt{\epsilon_{r2}} + iq,\, k_o)} \right) \right] \right\}$$

For the deformed double integral for SDP2,

$$H_{\phi SDP2^d}(\tau) = \frac{I_o l}{8\pi^2} Re \left\{ i \int_0^\infty dq \int_0^\infty du\, e^{-u\tau} I(-iu) \right.$$

$$\cdot \frac{(q - u\sqrt{\epsilon_{r2}})^2}{\sqrt{(q - u\sqrt{\epsilon_{r2}})^2 - u^2}} H_1^{(1)}(i(q + u\sqrt{\epsilon_{r2}})\rho) \quad (35)$$

$$\left. \cdot \left[-\frac{g_t^M(k_\rho,\, -iu)}{f_t^M(k_\rho,\, -iu)} + \frac{s_t^M(k_\rho,\, -iu)}{r_t^M(k_\rho,\, -iu)} \right]_{k_o = i(q - u\sqrt{\epsilon_{r2}})} \right\}$$

To summarize, the total time-domain solution of (5) for $\tau > \rho\sqrt{\epsilon_2}$ is expressible in terms of (15)–(16), (23)–(28), and (32)–(35), i.e.

$$H_\phi(\tau > \rho\sqrt{\epsilon_2}) = \sum_M H_{\phi MUU}(\tau) + \sum_M H_{\phi MLU}(\tau) + \sum_M H_{\phi Mg}(\tau)$$

$$+\sum_M H_{\phi Mf1}(\tau) + H_{\phi 1DP}(\tau) + \sum_M H_{\phi Mf2}(\tau) + \sum_M H_{\phi M\tau}(\tau)$$
$$+ H_{\phi 2DP}(\tau) + H_{\phi SDP1^d}(\tau) + H_{\phi SDP2^d}(\tau)$$

where again all components, except for $H_{\phi SDP1^d}$, and $H_{\phi SDP2^d}$, consist of single integrals and $H_{\phi SDP1^d}$ and $H_{\phi SDP2^d}$ are double integrals of rapid convergence by construction.

V. COMPUTATION OF POLE CONTRIBUTIONS

In the double deformation approach, we display responses corresponding to various sets of poles denoted by the integer M. Each M comprises poles from the k_ρ and k_o planes. We emphasize that the k_o plane poles are associated with the decomposition of the double integrals characterizing the time response of the k_ρ plane steepest descent paths. We also note that the evaluation of the *source-pole contribution* does not fall within the scheme to be discussed here but is performed in a straightforward manner based on (27) and (34).

For $\tau > \rho$, we remark on the scheme of evaluating the pole contributions. This is the only range of time to be considered and there are no solutions corresponding to P_{Mf2} and $P_{M\tau}$ [Section VI]. The evaluation of the pole contributions are greatly eased by the correspondence between positions of k_ρ poles and k_o poles at certain locations. In particular, the real frequencies at which the k_ρ plane pole loci intersect the steepest descent path are identical to the intersections of the k_o plane pole loci with the real frequency axis. This is expected, since at these points, the root equations (12) and (19) are identical and so are (13) and (20).

In the scheme employed [4,9], for each M, we locate the position and evaluate the contribution of each pole of the locus on the k_ρ as well as the k_o planes. Refering to Fig. 6, which depicts the situation for a general M, we begin the search for poles in the k_o plane starting with the P_{Mg} branch for $qd = 0$. At $q = q_{M2}$, the k_o pole will be k_{M2} corresponding precisely to the value for k_o when the k_ρ plane poles for the M th locus 'enters' the 'region of interest' [Fig. 3]. Moving then to the k_ρ plane and continuing on the corresponding k_ρ pole (K_{MUU}) locus [(15)] by lowering the frequency, we eventually leave the region of interest at $K_{MUU} = k_{M1} + iq_{M1}$. k_{M1} corresponds to the frequency at which the P_{Mg} pole loci 'returns' to the fourth k_o quadrant (when $q = q_{M1}$) for consideration when $\tau > \rho$.

The computation continues on the P_{Mg} locus [(19)] down into the fourth quadrant and converges quickly since the integrand has a $e^{-q\rho}$ dependence and is also proportional to $e^{k_o''(\tau-\rho)}$ for negative k_o''.

We return to the point for $qd = 0$ for the P_{Mf1} branch (which, by proper choice of M, may be coincident with the starting point for the P_{Mg} branch) and repeat the same procedure with the P_{Mf1} [(20)] branch and K_{MLU} locus [(16)] instead. For the M th locus, therefore, the computation terminates with the integration over the K_{MLU} pole contributions in the k_ρ plane. These poles lie

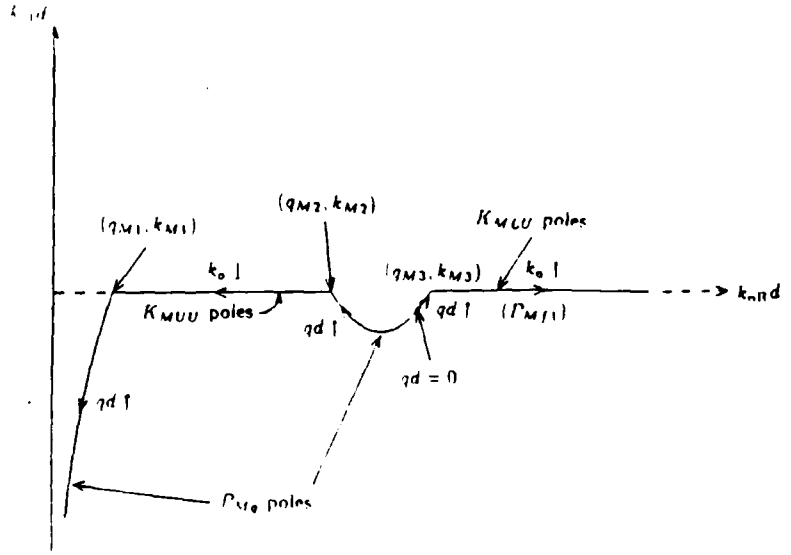

Figure 6. Example of summation path of pole contributions corresponding to general M.

closer to the real k_ρ axis and convergence of the pole contributions is slower than for those in the k_o plane.

Figure 6 shows the general situation. From the nature of the proof of causality [4,9], we find each M response to be causal if computed in accordance with the figure. In certain cases, for low orders of M, the P_{Mg} branch may not intersect the inversion contour on the k_o plane, implying that no corresponding K_{MUU} poles are in the region of interest and thus necessitating a slight modification to (19). This feature can easily be taken into account. In particular, the special case of $M = 0$ is considered in the Appendix.

VI. RESULTS AND DISCUSSION

In Figs. 7–11, we present results obtained for the time-domain magnetic field from the double deformation method in comparison with existing methods as well as for various sets of parameters. Unless explicitly stated otherwise, we shall consider the source function of the form,

$$i(t) = I_o\, t \sin(\omega_0 t) e^{-\alpha_0 t} u_{-1}(t) \tag{36}$$

The initial response due to such a function should begin from a zero value [1], so that a convenient check is immediately available for our numerical results. $I(k_o)$ has a pair of second order poles at $k_o = \pm 1.0 - i0.5$, of which only that in the fourth quadrant is of interest and will constitute the source-pole. To allow ready comparisons with alternate methods, we consider the lossless case. In addition, the parameters used shall be $\epsilon_1 = 3.2$, $\epsilon_2 = 80$, $\omega_0 = 1.0c$, $\alpha_0 = 0.5c$, $d = 1$ m and $\rho = 3$ m for most of the cases illustrated.

In Fig. 7, we show the results obtained via the single deformation method.

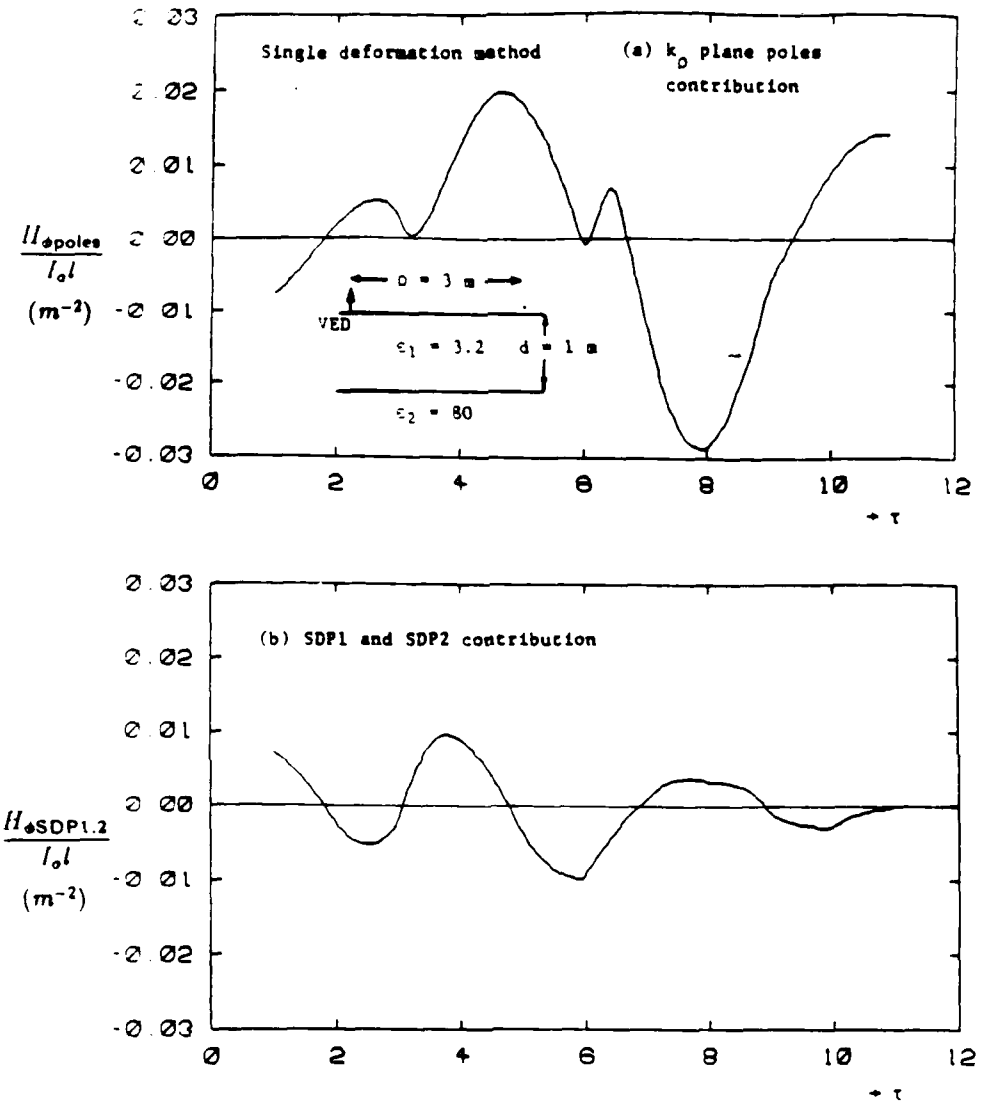

Figure 7. Time-domain magnetic field versus $\tau = ct$ for VED on two-layer medium using single deformation approach. $\epsilon_1 = 3.2$, $\epsilon_2 = 80$, $\rho = 3$ m, $d = 1$ m, $i(t) = I_o t \sin(ct) \cdot e^{-0.5ct} u_{-1}(t)$. (a) k_ρ plane poles contribution, (b) SDP1 and SDP2 contribution.

Figures 7(a) and (b) respectively depict the response due to the k_ρ poles and the steepest descent path integrals. The two responses are comparable in magnitude. The sum or total time response is plotted in Fig. 9(a) in comparison with the double deformation result.

Figurer 8(a)–(f) show the various contributions to the double deformation results. Figure 8(a) shows the source-pole contribution which follows the oscillating and decaying nature of the source function. Figures 8(b)–(f) show the responses corresponding to the various pole loci M and evaluated according to the scheme

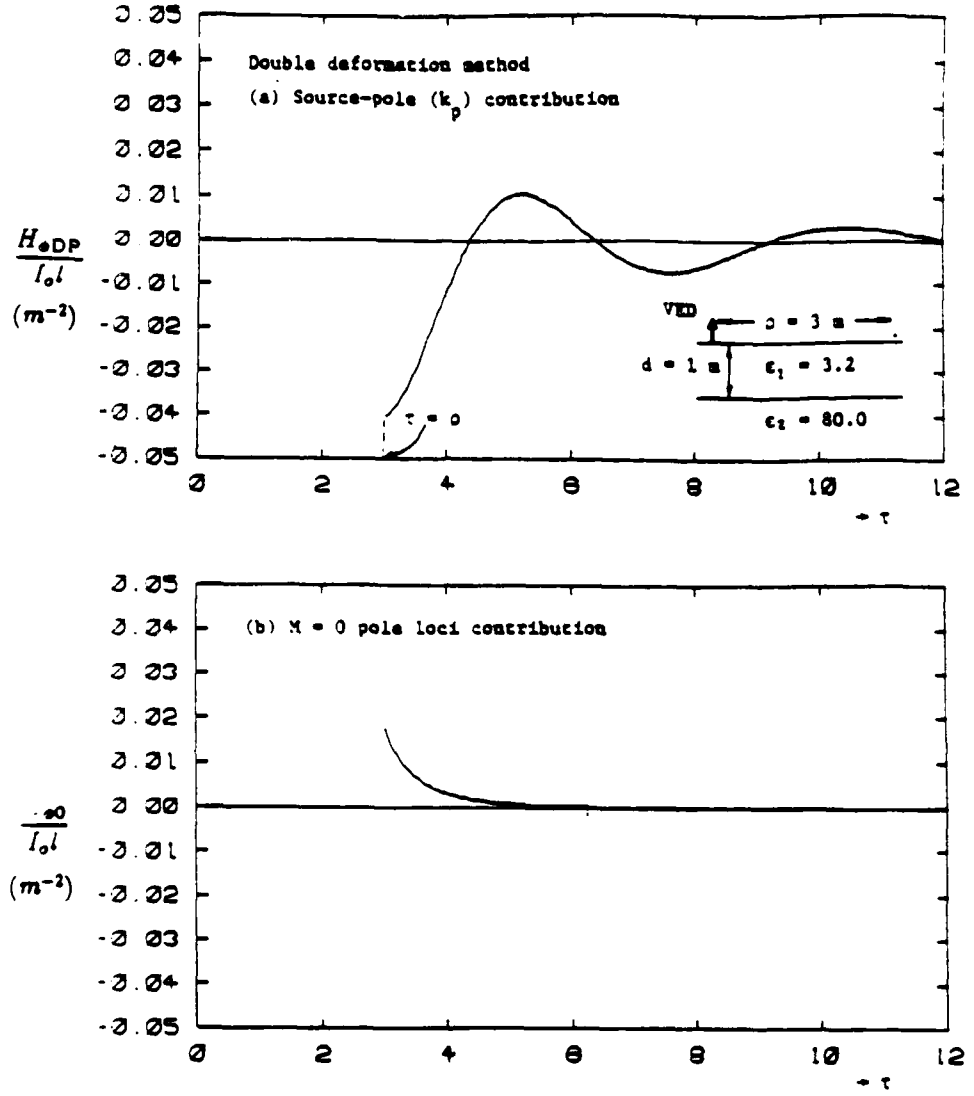

Figure 8. Magnetic field contributions versus $\tau = ct$ for VED on two-layer medium using double deformation approach. $\epsilon_1 = 3.2$, $\epsilon_2 = 80$, $\rho = 3$ m, $d = 1$ m, $i(t) = I_o t \sin(ct)\, e^{-0.5ct} u_{-1}(t)$. (a) Source-pole contribution. (b) Lowest order, $M = 0$, poles contribution.

described in Section V. In particular, we note that the $M = 0$ set in Fig. 8(b) is essentially an early time response due to its location on the negative imaginary k_o axis. We also find that the contributions fall rapidly with increasing M, and $M \leq 5$ should be sufficient to achieve reasonable convergence in results. The total response after summation is shown in Fig. 9(a).

We have not shown the double integral results corresponding to $H_{\phi SDP1^d}$ and $H_{\phi SDP2^{u,d}}$ because they are found to be negligibly small for all cases investigated and appear unnecessary for reasonable accuracy. Moreover, in [9], it is argued that

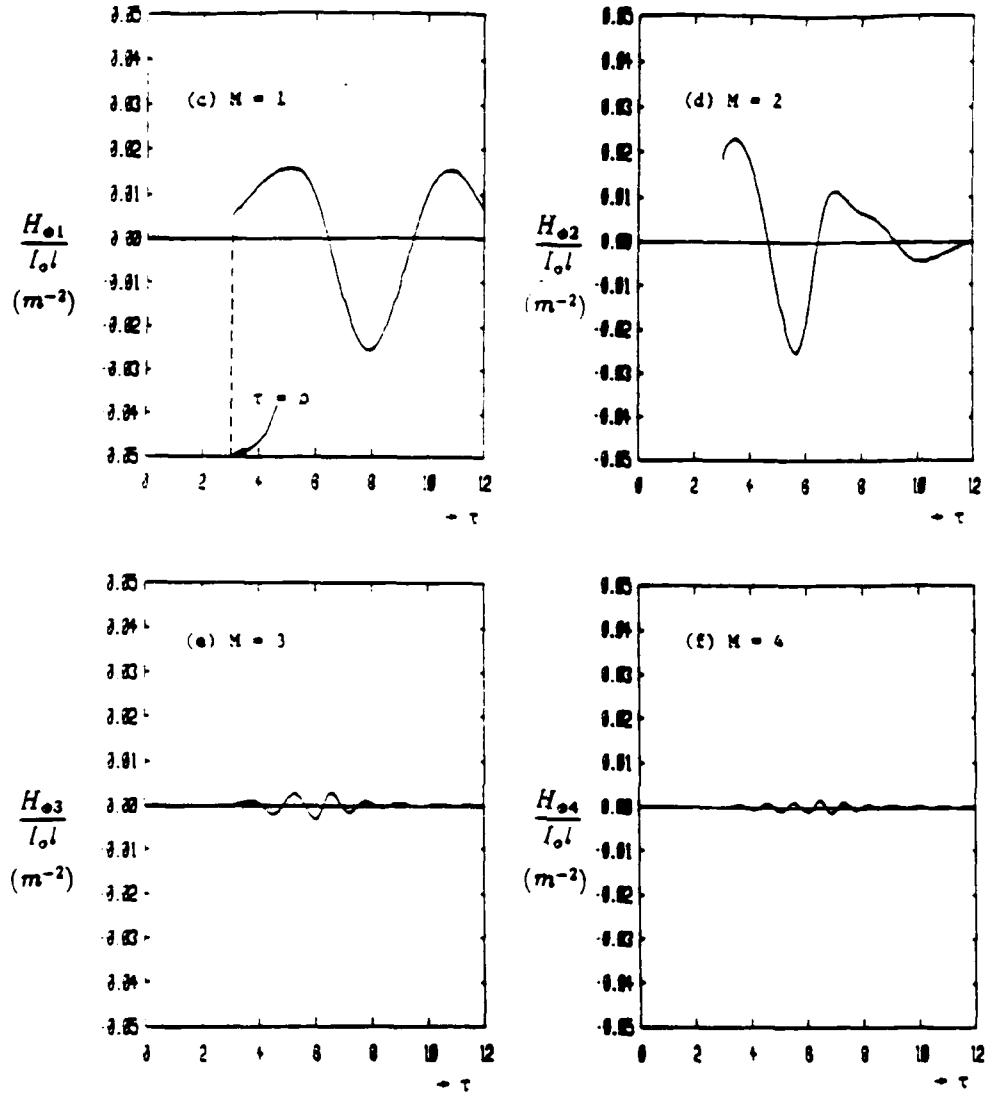

Figure 8. (cont'd)—Magnetic field contributions versus $\tau = ct$ for VED on two-layer medium using double deformation approach. $\epsilon_1 = 3.2$, $\epsilon_2 = 80$, $\rho = 3$ m, $d = 1$ m, $i(t) = I_o\, t \sin(ct) e^{-0.5ct} u_{-1}(t)$. (c) $M = 1$, (d) $M = 2$, (e) $M = 3$, and (f) $M = 4$.

the double integrals evaluate to zero for the non-dispersive half-space problem. This implies that our neglect of the small contribution of the double integrals becomes increasingly justified for larger layer thickness d in the lossless case.

The accuracy of the double deformation results is verified by comparison with the single deformation waveform in Fig. 9(a) and with the explicit inversion method [1] in Fig. 9(b). Figure 9(a) confirms the validity of the double deformation results. Further confirmation is obtained by matching with the half-space results [9] over an initial time-window and to be shown in Fig. 10(a). The comparison with the explicit inversion results shows slight discrepancies in value if

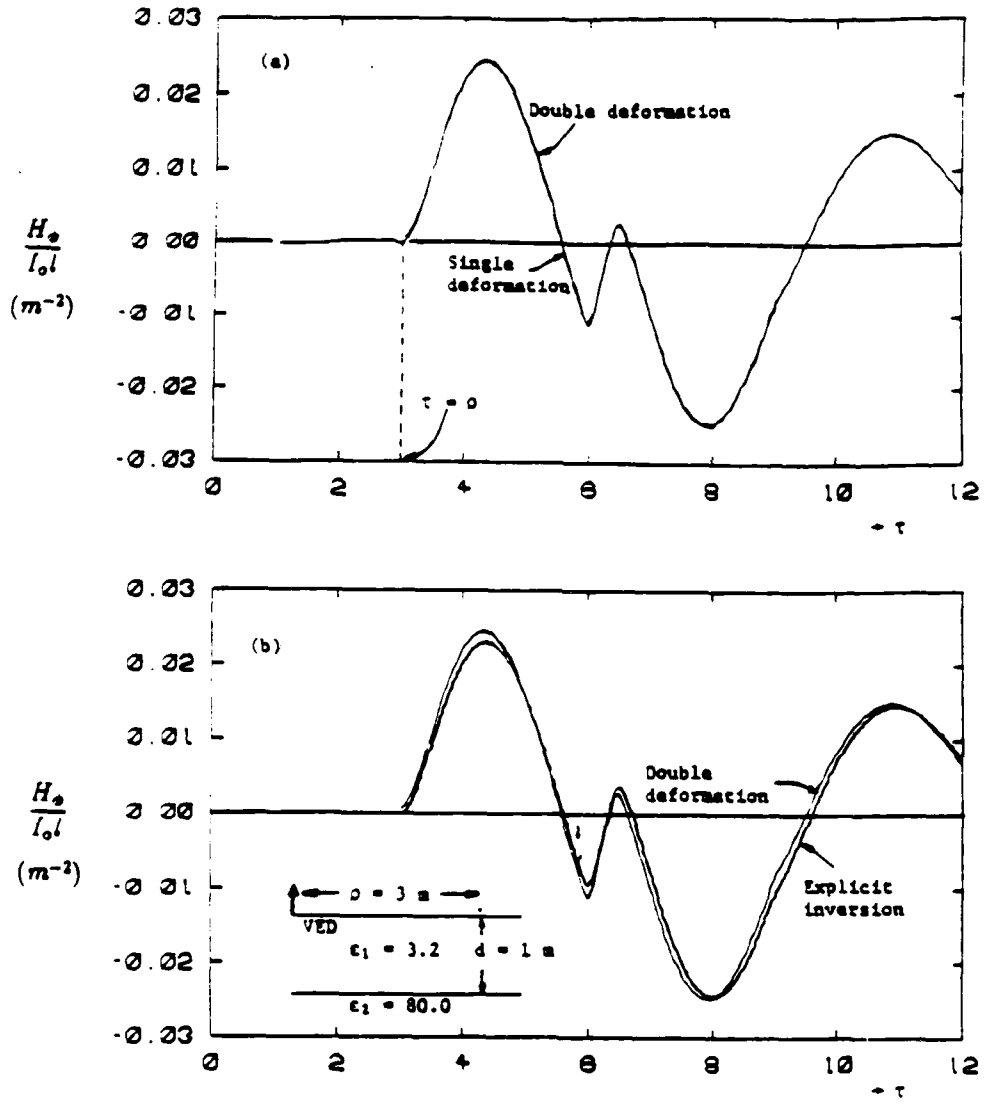

Figure 9. Total time-domain magnetic field versus $\tau = ct$ for VED on two-layer medium. $\epsilon_1 = 3.2$, $\epsilon_2 = 80$, $\rho = 3$ m, $d = 1$ m, $i(t) = I_o\, t \sin(ct) e^{-0.5ct} u_{-1}(t)$. (a) Single deformation and double deformation. (b) Explicit inversion and double deformation.

not in trend. In the explicit inversion scheme, the step response is first computed and subsequently convolved with the source function to obtain the required response. Much relies on the accuracy of the step response which has to be evaluated from an integral expression [1]. In Fig. 10 we compare the half-space solution, which may be readily obtained from the closed-form impulse response [10], with the double deformation results for $d = 1$ m and $d = 0.2$ m. The initial deviation from the half space solution indicates the first arrival due to reflection off the lower boundary.

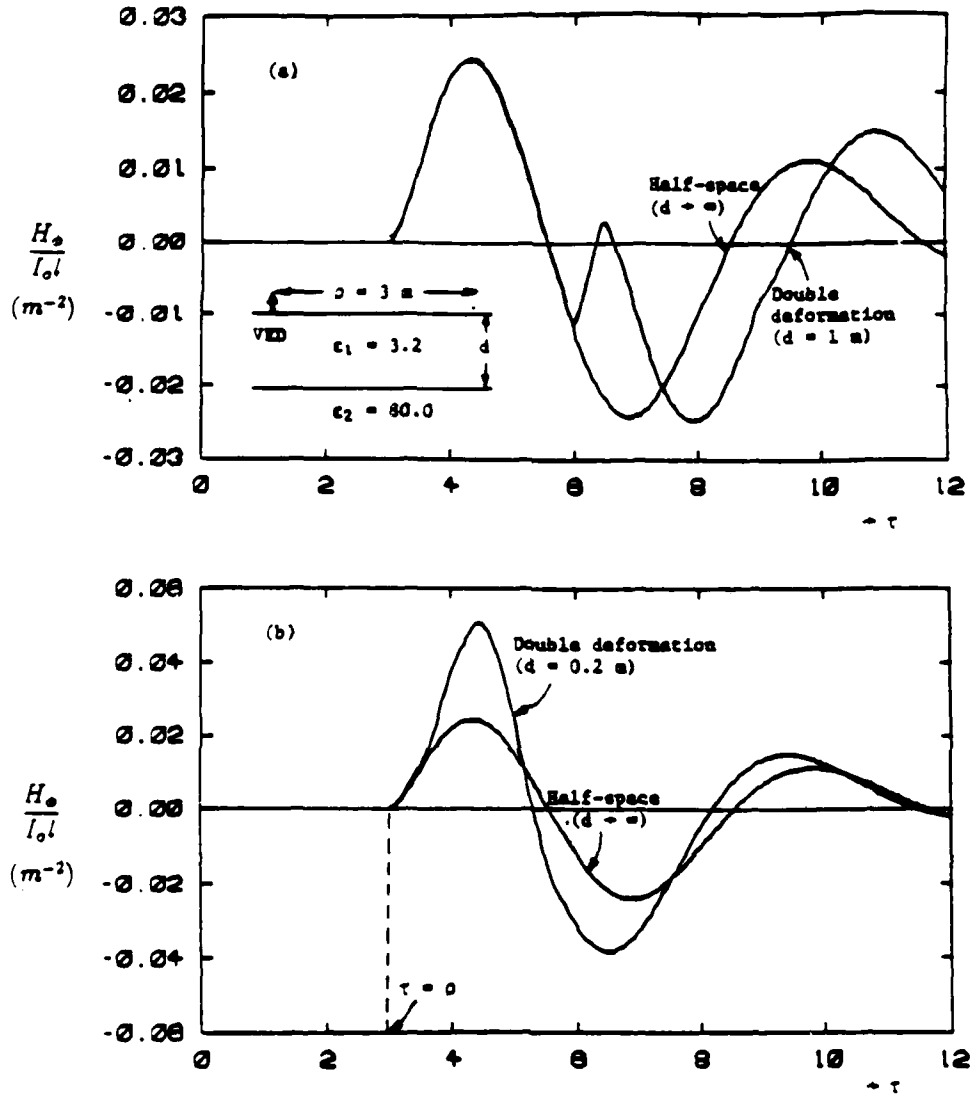

Figure 10. Magnetic field contributions versus $\tau = ct$ for VED on two-layer medium (double deformation) and a half-space, $d \to \infty$ (convolution with closed-form impulse response). $\epsilon_1 = 3.2$, $\epsilon_2 = 80$, $\rho = 3$ m, $i(t) = I_o t \sin(ct) e^{-0.5ct} u_{-1}(t)$. (a) $d = 1$ m, (b) $d = 0.2$ m.

In Fig. 11(a) we show the results for single and double deformation for the case of $\epsilon_2 = 12$, all other parameters unchanged. Due to the smaller dielectric contrast at the lower boundary, the effect of the first reflected wave is not as pronounced as in the previous case of $\epsilon_2 = 80$. In addition, we have again not included any of the double integrals corresponding to $H_{\phi SDP1^d}$ and $H_{\phi SDP2^{u,d}}$ in our computation. We find that, in comparison with single deformation results, this does not affect the accuracy of the double deformation method.

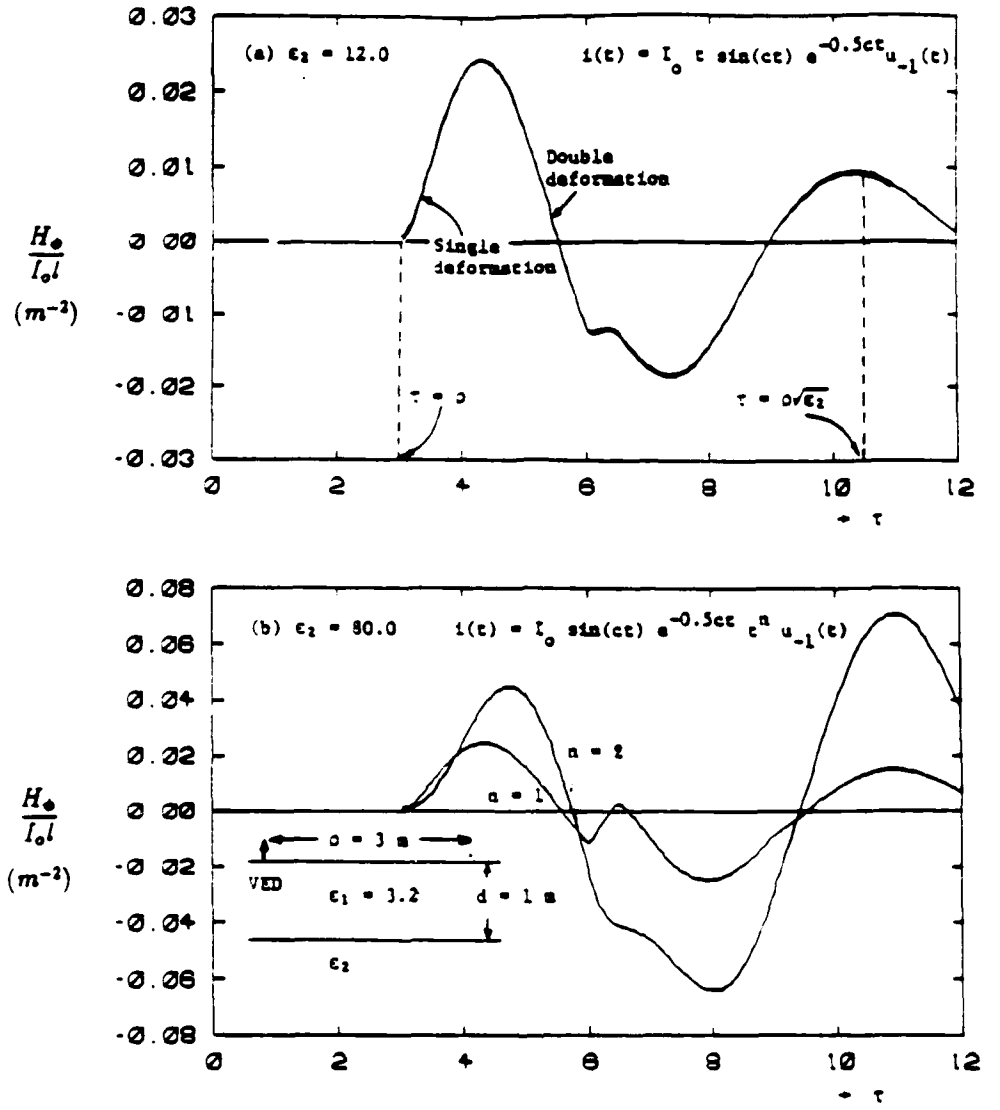

Figure 11. Magnetic field contributions versus $\tau = ct$ for VED on two-layer medium. $\rho = 3$ m, $d = 1$ m, $\epsilon_1 = 3.2$. (a) $\epsilon_2 = 12$, $i(t) = I_o\, t \sin(ct) e^{-0.5ct} u_{-1}(t)$. Single and double deformation. (b) $\epsilon_2 = 80$, $i(t) = I_o\, t^n \sin(ct) e^{-0.5ct} u_{-1}(t)$, with $n = 1$ and 2. Double deformation.

The effect of using a smoother source function $i(t) = I_o\, t^2 \sin(ct) e^{-0.5ct} u_{-1}(t)$ is illustrated in Fig. 11(b), in comparison with the source described by (36). Here the most outstanding difference is the slower and smaller change in the waveform due to the first reflected arrival. The smoothness of the source accounts for the delayed effect and also allows the falling portion of the half-space solution to smooth out much of the early contribution of the reflected signal.

We have illustrated, by means of a few examples, the feasibility of the double deformation method applied to transient dipole radiation over a two-layer

medium. In comparison with a previous attempt in this direction [4], the identification of the $M = 0$ pole locus enables us to obtain a complete response to the time-domain problem.

APPENDIX: EXISTENCE OF P_{0g} LOCUS

In this appendix, we show how the pole locus, designated $M = 0$ for P_{Mg}, satisfying the equation $g_t^{\mathrm{M}} = 0$, on SDP1, is found to exist on the negative imaginary k_o axis.

For the sake of illustration, we consider $\epsilon_2 > \epsilon_1$. In the k_o plane, for SDP1, k_{oz}, k_{1z} and k_{2z} may be written as

$$k_{oz} = e^{-i\pi/4}\sqrt{2q}\sqrt{k_o + i\frac{q}{2}}$$

$$k_{1z} = \sqrt{\epsilon_1 - 1}\sqrt{\left(k_o - i\frac{q}{\sqrt{\epsilon_1}-1}\right)\left(k_o + i\frac{q}{\sqrt{\epsilon_1}+1}\right)}$$

$$k_{1z} = \sqrt{\epsilon_2 - 1}\sqrt{\left(k_o - i\frac{q}{\sqrt{\epsilon_2}-1}\right)\left(k_o + i\frac{q}{\sqrt{\epsilon_2}+1}\right)}$$

so that there are branch points at $k_o = -iq/2$ corresponding to k_{oz} and $k_o = iq/(\sqrt{\epsilon_2} - 1)$ and $k_o = -iq/(\sqrt{\epsilon_2} + 1)$ corresponding to k_{2z}. The locations of these singularities, the corresponding choice of branch cuts and the critical points at $k_o = iq/(\sqrt{\epsilon_1} - 1)$ and $k_o = -iq/(\sqrt{\epsilon_1} + 1)$ for k_{1z} are shown in Fig. A.1.

Refering to Fig. A.1, we may divide the negative imaginary axis into four intervals namely, $0 < X < q/(\sqrt{\epsilon_2}+1)$, $q/(\sqrt{\epsilon_2}+1) < X < q/(\sqrt{\epsilon_1}+1)$, $q/(\sqrt{\epsilon_1}+1) < X < q/2$ and $X > q/2$. We have let $k_o = -iX$, where $X > 0$. We note that only in the interval $X > q/2$, are all of k_{oz}, k_{1z} and k_{2z} purely imaginary, i.e.

$$k_{oz} = -i\sqrt{2q}\sqrt{X - q/2}$$

$$k_{1z} = i\sqrt{\epsilon_1 - 1}\sqrt{\left(X + \frac{q}{\sqrt{\epsilon_1}-1}\right)\left(X - \frac{q}{\sqrt{\epsilon_1}+1}\right)}$$

$$k_{2z} = i\sqrt{\epsilon_2 - 1}\sqrt{\left(X + \frac{q}{\sqrt{\epsilon_2}-1}\right)\left(X - \frac{q}{\sqrt{\epsilon_2}+1}\right)}$$

so that all of R_{01}, R_{12} and $e^{i2k_{1z}d}$ are real.

We find that over this portion of the imaginary axis, $g_t^{\mathrm{M}} = 0$ and $f_t^{\mathrm{M}} = 0$ become real equations in X, i.e.

$$g_t^{\mathrm{M}}(k_o + iq, k_o) = 1 + R_{01}R_{12}e^{i2k_{1z}d}\Big|_{k_\rho = k_o + iq} = 0 \qquad (A.1)$$

$$f_t^{\mathrm{M}}(k_o + iq, k_o) = R_{01} + R_{12}e^{i2k_{1z}d}\Big|_{k_\rho = k_o + iq} = 0 \qquad (A.2)$$

are real equations, for $k_o = -iX$ and $X > q/2$. Consequently, $(A.1)$ and $(A.2)$ may be readily solved using algorithms for real functions. This would be far simpler than attempting to determine the pole positions from the complex equations

as given in (19) and (20). The real solutions, multiplied by $-i$, would give P_{0g} and P_{0f} ($M = 0$) respectively. We find that only (A.1) supports any solution and that there are two sets of solution for varying q, one lying entirely between $X = q/2$ and $X = q$ and the other entirely in the range $X > q$. Refering to (25) we find that only the *second* set gives a non-zero contribution to the real magnetic field and it is this set that we refer to as P_{0g} and is depicted as the $M = 0$ loci in Fig. 5(a).

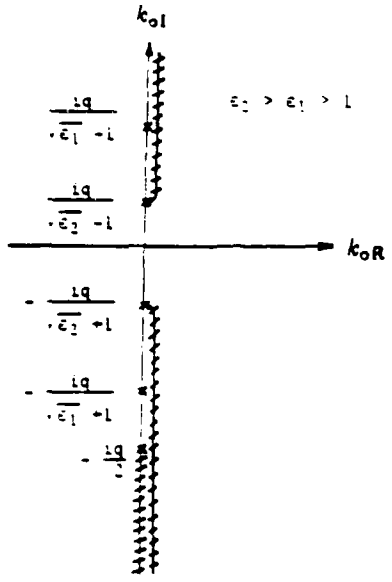

Figure A.1. Branch points and branch cuts in the k_o plane for SDP1.

The magnetic field, as a modification to (25), is therefore

$$H_{\phi 0g}(\tau > \rho) = -\frac{I_o l}{8\pi} Re \left\{ i \int_0^\infty dq\, e^{-iP_{Mg}\tau} I(P_{Mg}) \frac{(P_{Mg}+iq)^2}{\sqrt{P_{Mg}^2 - (P_{Mg}+iq)^2}} \right.$$

$$\left. \cdot \mathcal{H}_1^{(1)}((P_{Mg}+iq)\rho) \frac{f_t^M(P_{Mg}+iq,\, P_{Mg})}{\dfrac{\partial}{\partial k_o} g_t^M(k_o+iq,\, \kappa_o)\Big|_{k_o=P_{Mg}}} \right\}_{M=0}$$

where analytical simplification may be performed before computation by recognizing that P_{0g} is purely imaginary and that the loci lies entirely on $k_o = -iX$, and $X > q$. Half the residue is taken due to the location of the poles and the nature of the deformation.

ACKNOWLEDGMENTS

This work was supported by the IBM Corporation, the Joint Service Electronics Program under Contract DAAL03-86-K-0002, the Army Research Office Contract DAAG29-85-K-0079, and the Office of Naval Research Contract N00014-86-K-0533.

The Editor thanks S. Ali, W. Chew, A. T. de Hoop, T. Habashy, D. Hill, E. Kuester, and M. Tsuk for reviewing the paper.

REFERENCES

1. Ezseddine, A., J. A. Kong, and L. Tsang, "Transient fields of a vertical electric dipole over a two-layer nondispersive dielectric," *J. Appl. Phys.*, Vol. 52, 1202–1208, March 1981.
2. de Hoop, A. T., "A modification of Cagniard's method for solving seismic pulse problems," *Appl. Sci. Res.*, Vol. B8, 349–356, 1960.
3. Langenberg, K. J., "The transient response of a dielectric layer," *Appl. Phys.*, Vol. 3, 179–188, 1974.
4. Ezseddine, A., J. A. Kong, and L. Tsang, "Time response of a vertical electric dipole over a two-layer medium by the double deformation technique," *J. Appl. Phys.*, Vol. 53, 813–822, Feb. 1982.
5. Tsang, L., and J. A. Kong, "Modified modal theory of transient response in layered media," *J. Math. Phys.*, Vol. 20, 1170–1182, June 1979.
6. Kong, J. A., *Electromagnetic Wave Theory,* Wiley-Interscience, New York, 1986.
7. Tsang, L., R. Brown, J. A. Kong, and G. Simmons, "Numerical evaluation of electromagnetic fields due to dipole antennas in the presence of stratified media," *J. Geophys. Res.*, Vol. 79, 2077–2080, May 1974.
8. Tsang, L., and D. Rader, "Numerical evaluation of the transient acoustic waveform due to a point source in a fluid-filled borehole," *Geophysics*, Vol. 44, 1706–1720, Oct. 1979.
9. Poh, S. Y., "Transient electromagnetic dipole radiation over a stratified medium," Ph.D. thesis, Massachusetts Institute of Technology; Cambridge, MA, June 1986.
10. Hill, D., "The transient fields of a Hertzian dipole in the presence of a dielectric half-space," *Radio Sci.*, Vol. 6, Nos. 8,9, 787–794, Aug.–Sept. 1971.

Soon Yun Poh is currently an adjunct staff member in the General Technology Division of the IBM Corporation, East Fishkill, New York. He received his B.S., M.S. and Ph.D. degrees, all in electrical engineering, from the Massachusetts Institute of Technology, Cambridge, Massachusetts. His professional interest is in the area of transient electromagnetic wave guidance and radiation in media. He is a member of Tau Beta Pi and Eta Kappa Nu.

Journal of Electromagnetic Waves and Applications, Vol. 1, No. 2, 109-132, 1987

Time Domain Analysis of Nonuniformly Coupled Line Systems

Q. Gu, J. A. Kong, and Y. E. Yang

Research Laboratory of Electronics
Department of Electrical Engineering and Computer Science
Massachusetts Institute of Technology
Cambridge, MA 02139, USA

Abstract– A general method of analyzing the time-domain bi-directional coupling of a pair of nonuniformly coupled dispersionless transmission lines is presented. The transmission line equations are decoupled using the method of characteristics and the equations are solved iteratively. In the cases with linear loads, the unit-step response can be obtained in closed-form to the first order, and arbitrary excitations can be handled by convolution. Numerical integration for the cases with nonlinear loads is also shown to be more efficient than integration based on the original coupled partial differential equations.

INTRODUCTION

Previous analyses on coupled line systems have often emphasized mono-directional (codirectional or contradirectional) coupling problems [1]-[5]. The interest in such problems is due to the fact that the mono-directionally coupled line system is a very accurate model for many practical situations such as coupled TEM transmission lines and dielectric waveguides, and that the model simplifies the analysis of the corresponding coupling problem. With increasingly compact packaging of electronic circuits, especially in the high-speed digital integrated circuits used in computers, crosstalk between adjacent signal lines in circuits becomes a significant problem in that it limits the speed of circuits as well as the maximum packaging density. It is well known that crosstalk is caused by electromagnetic coupling. However, the coupled system consisting of signal lines, i.e. interconnecting lines in integrated circuits, is no longer a mono-directionally coupled system as a result of the inhomogeneities caused by the complex configurations [6]-[8].

The crosstalk in low speed integrated circuits or low frequency printed circuit boards is usually dealt with using a lumped parameter model [9]-[10]. Yet recent progresses in digital integrated circuits have extended clock speeds into the 3 GHz region, with rise times of signals dropping below 200 ps, hence the bandwidths of the signals on these circuits have increased to several GHz or more. Obviously lumped parameter analysis is no longer accurate and all interconnecting lines in circuits must be treated as microwave transmission lines. To be specific, they should be modeled as nonuniformly coupled transmission line systems, and the coupling is bi-directional. This is harder to deal with than the mono-directional coupling problem. In [12]-[14] the authors used approximate differential equations under the assumption of weak coupling to discuss transmission properties

and coupling effects of high-speed integrated circuits and printed circuit boards. With the method of characteristics, computer simulation based on the equivalent circuit of individual modes is commonly employed to analyze transients in coupled transmission line systems, and gives rather accurate results [15]-[18], but such a technique could be time-consuming when nonuniform coupling is involved. In fact, until recently most analyses of the transient responses in integrated circuits were based on uniformly coupled transmission line models. Yang et al. [19] solved the nonuniformly coupled transmission lines problem with an elegant time domain formulation, but only the contradirectional coupling can be handled without much effort. In addition, some special kinds of transmission line systems with periodically varying coupling properties were analyzed with the odd and even-mode equivalent circuits and transform technique [20]-[21].

The purpose of this paper is to generalize the transient analysis method given in [19]. A new set of variables is introduced such that the transformed equations are simpler and both the codirectional and contradirectional coupling can be easily calculated. By virtue of the formulation, causality is preserved and each higher order term in the perturbational series can be interpreted as a partial reflection along the lines due to nonuniform coupling. Since, in practice, the terminations for interconnecting lines in integrated circuits can be linear or nonlinear, we shall investigate both cases. Solutions accurate to the first order in spatial derivatives of the coupling coefficients, which is analytically manageable, will be presented.

FORMULATION AND CHARACTERIZATION

Consider two nonuniformly coupled non-dispersive transmission lines as depicted in Fig. 1, where $a_1^{\pm}(z,t)$ and $a_2^{\pm}(z,t)$ are the forward and backward modes on each of lines 1 and 2 [22]. Define the column matrix A as

$$A = (a_1^+, a_1^-, a_2^+, a_2^-)^t$$

then the general coupled mode equation can be written in matrix form

$$\frac{\partial A}{\partial z} + \frac{1}{v}\begin{bmatrix} 1 & 0 & -k_+ & -k_- \\ 0 & -1 & k_- & k_+ \\ -k_+ & -k_- & 1 & 0 \\ k_- & k_+ & 0 & -1 \end{bmatrix} \frac{\partial A}{\partial t} + \begin{bmatrix} 0 & p_1 & 0 & 0 \\ p_1 & 0 & 0 & 0 \\ 0 & 0 & 0 & p_2 \\ 0 & 0 & p_2 & 0 \end{bmatrix} A = 0 \qquad (1)$$

where we assume that two lines have identical phase velocity

$$v = \frac{1}{\sqrt{L_1 C_1}} = \frac{1}{\sqrt{L_2 C_2}} \qquad (2)$$

and that the propagating modes on each line are quasi-TEM. L_i and C_i $(i = 1, 2)$ are the inductance and capacitance per unit length of each line, and are all functions of position z. The elements k_+ and k_- in the coupling coefficient matrix are referred to as the codirectional and contradirectional coupling coefficients of the coupled transmission lines respectively. They are related to the capacitive coupling coefficient k_C and inductive coupling coefficient k_L via

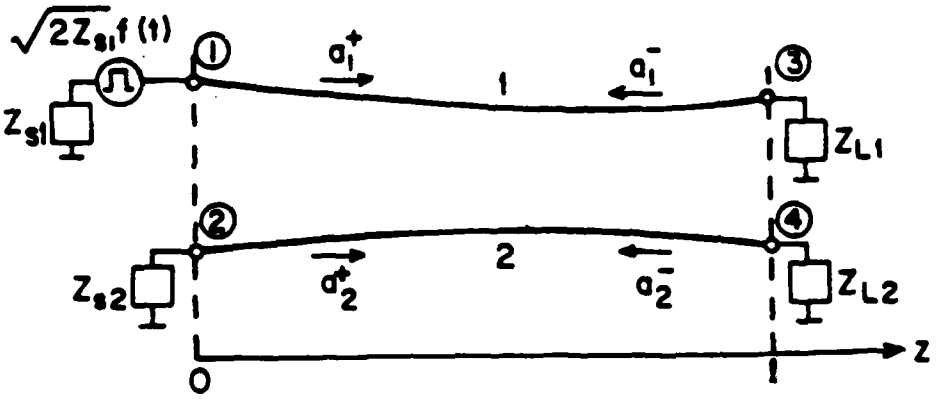

Figure 1. Two nonuniformly coupled transmission lines.

$$k_+ = \frac{k_C(z) - k_L(z)}{2}, \qquad k_- = \frac{k_C(z) + k_L(z)}{2} \tag{3}$$

and it is well known that k_C and k_L are associated with the mutual capacitance C_{12} and the mutual inductance L_{12} in the following forms

$$k_C = \frac{C_{12}(z)}{\sqrt{C_1(z)C_2(z)}}, \qquad k_L = \frac{L_{12}(z)}{\sqrt{L_1(z)L_2(z)}} \tag{4}$$

The elements p_i $(i = 1, 2)$ of the coefficient matrix account for the effects of nonuniform coupling:

$$p_i = \frac{d}{dz}[\ln \sqrt{Z_i(z)}] = \frac{d}{dz} \ln \left[Z_{0i} \sqrt{\frac{1 - k_+ - k_-}{1 - k_+ + k_-}} \right]^{1/2} \qquad (i = 1, 2) \tag{5}$$

where $Z_i(z) = \sqrt{L_i(z) 1 C_i(z)}$ and Z_{0i} are the self-impedances of the same transmission lines with infinite separation, i.e., lines without coupling.

The matrices in (1) can be recast in partitioned form

$$\frac{\partial A}{\partial z} + \begin{bmatrix} K_v & \vdots & K_o \\ \cdots & \cdots & \cdots \\ K_o & \vdots & K_v \end{bmatrix} \frac{\partial A}{\partial t} + \begin{bmatrix} P_1 & \vdots & 0 \\ \cdots & \cdots & \cdots \\ 0 & \vdots & P_2 \end{bmatrix} A = 0 \tag{6}$$

where the coupling coefficient matrix K consists of the following elementary blocks:

$$K_v = \frac{1}{v} \begin{bmatrix} 1 & 0 \\ 0 & -1 \end{bmatrix} \qquad \text{and} \qquad K_o = \frac{1}{v} \begin{bmatrix} -k_+ & -k_- \\ k_- & k_+ \end{bmatrix} \tag{7}$$

and the submatrices P_1 and P_2 are

$$P_1 = \begin{bmatrix} 0 & p_1 \\ p_1 & 0 \end{bmatrix} \qquad \text{and} \qquad P_2 = \begin{bmatrix} 0 & p_2 \\ p_2 & 0 \end{bmatrix} \tag{8}$$

The coupled mode equation (1) can be cast into normal form by diagonalizing the coupling coefficient matrix K in two steps. First, using the rotation transformation

$$T_0 = \frac{1}{\sqrt{2}} \begin{bmatrix} I & \vdots & I \\ \cdots & \cdots & \cdots \\ I & \vdots & -I \end{bmatrix} \tag{9}$$

where I is the identity matrix, we eliminate the off-diagonal submatrices in K

$$T_0 K T_0^{-1} = \begin{bmatrix} K_v + K_o & \vdots & 0 \\ \cdots & \cdots & \cdots \\ 0 & \vdots & K_v - K_o \end{bmatrix} = \begin{bmatrix} K_1 & \vdots & 0 \\ \cdots & \cdots & \cdots \\ 0 & \vdots & K_2 \end{bmatrix} \tag{10}$$

Next, we diagonalize the submatrices K_1 and K_2 in (10). This can be performed by using the following transformation matrices

$$T_1 = \frac{1}{2\sqrt[4]{(1-k_+)^2 - k_-^2}} \begin{bmatrix} \sqrt{(1-k_+)+k_-} + \sqrt{(1-k_+)-k_-} & \sqrt{(1-k_+)-k_-} - \sqrt{(1-k_+)+k_-} \\ \sqrt{(1-k_+)-k_-} - \sqrt{(1-k_+)+k_-} & \sqrt{(1-k_+)+k_-} + \sqrt{(1-k_+)-k_-} \end{bmatrix} \tag{11}$$

and

$$T_2 = \frac{1}{2\sqrt[4]{(1+k_+)^2 - k_-^2}} \begin{bmatrix} \sqrt{(1+k_+)+k_-} + \sqrt{(1+k_+)-k_-} & \sqrt{(1+k_+)+k_-} - \sqrt{(1+k_+)-k_-} \\ \sqrt{(1+k_+)+k_-} - \sqrt{(1+k_+)-k_-} & \sqrt{(1+k_+)+k_-} + \sqrt{(1+k_+)-k_-} \end{bmatrix} \tag{12}$$

The corresponding diagonalized submatrices will be

$$\Lambda_i = \begin{bmatrix} \lambda_i^+ & 0 \\ 0 & \lambda_i^- \end{bmatrix} = T_i K_i T_i^{-1} = \frac{1}{v} \begin{bmatrix} \left[(1 \mp k_+)^2 - k_-^2\right]^{1/2} & 0 \\ 0 & -\left[(1 \mp k_+)^2 - k_-^2\right]^{1/2} \end{bmatrix} \tag{13}$$

$$(i = 1, 2)$$

Here the top sign is for $i = 1$ and the bottom sign for $i = 2$. The composite transformation matrix T which reduces the coupling coefficient matrix K into diagonal form is then

$$T = \begin{bmatrix} T_1 & \vdots & 0 \\ \cdots & \cdots & \cdots \\ 0 & \vdots & T_2 \end{bmatrix} \begin{bmatrix} I & \vdots & I \\ \cdots & \cdots & \cdots \\ I & \vdots & -I \end{bmatrix} = \begin{bmatrix} T_1 & \vdots & T_1 \\ \cdots & \cdots & \cdots \\ T_2 & \vdots & -T_2 \end{bmatrix} \tag{14}$$

The diagonal matrix Λ is related to K by

$$\Lambda = \begin{bmatrix} \Lambda_1 & \vdots & 0 \\ \cdots & \cdots & \cdots \\ 0 & \vdots & \Lambda_2 \end{bmatrix} = TKT^{-1} \tag{15}$$

Applying transformation T to (1), and after some algebraic manipulations, (1) becomes

$$\frac{\partial V}{\partial z} + \begin{bmatrix} \Lambda_1 & \vdots & 0 \\ \cdots & \cdots & \cdots \\ 0 & \vdots & \Lambda_2 \end{bmatrix} \frac{\partial V}{\partial t} = \begin{bmatrix} \frac{\partial T_1}{\partial z}T_1^{-1} - \frac{1}{2}T_1(P_1+P_2)T_1^{-1} & -\frac{1}{2}T_1(P_1-P_2)T_2^{-1} \\ -\frac{1}{2}T_2(P_1-P_2)T_1^{-1} & \frac{\partial T_2}{\partial z}T_2^{-1} - \frac{1}{2}T_2(P_1+P_2)T_2^{-1} \end{bmatrix} V \tag{16}$$

where

$$V = (V_1^+, V_1^-, V_2^+, V_2^-)^t = TA \tag{17}$$

When both of the coupled transmission lines have the same parameters, (16) is simplified to

$$\frac{\partial V}{\partial z} + \begin{bmatrix} \lambda_1^+ & 0 & 0 & 0 \\ 0 & \lambda_1^- & 0 & 0 \\ 0 & 0 & \lambda_2^+ & 0 \\ 0 & 0 & 0 & \lambda_2^- \end{bmatrix} \frac{\partial V}{\partial t} = \begin{bmatrix} 0 & b_1 & 0 & 0 \\ b_1 & 0 & 0 & 0 \\ 0 & 0 & 0 & b_2 \\ 0 & 0 & b_2 & 0 \end{bmatrix} V \tag{18}$$

where

$$\lambda_i^{\pm} = \pm\lambda_i = \pm\frac{1}{v}\left[(1 \mp k_+)^2 - k_-^2\right]^{1/2} \quad (i = 1,2) \tag{19}$$

and

$$b_i = \mp\frac{1}{2}\frac{k'_-(1 \mp k_+) \pm k'_+k_-}{(1 \mp k_+)^2 - k_-^2} - \frac{p_1 + p_2}{2} \quad (i = 1,2) \tag{20}$$

Equation (18) is effectively decoupled. The energy exchange between the forward wave V_i^+ and backward wave V_i^- occurs only because of nonuniform coupling. If the impedance Z_{01} of line 1 is independent of position z, b_1 in (18) will be zero, and the forward wave V_1^+ and the backward wave V_1^- are completely decoupled.

Equation (18) can be further simplified by introducing four families of characteristic curves which satisfy the following ordinary differential equations [23]

$$\frac{dt}{dz} = \lambda_i^+$$

and

$$\frac{dt}{dz} = \lambda_i^- \quad (i = 1,2) \tag{21}$$

The explicit expressions of the characteristic curves are

$$C_i^+ : \quad t - \int dz\ \lambda_i^+ = \text{constant}$$

and

$$C_i^-: \quad t - \int dz\, \lambda_i^- = \text{constant} \quad (i = 1, 2) \tag{22}$$

On these four characteristic curve families, the corresponding equations of (18) become

$$\frac{dV_i^+}{dz} = b_i V_i^-$$

and

$$\frac{dV_i^-}{dz} = b_i V_i^+ \qquad (i = 1,\ 2) \tag{23}$$

It is known from the expressions of the characteristic curves that the solutions of V_i^+ and V_i^- represent wave travelling in the positive and negative z-directions respectively. Equation (23) further demonstrates the fact that there is energy exchange between positive-going and negative-going waves between two boundaries, or we can interpret it as continuous reflection along the lines. This type of reflection is due to nonuniform coupling.

The solution to (23) are to be constructed iteratively, making use of time-marching properties of wave equations [23]. Assuming that the solutions before time t have been obtained at any position along the lines, then

$$V_i^{\pm(0)}(z,t) = V_{i0}^{\pm}(z_{i0}, t_{i0}) \tag{24a}$$

$$V_i^{\pm(n)}(z,t) = V_{i0}^{\pm}(z_{i0}, t_{i0}) + \int_{z_{i0}}^{z} dz' b_i(z') V_i^{\mp(n-1)}(z', t - \int_{z'}^{z} dz'' \lambda_i^{\mp}) \tag{24b}$$

$$(i = 1, 2; \quad n = 0, 1, 2, 3, \ldots)$$

where $V_{i0}^{\pm}$ stand for solutions to (23) with the right-hand sides equal to zero, which are simply uniform travelling waves, and z_{i0} and $t_{i0} = t - \int_{z_{i0}}^{z} dz' \lambda^{\pm}$ can be chosen such that $t_{i0} < t$. Both $V_{i0}^{\pm}(z_{i0}, t_{i0})$ and the integrand in (24b), which is taken along the characteristic curve between (z_{i0}, t_{i0}) and (z, t), are obtained before time t. Therefore calculating the solutions to (23) becomes very straightforward. Note that the notations $V_i^{\pm(n)}$ stand for the nth order approximation, rather than the nth order term in the perturbational series, as used in [19]. Since b_1' and b_2' are proportional to k_+' and k_-', the iteration scheme converges to the correct answer provided that k_C and k_L are slowly varying continuous functions of Z. The general discussion on convergence can be found in [23], Chapter II, § 3. The solutions for forward modes a_i^+ and backward modes a_i^- on coupled transmission lines are obtained by applying the inverse transformation of (17)

$$A = (a_1^+, a_1^-, a_2^+, a_2^-)^t = T^{-1} V \tag{25}$$

SOLUTION FOR THE CASE OF LINEAR TERMINAL CONDITIONS

We shall discuss the solution of two transmission lines possessing identical parameters and terminated with matched loads at their ends, i.e. $Z_s = Z(0)$ and $Z_L = Z(\ell)$, and excited by a step voltage source $f(t) = u(t)$. According to the

relations between $a_i^{\pm}$ and voltage e_i and current i_i on the lines [22]

$$a_i^{\pm} = \frac{1}{\sqrt{2}}\left(\frac{e_i}{\sqrt{Z_i}} \pm \sqrt{Z_i} i_i\right) \tag{26}$$

The initial conditions are zero, and the boundary conditions will be

$$a_1^+(0,t) = u(t) \tag{27a}$$

$$a_1^-(\ell,t) = 0 \tag{27b}$$

$$a_2^+(0,t) = 0 \tag{27c}$$

and

$$a_2^-(\ell,t) = 0 \tag{27d}$$

The boundary conditions of variables $v_i^{\pm}$ can be obtained from the transformation relation as expressed in (17). For convenience of expressing the boundary conditions, we rewrite (17) in the following form

$$V_1^+ = \frac{1}{(t_{11})_1}(a_1^+ + a_2^+) + \frac{(t_{12})_1}{(t_{11})_1} V_1^- \tag{28a}$$

$$V_1^- = \frac{(t_{12})_1}{(t_{11})_1} V_1^+ + \frac{1}{(t_{11})_1}(a_1^- + a_2^-) \tag{28b}$$

$$V_2^+ = \frac{1}{(t_{11})_2}(a_1^+ - a_2^+) + \frac{(t_{12})_2}{(t_{11})_2} V_2^- \tag{28c}$$

$$V_2^- = \frac{(t_{12})_2}{(t_{11})_2} V_2^+ + \frac{1}{(t_{11})_2}(a_1^- - a_2^-) \tag{28d}$$

where

$$\begin{aligned}(t_{11})_i &= \frac{\sqrt{(1 \mp k_+) + k_-} + \sqrt{(1 \mp k_+) - k_-}}{2\sqrt[4]{(1 \mp k_+)^2 - k_-^2}} \\ (t_{12})_i &= \pm \frac{\sqrt{(1 \mp k_+) - k_-} - \sqrt{(1 \mp k_+) + k_-}}{2\sqrt[4]{(1 \mp k_+)^2 - k_-^2}}\end{aligned} \tag{29}$$

From (27) and (28), the boundary conditions of V are

$$V_{10}^+(0,t) = \frac{2\sqrt[4]{(1-k_+)^2 - k_-^2}}{\sqrt{(1-k_+) - k_-} + \sqrt{(1-k_+) + k_-}} u(t) + R_1(0) V_{10}^-(0,t) \tag{30a}$$

$$V_{10}^-(\ell,t) = R_1(\ell) V_{10}^-(\ell,t) \tag{30b}$$

$$V_{20}^+(0,t) = \frac{2\sqrt[4]{(1+k_+)^2 - k_-^2}}{\sqrt{(1-k_+) - k_-} + \sqrt{(1-k_+) + k_-}} u(t) + R_2(0) V_{20}^-(0,t) \tag{30c}$$

and

$$V_{20}^-(\ell,t) = R_2(\ell) V_{20}^+(\ell,t) \tag{30d}$$

where

$$R_i(z) = \frac{(t_{12}(z))_i}{(t_{11}(z))_i} \qquad (i = 1,\ 2) \tag{31}$$

are the reflection coefficients at the boundaries.

Based on (24), we can use a similar method given in [19] to obtain closed form solutions to V and A under conditions (30). The characteristic curves $C_1^{\pm}$ associated with $V_1^{\pm}$ are straight lines as in [19]. Since

$$\lambda_1^{\pm} = \pm\frac{1}{v_0} \tag{32}$$

where v_0 is the phase velocity of the waves propagating along the uncoupled transmission line, the corresponding characteristic curves are

$$t \mp \tau_1(z) = \text{ constant} \tag{33}$$

where

$$\tau_1(z) = \frac{z}{v_0}$$

But the characteristic curves $C_2^{\pm}$ are usually not straight lines, they are

$$t \mp \tau_2(z) = \text{ constant} \tag{34}$$

where

$$\tau_2(z) = \int_0^z dz' \frac{1}{v_0}\sqrt{\frac{(1+k_+(z'))^2 - k_-^2(z')}{(1-k_+(z'))^2 - k_-^2(z')}} \tag{35}$$

Along these characteristic curves, the zeroth order solutions to V, which correspond to the solutions of differential equations (23) with zero right-hand sides, are waves of constant amplitudes,

$$V_{1,n}^{+(0)}(z,t) = \frac{2\sqrt[4]{(1-k_+(0))^2 - k_-(0)^2}}{\sqrt{1-k_+(0)+k_-(0)} + \sqrt{1-k_+(0)-k_-(0)}} \sum_{j=0}^{n}[R_1(0)R_1(\ell)]^j u\left(t - \frac{z}{v_0} - 2jT_1\right)$$

$$V_{1,n}^{-(0)}(z,t) = \frac{2R_1(\ell)\sqrt[4]{(1-k_+(0))^2 - k_-(0)^2}}{\sqrt{1-k_+(0)+k_-(0)} + \sqrt{1-k_+(0)-k_-(0)}} \sum_{j=0}^{n}[R_1(0)R_1(\ell)]^j u\left(t + \frac{z}{v_0} - 2(j+1)T_1\right)$$

$$V_{2,n}^{+(0)}(z,t) = \frac{2\sqrt[4]{(1+k_+(0))^2 - k_-(0)^2}}{\sqrt{1+k_+(0)-k_-(0)} + \sqrt{1+k_+(0)+k_-(0)}} \sum_{j=0}^{n}[R_2(0)R_2(\ell)]^j u(t - \tau_2(z) - 2jT_2)$$

and

$$V_{2,n}^{-(0)}(z,t) = \frac{2R_2(\ell)\sqrt[4]{(1+k_+(0))^2 - k_-(0)^2}}{\sqrt{1+k_+(0)-k_-(0)} + \sqrt{1+k_+(0)+k_-(0)}} \sum_{j=0}^{n}[R_2(0)R_2(\ell)]^j u(t - \tau_2(z) - 2(j+1)T_2)$$

(36)

where

$$T_1 = \frac{\ell}{v_0}$$

$$T_2 = \int_0^\ell dz' \frac{1}{v_0} \sqrt{\frac{(1+k_+(z'))^2 - k_-^2(z')}{(1-k_+(z'))^2 - k_-^2(z')}}$$

and ℓ is the length of the coupled region.

Higher order solutions to V can be obtained by making use of the iterative formula (24). The general form of the first order solutions, which are directly derivable from the zeroth order solutions $V^{\pm(0)}$, are as follows:

In region (nf): $2nT_i + \tau_i(z) \le t < 2(n+1)T_i - \tau_i(z)$

$$V_{i,nf}^{-(1)}(z,t) = V_{i,n}^{+(0)} R_{kz,i}(z, z_{i,n}^+) + V_{i,(n-1)b}^{-(1)}(z_{i,n}^+, t_{i,n}^+)$$

$$V_{i,nf}^{+(1)}(z,t) = V_{i,n-1}^{-(0)} R_{kz,i}(z,0) + R_i(\ell) V_{i,nf}^{+(1)}(0, t-\tau_i(z))$$

In region (nb) : $2(n+1)T_i - \tau_i(z) \le t < 2(n+1)T_i + \tau_i(z)$

$$V_{i,nb}^{+(1)}(z,t) = V_{i,n}^{-(0)} R_{kz,i}(z, z_{i,n}^-) + V_{i,nf}^{-(1)}(z_{i,n}^-, t_{i,n}^-)$$

$$V_{i,nb}^{-(1)}(z,t) = V_{i,n}^{+(0)} R_{kz,i}(z,\ell) + R_i(\ell) V_{i,nb}^{+(1)}(\ell, t+\tau_i(z)-T_i)$$

$$(i = 1,2) \qquad (37)$$

and $V_i^{\pm(1)} = 0$ in the region below the characteristics passing through $(z_{i,0}^-, t_{i,0}^-)$. Here

$$R_{kz,i}(z,z_i) = \frac{1}{4}\left\{ \ln \frac{1 \mp k_+(z) \mp k_-(z)}{1 \mp k_+(z) \pm k_-(z)} \frac{1 \mp k_+(z_i) \pm k_-(z_i)}{1 \mp k_+(z_i) \mp k_-(z_i)} \right.$$
$$\left. + \ln \frac{1 - k_+(z) + k_-(z)}{1 - k_+(z) - k_+(z)} \frac{1 - k_+(z_i) - k_-(z_i)}{1 - k_+(z_i) + k_-(z_i)} \right\}$$
$$+ \ln \frac{Z_0(z)}{Z_0(z_i)} \qquad (i = 1,2) \qquad (38)$$

$$z_{i,n}^+ = \tau_i^{-1}\left[\frac{1}{2}(\tau_i(z) + (t - 2jT_i))\right], \quad t_{i,n}^+ = \frac{1}{2}[t + \tau_i(z)] + nT_i \qquad (39a)$$

$$z_{i,n}^- = \tau_i^{-1}\left[\frac{1}{2}(\tau_i(z) - (t - 2(j+1)T_i))\right], \quad t_{i,n}^- = \frac{1}{2}[t - \tau_i(z)] + (n+1)T_i \qquad (39b)$$

where $\tau_i^{-1}(t)$ is the inverse function of $\tau_i(z)$.

The forward and backward modes $a_i^{\pm}(z,t)$ can be obtained by (25). From $V_i^{\pm}(z,t)$ we know that the first order approximation to $a_i^{\pm}(z,t)$ also have closed form expressions.

While the analysis in this section is for unit step excitation, the transient response for the case of linear terminal conditions to general input waveforms can be easily obtained through convolution.

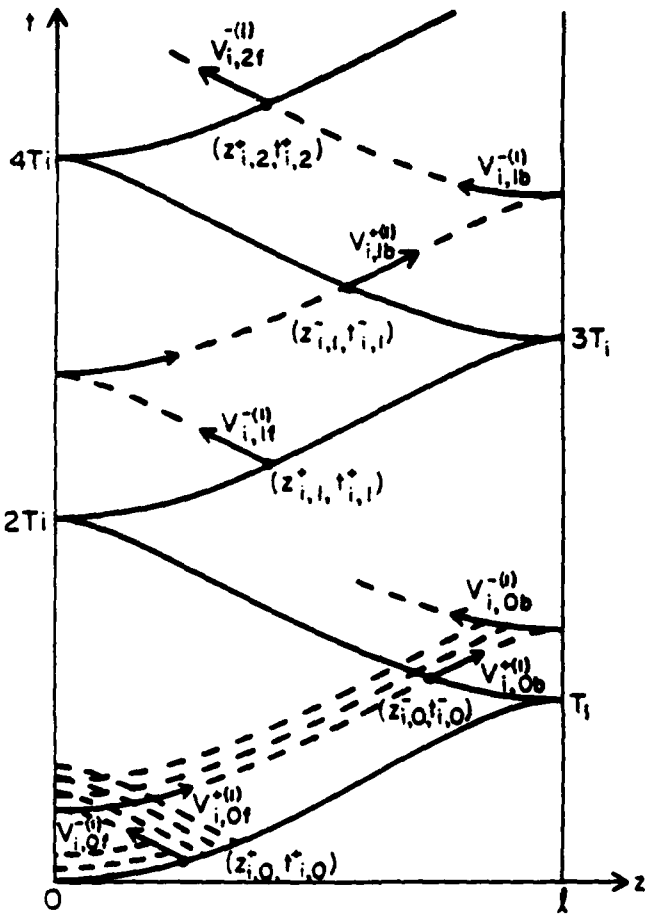

Figure 2. Integration paths on z-t plane.

SYSTEM TERMINATED WITH NONLINEAR LOADS

Interconnecting lines in integrated circuits are usually terminated with nonlinear loads, e.g., the input impedances of transistors. It is therefore important to investigate the transient response for such coupled systems. For simplicity, in the following analysis we assume that the only nonlinear load is at the far end of the active line (line 1 in Fig. 1), and the other ends of the coupled line system are matched. In this case, the boundary conditions become

$$a_1^+(0,t) = f(t) \tag{40a}$$

$$a_1^-(\ell,t) = r_{nl}(a_1^+)a_1^+(\ell,t) \tag{40b}$$

$$a_2^+(0,t) = 0 \tag{40c}$$

$$a_2^-(\ell,t) = 0 \tag{40d}$$

We also assume that the initial states for all independent variables are zero.

As in the previous section, the solutions are still given by (24) except that the

boundary conditions of V are

$$V_1^+(0,t) = \frac{1}{(t_{11}(0))_1} a_1^+(0,t) + \frac{(t_{12}(0))_1}{(t_{11}(0))_1} V_1^-(0,t) \tag{41a}$$

$$V_1^-(\ell,t) = \frac{(t_{12}(\ell))_1}{(t_{11}(\ell))_1} V_1^+(\ell,t) + \frac{1}{(t_{11}(\ell))_1} r_{n\ell}(a_1^+(\ell,t)) a_1^+(\ell,t) \tag{41b}$$

$$V_2^+(0,t) = \frac{1}{(t_{11}(0))_2} a_1^+(0,t) + \frac{(t_{12}(0))_2}{(t_{22}(0))_2} V_2^-(0,t) \tag{41c}$$

$$V_2^-(\ell,t) = \frac{(t_{12}(\ell))_2}{(t_{11}(\ell))_2} V_2^+(\ell,t) + \frac{1}{(t_{11}(\ell))_2} r_{n\ell}(a_1^+(\ell,t)) a_1^+(\ell,t) \tag{41d}$$

We will not elaborate on how to solve $V_i^{\pm}$ from the nonlinear equations (41a)–(41d), but wish to point out that the zeroth order solutions to (23) will consist not only of the terms generated by the excitation but also the reflections due to the nonlinear terminal load. The expressions of the zeroth order solutions are

$$\begin{aligned} V_{i,n}^{+(0)}(z,t) = 2 & \frac{\sqrt[4]{(1 \mp k_+(0))^2 - k_-^2(0)}}{\sqrt{1 \mp k_+(0) + k_-(0)} + \sqrt{1 \mp k_+(0) - k_-(0)}} \\ & \sum_{j=0}^{n} [R_i(0) R_i(\ell)]^j f(t - \tau_i(z) - 2jT_i) \\ & + R_i(0) \sum_{m=0}^{n} [R_i(0) R_i(\ell)]^m r_{n\ell i}\left(a_{i,n-m}^{+(0)}\right) \\ & a_{i,n-m}^{+(0)}(t - \tau_i(z) - 2(m+1)T_i) \end{aligned}$$

$$\begin{aligned} V_{i,n}^{-(0)}(z,t) = 2 & \frac{\sqrt[4]{(1 \mp k_+(0))^2 - k_-^2(0)}}{\sqrt{1 \mp k_+(0) + k_-(0)} + \sqrt{1 \mp k_+(0) - k_-(0)}} \\ & \sum_{j=0}^{n} [R_i(0) R_i(\ell)]^j f(t + \tau_i(z) - 2(j+1)T_i) \\ & + \sum_{m=0}^{n} [R_i(0) R_i(\ell)]^m r_{n\ell i}\left(a_{i,n-m}^{+(0)}\right) \\ & a_{i,n-m}^{+(0)}(t + \tau_i(z) - 2(m+1)T_i) \\ & (i = 1,2) \end{aligned} \tag{42}$$

where

$$r_{n\ell,i}(z) = \frac{2\sqrt[4]{(1 \mp k_+(\ell))^2 - k_-^2(\ell)}\, r_{n\ell}(z)}{\sqrt{1 \mp k_+(\ell) - k_-(\ell)} + \sqrt{1 \mp k_+(\ell) + k_-(\ell)}} \tag{43}$$

$$a_{1,j}^{+(0)}(t) = \begin{cases} \frac{1}{2}\left[(t_{11}(\ell))_1 V_{1j}^{+(0)}(\ell,t) - (t_{12}(\ell))_1 V_{1j}^{-(0)}(\ell,t)\right. \\ \quad \left. +(t_{11}(\ell))_2 V_{2j}^{+(0)}(\ell,t) - (t_{12}(\ell))_2 V_{2j}^{-(0)}(\ell,t)\right] \\ 0, \qquad \text{if } t < 2jT_i \text{ and } t > 2(j+1)T_i \end{cases} \tag{44}$$

and $(t_{11})_i$ and $(t_{12})_i$, $(i = 1,2)$ are given by (29).

Higher order terms are easier to calculate because a linearized model can be used to characterize small perturbations. In summary, the first order solutions have the following form:

In region (nf): $\quad 2nT_i \le t_{in}^+ < (2n+1)T_i$

$$V_{i,nf}^{-(1)}(z,t) = \int_{z_{i,n}^+}^{z} dz' b_i(z') V_{i,n-1}^{+(0)}\left(z', t + \tau_i(z) - \tau_i(z')\right) + V_{i,(n-1)b}^{-(1)}\left(z_{i,n}^+, t_{i,n}^+\right) \qquad (t_{i,n}^+ \le t \le t_{i,n}^+ + \tau_i(z_{i,n}^+)) \tag{45a}$$

$$V_{i,nf}^{+(1)}(z,t) = \int_{0}^{z} dz' b_i(z') V_{i,n-1}^{-(0)}\left(z', t - \tau_i(z) + \tau_i(z')\right) + R_i(0) V_{i,nf}^{-(1)}\left(0, t - \tau_i(z)\right) \qquad (2nT_i \le t \le 2t_{i,n}^+ - 2nT_i) \tag{45b}$$

In region (nb): $\quad (2n+1)T_i \le t_{in}^- < 2(n+1)T_i$

$$V_{i,nb}^{+(1)}(z,t) = \int_{z_{i,n}^-}^{z} dz' b_i(z') V_{i,n}^{-(0)}\left(z', t - \tau_i(z) + \tau_i(z')\right) + V_{i,nf}^{+(1)}\left(z_{i,n}^-, t_{i,n}^-\right) \qquad (t_{i,n}^- \le t \le t_{i,n}^- + \tau_i(\ell) - \tau_i(t_{i,n}^-)) \tag{45c}$$

$$V_{i,nb}^{-(1)}(z,t) = \int_{\ell}^{z} dz' b_i(z') V_{i,n}^{+(0)}\left(z', t + \tau_i(z) - \tau_i(z')\right) + R_i(\ell) V_{i,nb}^{+(1)}(\ell, t + \tau_i(z) - T_i) + \Delta R_{n\ell i} \qquad ((2n+1)T_i \le t \le 2t_{i,n}^- - 2nT_i) \tag{45d}$$

$$(i = 1,2; \quad n = 0,1,2,\ldots)$$

where

$$\Delta R_{n\ell i} = r_{n\ell i}(a_{1,n}^{+(1)}) a_{1,n}^{+(1)}(\ell,t) - r_{n\ell i}(a_{1,n}^{+(0)}) a_{1,n}^{+(0)}(\ell,t)$$
$$\doteq r_{n\ell i}(a_{1,n}^{+(0)}) \Delta a_{1,n}^{+}(\ell,t) + \Delta r_{n\ell i}(a_{1,n}^{+(0)}) a_{1,n}^{+(0)}(\ell,t),$$
$$z_{i,n}^+ = \frac{1}{2}\left(z + \tau_i^{-1}(t - 2nT_i)\right), \quad t_{i,n}^+ = \frac{1}{2}\left[(t + 2nT_i) + \tau_i(z)\right]$$

and

$$z_{i,n}^- = \frac{1}{2}\left(z - \tau_i^{-1}(t - 2(n+1)T_i)\right), \quad t_{i,n}^- = \frac{1}{2}\left[(t + 2(n+1)T_i) - \tau_i(z)\right]$$

The remaining steps are the same as in the previous section, viz. applying (25) to get

$$a_i^+(z,t) = \frac{1}{2}[(t_{11}(z))_1 V_1^+(z,t) - (t_{12}(z))_1 V_1^-(z,t) \pm (t_{11}(z))_2 V_2^-(z,t) \mp (t_{12}(z))_2 V_2^-(z,t)] \quad (46a)$$

$$a_i^-(z,t) = \frac{1}{2}[-(t_{12}(z))_1 V_1^+(z,t) + (t_{11}(z))_1 V_1^-(z,t) \mp (t_{12}(z))_2 V_2^+(z,t) \pm (t_{11}(z))_2 V_2^-(z,t)] \quad (46b)$$

$$(i = 1, 2)$$

NUMERICAL RESULTS

To verify our formulation, we first examine a special case where $k_C = k_L$. The parameters of Fig. 3 are taken from Fig. 14 of [19], i.e. $k_C = k_L = k(z) = 0.45 + 0.2\tanh(2.5z - 1.25)$. Both Z_s and Z_L are matched to the line, and the units of distance and time are normalized to the lengths of the lines and the corresponding signal travel times, respectively. The excitation $e_s(t)$ is assumed to be a pulse of amplitude 4 with rise time of $0.25T$, fall time of $0.1T$, and duration of $0.15T$ * The first order approximation shown here matches very well with the result in [19].

The power of the present approach is in its capability of computing codirectional as well as contra-directional coupling. For the rest of the calculation, we assume that the transmission line is in a medium with relative permittivity $\epsilon_r = 9$ and line length 10 mm and the input signal is a pulse of amplitude 5. Figures 4 through 7 show the far-end crosstalks when both lines have linear, matched loads. For Figs. 4 and 5, $k_C(z) = 0.15 + 0.05\sin(0.1\pi z + \pi/4)$ and $k_L(z) = 0.10 + 0.05\sin(0.1\pi z + \pi/4)$ where the unit of length is mm. Hence the co-directional coupling coefficient $k_+ = (k_C - k_L)/2 = 0.025$ is a constant. The only difference is that the rise time and the fall time are 10 ps for Fig. 4, but 20 ps for Fig. 5. The durations of the pulses are also different: 20 ps for Fig. 4 and 30 ps for Fig. 5. The results show good agreement with the approximate formula in [12]. Indeed, the far-end crosstalk is inversely proportional to the rise time since k_C and k_L are so close that the difference between end-to-end traveling times of modes V_1^+ and V_2^+ (or V_1^- and V_2^-) is less than the rise time. Note, however, that the formula in [12] is rendered invalid when $k_+(z)$ is no longer uniform. Figures 6 and 7 both have $k_L = 0.25 + 0.10\tanh(0.25z - 1.25)$. k_C is $0.25 + 0.15\tanh(0.25z - 1.25)$ for Fig. 6 and $0.25 + 0.20\tanh(0.25z - 1.25)$ for Fig. 7. Equivalently, $k_+(z) = 0.025\tanh(0.25z - 1.25)$ for Fig. 6 and $k_+ = 0.05\tanh(0.25z - 1.25)$ for Fig. 7. Qualitatively, the results are consistent with the formula in [12]. However, the peak values are significantly smaller than those predicted by the previous approximate formula if the maximum $k_+(z)$ is substituted. This is understandable, since the positive and negative parts of $k_+(z)$ tend to average out.

* The rise time and the fall time are mistakenly written as $0.125T$ and $0.0625T$ in [19].

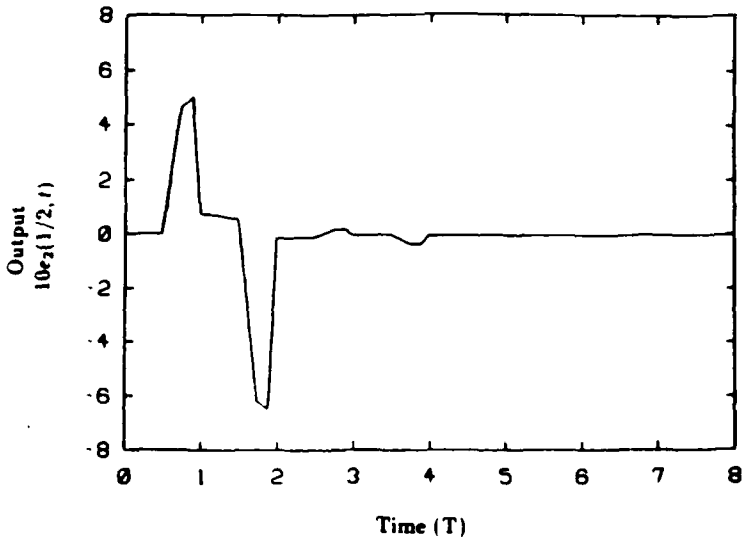

Figure 3. Response in the middle of line 2 when $k_L(z) = k_C(z) = 0.45 + 0.2\tanh(2.5z - 1.25)$.

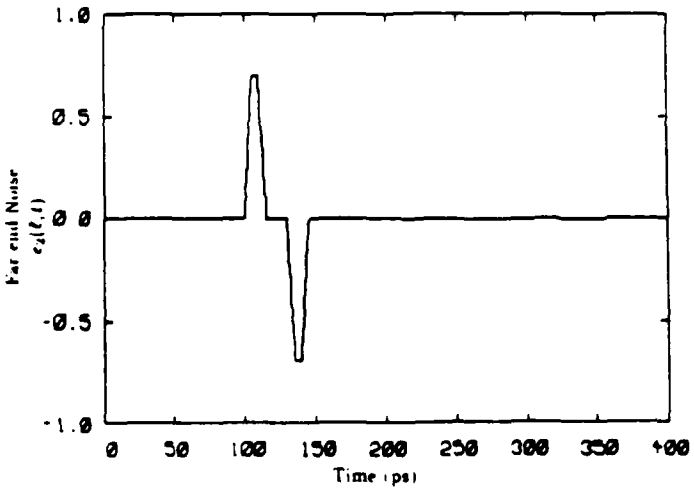

Figure 4. Response of line 2 if $k_C(z) = 0.15 + 0.05\sin(0.1\pi z + \pi/4)$ and $k_L(z) = 0.10 + 0.05\sin(0.1\pi z + \pi/4)$. $t_r = 10\,\text{ps}$

In the following figures we consider systems having coupling coefficients of the form:

$$k_-(z) = k_o + \frac{\Delta k}{2}[1 - \cos(\alpha z + \beta)] \tag{47a}$$

and

$$k_+(z) = \frac{\Delta k}{2}[1 - \cos(\alpha z + \beta)] \tag{47b}$$

and a nonlinear load at the far-end of the active line (port 3 in Fig. 1) characterized by

$$r_{n\ell}(a_1) = r_m[1 + \tanh(\gamma(a_1 - a_0))] + r_o \tag{48}$$

where $a_1 = a_1^+(\ell, t) + a_1^-(\ell, t)$. The remaining ports are assumed to be matched. The input signal, as shown in Fig. 8, has both rise time and fall time of 10 ps, duration 20 ps and amplitude 5. The parameters of Fig. 8 are given as follows:

$$k_o = 0.2, \quad \Delta k = -0.05, \quad \alpha = 2\pi \text{ rad/mm}, \quad \beta = 0$$

and

$$r_m = -0.3, \quad \gamma = 1.0, \quad a_o = 2.5 \text{ and } r_o = -r_m(1 - \tanh(\gamma a_o))$$

In Fig. 8, the first order transmitted signal, reflected signal, near-end and far-end crosstalks are displayed together to allow comparison of their relative magnitudes. Figs. 9–12 show the differences between the zeroth order and the first order solutions for the reflected, transmitted signal, near-end and far-end crosstalks. The small discrepancies justify the use of the iterative method.

It is of interest to see what happens when $k_+(z)$ is positive instead of negative. In Figs. 13–17, we choose $\Delta k = +0.05$, and the coupling coefficients become

$$k_-(z) = 0.2 + 0.025[1 - \cos(2\pi z)]$$
$$k_+(z) = 0.025[1 - \cos(2\pi z)]$$

The responses at all four ports are shown in Fig. 13 whereas Figs. 14–17 provide comparison with the previous example in which $\Delta k = -0.05$. We notice that the far-end crosstalk for this case is nearly the negative of that for the previous case. This can be explained in terms of the differences in mode velocities. From the theory of coupled transmission lines one can show that the far-end crosstalk is equal to the difference of odd and even modes, which correspond to our $V_1^{\pm}$ and $V_2^{\pm}$. The velocity of the even mode may be larger or smaller than that of the odd mode, depending on whether k_+ is positive or negative. Therefore, the initial arrival of the faster mode at the far end results in positive crosstalk in one case and negative in the other. The deviation after the first arrival (~ 100 ps) is due to the nonlinear load.

CONCLUSIONS

General approximate solutions to the transient response on two identical, nonuniformly coupled transmission lines terminated with linear or nonlinear loads have been obtained through an iterative scheme that was previously applied to a smaller class of problems in [19]. The iterative method is very useful when the coupling

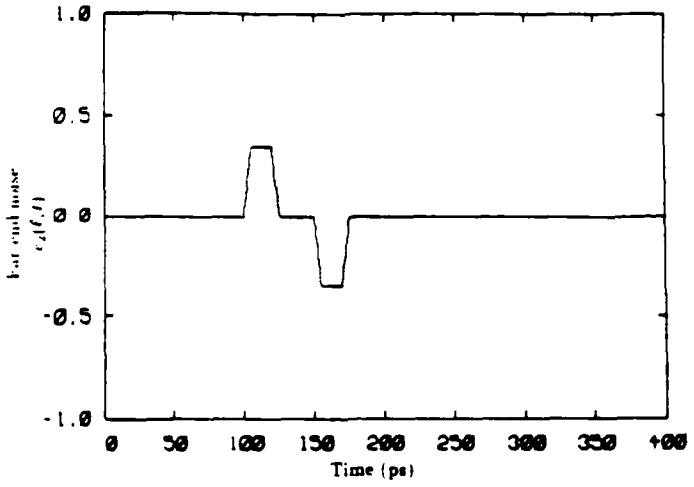

Figure 5. Response of line 2 if $k_C(z) = 0.15 + 0.05\sin(0.1\pi z + \pi/4)$ and $k_L(z) = 0.10 + 0.05\sin(0.1\pi z + \pi/4)$. $t_r = 20\,\text{ps}$

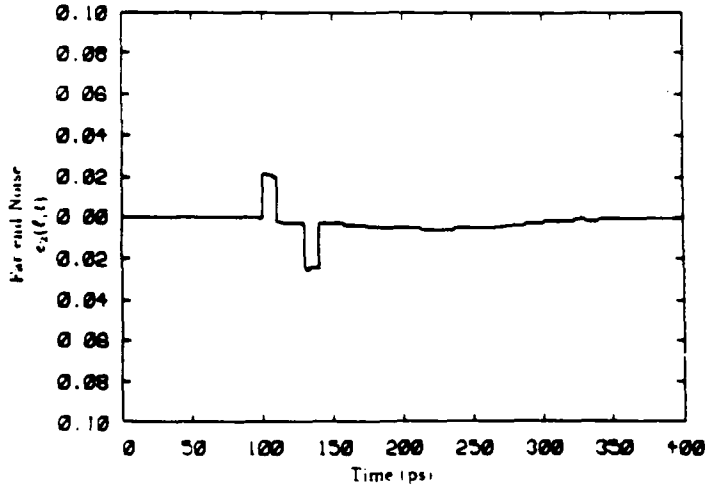

Figure 6. Response of line 2 if $k_C(z) = 0.25 + 0.15\tanh(0.25z - 1.25)$ and $k_L(z) = 0.25 + 0.10\tanh(0.25z - 1.25)$. $t_r = 10\,\text{ps}$

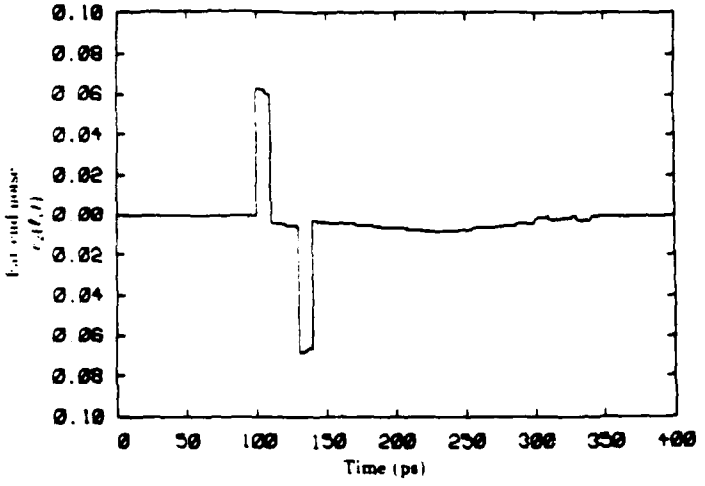

Figure 7. Response of line 2 if $k_C(z) = 0.25 + 0.20\tanh(0.25z - 1.25)$ and $k_L(z) = 0.25 + 0.10\tanh(0.25z - 1.25)$. $t_r = 10\,\text{ps}$

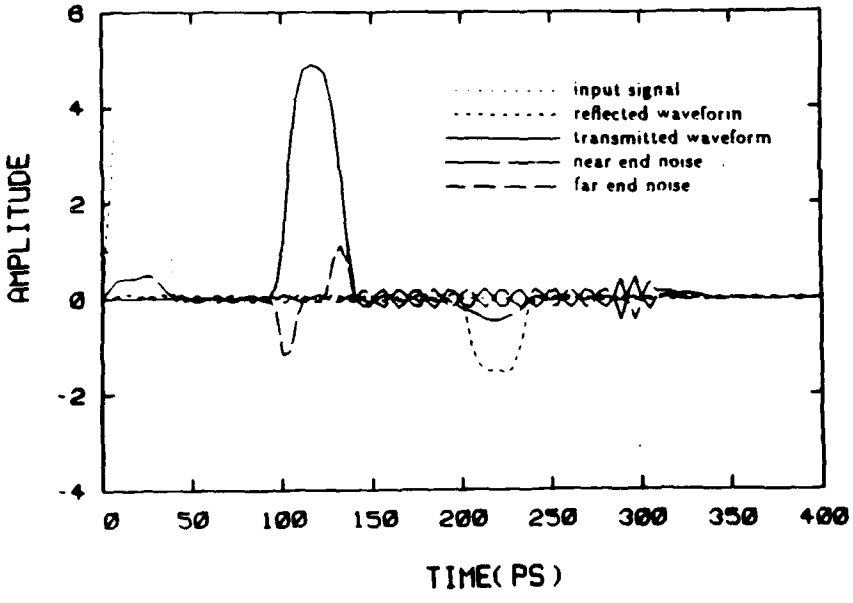

Figure 8. Response at different ports of a system with $k_-(z) = 0.20 - 0.025(1 - \cos 2\pi z)$ and $k_+(z) = -0.025(1 - \cos 2\pi z)$.

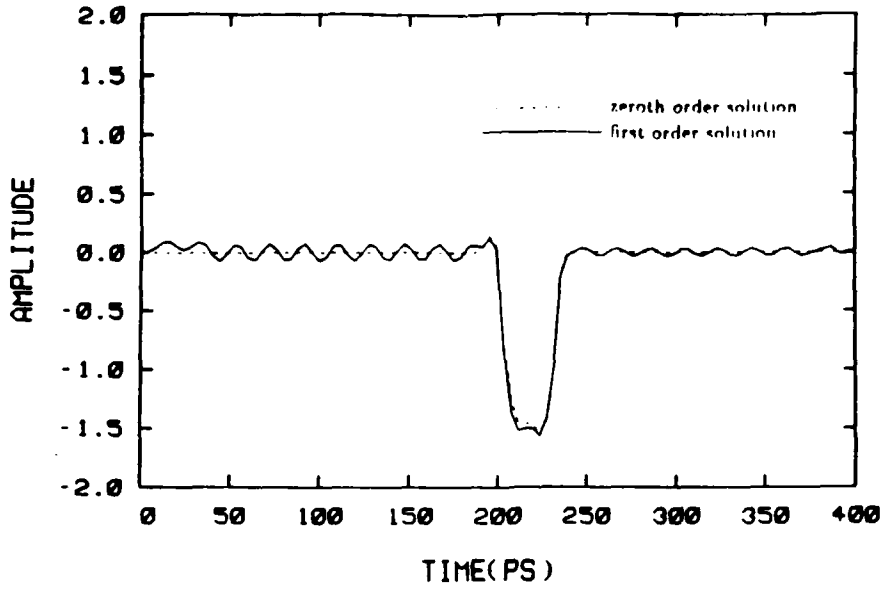

Figure 9. Comparison of the zeroth and the first order solutions of the reflected signal. $k_{-}(z) = 0.2 - 0.025(1 - \cos 2\pi z)$, $k_{+}(z) = -0.025(1 - \cos 2\pi z)$

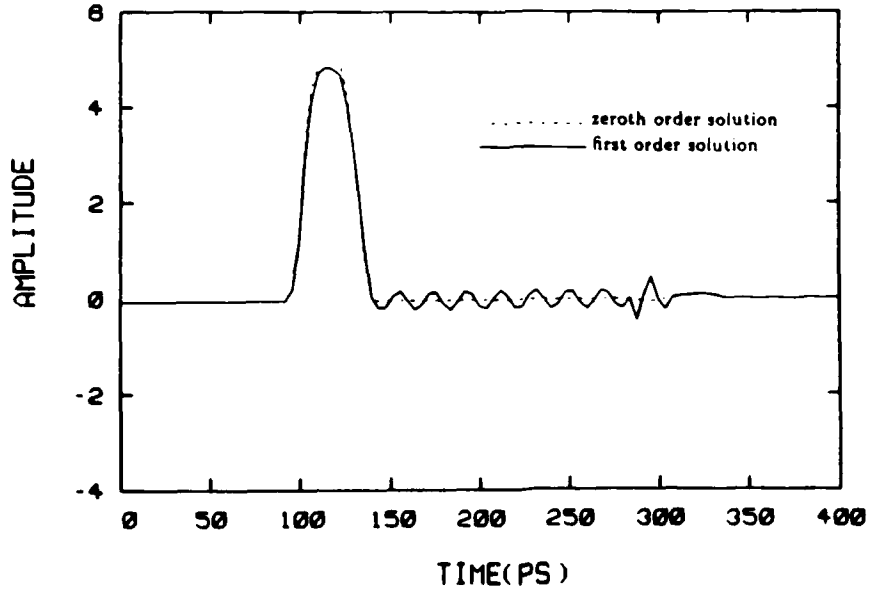

Figure 10. Comparison of the zeroth and the first order solutions of the transmitted signal. $k_{-}(z) = 0.2 - 0.025(1 - \cos 2\pi z)$, $k_{+}(z) = -0.025(1 - \cos 2\pi z)$

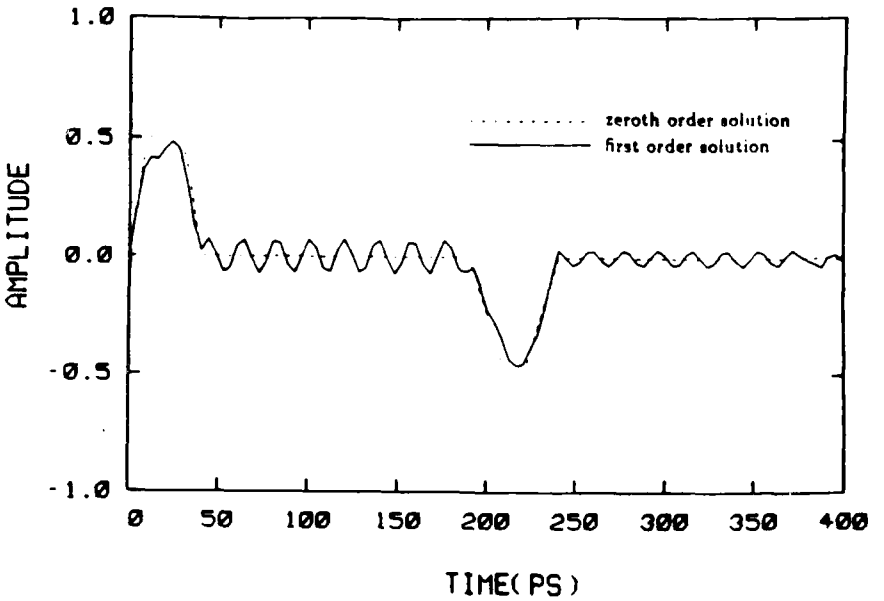

Figure 11. Comparison of the zeroth and the first order solutions of the near-end crosstalk. $k_-(z) = 0.2 - 0.025(1 - \cos 2\pi z)$, $k_+(z) = -0.025(1 - \cos 2\pi z)$

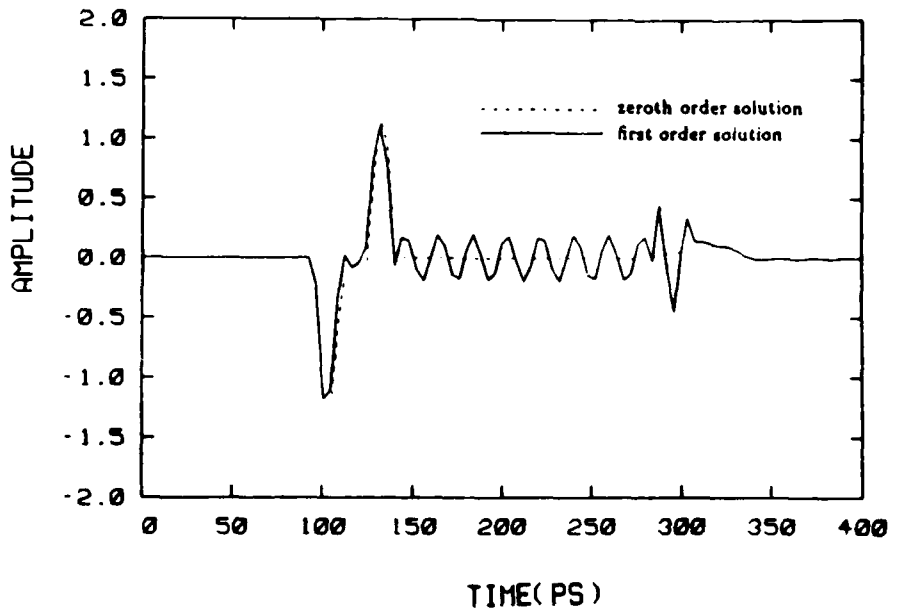

Figure 12. Comparison of the zeroth and the first order solutions of the far end crosstalk. $k_-(z) = 0.2 - 0.025(1 - \cos 2\pi z)$, $k_+(z) = -0.025(1 - \cos 2\pi z)$

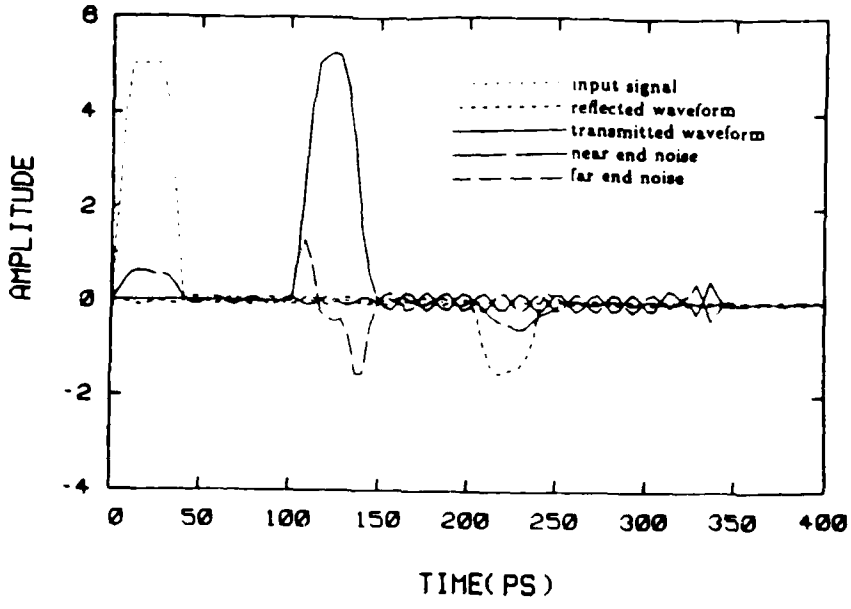

Figure 13. Response at different ports of a system with $k_{-}(z) = 0.20 + 0.025(1 - \cos 2\pi z)$ and $k_{+}(z) = +0.025(1 - \cos 2\pi z)$.

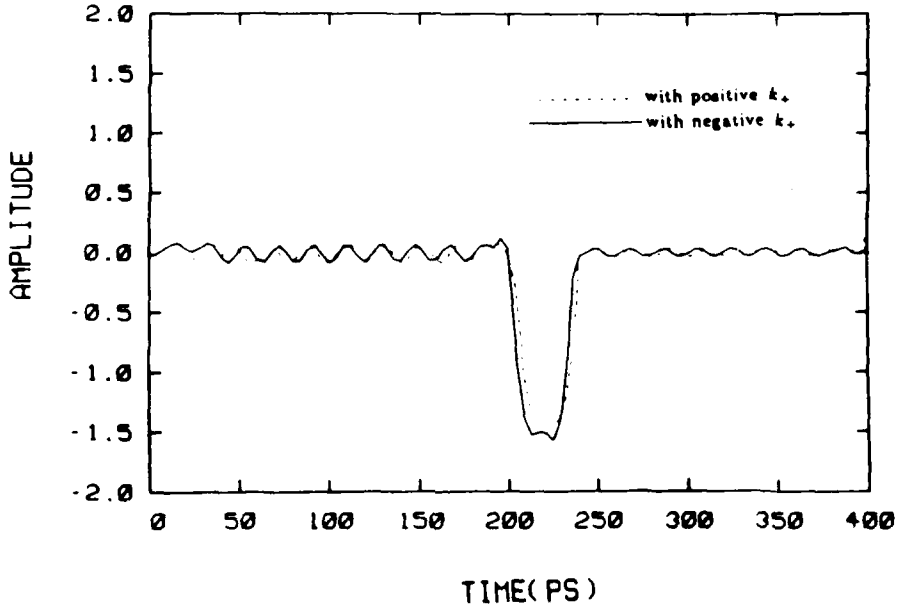

Figure 14. Comparison of reflected signals on lines terminated nonlinear loads with $k_{+}(z)$ of opposite signs.

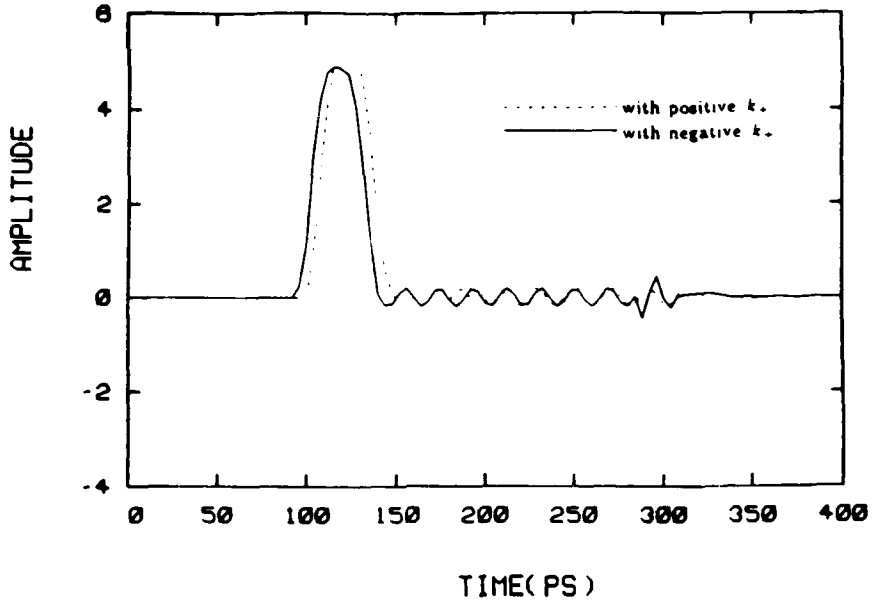

Figure 15. Comparison of transmitted signals on lines terminated nonlinear loads with $k_+(z)$ of opposite signs.

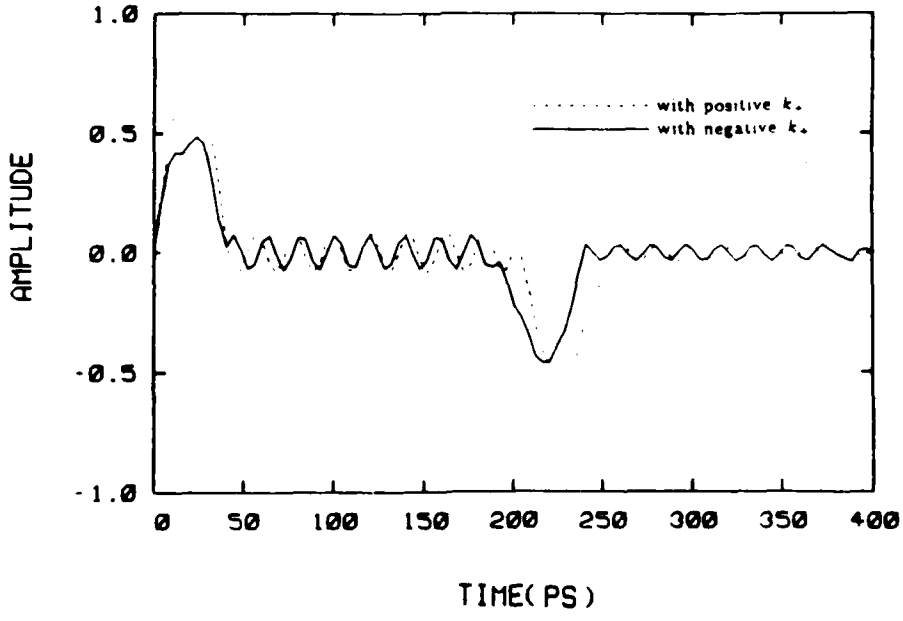

Figure 16. Comparison of near end crosstalk on lines terminated nonlinear loads with $k_+(z)$ of opposite signs.

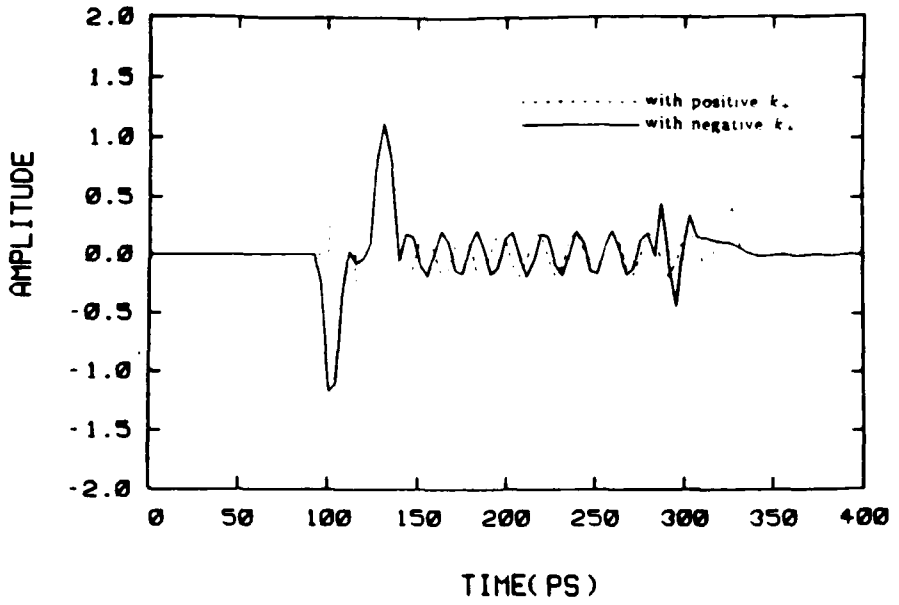

Figure 17. Comparison of far end crosstalk on lines terminated nonlinear loads with $k_+(z)$ of opposite signs.

coefficients are slowly varying with position since the zeroth order or first order approximation would be sufficiently accurate yet much easier to calculate. Furthermore, with the help of newly devised special transformations, we have shown that both the codirectional coupling and contradirectional coupling of the problem with unit-step excitation and linear loads have closed form expressions up to the first order approximation. Arbitrary excitation can then be taken into account by convolution. This method is hence most efficient. As for nonlinear terminations, numerical integrations are performed along the characteristics. Examples have been given for both cases to illustrate the use of this method. Extension to problems in which the phase velocities of coupled lines are not equal, or where more than two coupled lines are involved is also under consideration.

ACKNOWLEDGMENTS

This work was supported by the IBM Corporation, the Joint Service Electronics Program under Contract DAAL03-86-K-0002, the Army Research Office Contract DAAG29-85-K-0079, and the Office of Naval Research Contract N00014-86-K-0533.

The Editor thanks I. Lindell, A. Sezginer and R. B. Wu for reviewing the paper.

REFERENCES

1. Pierce, J. R., "Coupling of modes of propagation," *J. Appl. Phys.*, Vol. 25, 179–183, 1954.
2. Oliver, B. M., "Directional electromagnetic couplers," *Proc. IRE*, Vol. 42, 1686–

1693, Nov. 1954.
3. Cohn, S. B., "Shielded coupled-strip transmission line," *IRE Trans. Microwave Theory Tech.*, Vol. MTT-3, 29–38, Oct. 1955.
4. Krage, M. K., and G. I. Haddad, "Characteristics of coupled microstrip transmission lines – I: Coupled mode formulation of inhomogeneous lines and – II: Evaluation of coupled line parameters," *IEEE Trans. Microwave Theory Tech.*, Vol. MTT-18, 217–228, April 1970.
5. Marcatili, E. A. J., "Dielectric rectangular waveguide and directional coupler for integrated optics," *B. S. T. J.*, Vol. 48, 207–2102, 1969.
6. Clark, B. T., and V. M. Hill, "IBM multichip multilayer ceramic modules for LSI chips – design for performance and density," *IEEE Trans. Components, Hybrids, Manuf. Technology*, Vol. CHMT-3, 89–93, March 1980.
7. Ho, C. W., D. A. Chance, C. H. Bajorek, and R. E. Acosta, "The thin-film module as a high-performance semiconductor package, *IBM. J. Res. Develop.*, Vol. 26, 286–296, May 1982.
8. Venkatachalam, P. N., "Pulse propagation properties of multilayer ceramic multichip modules for VLSI circuits," *Proc. 1983 Electronic Components Conference*, 130–134.
9. Paul, C. R., and W. W. Everatt III, "Modeling crosstalk on printed circuit boards," *RADC-TR-85-107*, Phase Report, July 1985.
10. Smith, W. R., and D. E. Snyder, "Circuit loading and crosstalk signals from capacitance in SOS and bulk-silicon interconnect channels," *IEEE 1984 V-MIC Conf.*, 218–227, June 1984.
11. Sainati, R., "High speed packaging analysis and modeling," *Proc. IEEE 1985 Electronic Components Conference*, 365–375, May 1985.
12. Feller, A., H. R. Kaupp, and J. J. Digiacomo, "Crosstalk and reflections in high-speed digital systems," *Proc. – Fall Joint Computer Conference*, 511–525, Dec. 1965.
13. Rainal, A. J., "Transmission properties of various styles of printed wiring boards," *B. S. T. J.*, Vol. 58, 995–1025, May-June 1979.
14. Chang, C. S., G. Crowder, and M. F. McAllister, "Crosstalk in multilayer ceramic packaging," *1981 IEEE International Symposium on Circuits and Systems Proceedings*, 6–11.
15. Chang, F. Y., "Transient analysis of lossless coupled transmission lines in a nonhomogeneous dielectric medium," *IEEE Trans. Microwave Theory Tech.*, Vol. MTT-18, 616–626, Sept. 1970.
16. Chilo, J., and T. Arnaud, "Coupling effects in the time domain for an interconnecting bus in high-speed GaAs logic circuits," *IEEE Trans. Electron. Devices*, Vol. ED-31, 347–352, March 1984.
17. Gruodis, A. J., "Transient analysis of uniform resistive transmission lines in a homogeneous medium," *IBM J. Res. Develop.*, Vol. 23, 676–681, Nov. 1979.
18. Gruodis, A. J., and C. S. Chang, "Coupled lossy transmission line characterization and simulation," *IBM J. Res. Develop.*, Vol. 25. 25–41, Jan. 1981.
19. Yang, Y. C. E., J. A. Kong, and Q. Gu, "Time-domain perturbational analysis of nonuniformly coupled transmission lines," *IEEE Trans. Microwave Theory Tech.*, Vol. MTT-33, 1120–1130, Nov. 1985.
20. Gu, Q., and J. A. Kong, "Transient analysis of single and coupled lines with capacitively-loaded junctions," *IEEE Trans. Microwave Theory Tech.*, Vol. MTT-34, 952–964, Sept. 1986.
21. Gu, Q., and J. A. Kong, "Transient analysis of single transmission line system with mesh ground planes," to be published.
22. Adair, J. E., and G. I. Haddad, "Coupled-mode analysis of non-uniform coupled transmission lines," *IEEE Trans. Microwave Theory Tech.*, Vol. MTT-17, 746–752, Oct. 1969.
23. Courant, R., and D. Hilbert, *Methods of Mathematical Physics*, Vol. II, Chap. II, Wiley-Interscience, 1966.

Qisheng Gu was born in Jiangsu, China. He graduated from Fudan University, Shanghai, China, in 1960. From 1960 to 1962, he worked on automatic control systems at Shanghai Designing Institute of Machinery and Electrical Engineering, China. In 1962, he joined the Department for Research and Development at Shanghai Xinhua Radio Factory, where he was engaged in research of microwave systems and circuits. Since October 1982, he has been a senior engineer and the Deputy Director of the Department. In June 1983, he came to the United States as a visiting scientist in the Research Laboratory of Electronics, Massachusetts Institute of Technology. He is a member of the Shanghai Electronics Association Council and the Microwave Committee of the Chinese Institute of Electronics.

Jin Au Kong is Professor of Electrical Engineering and Chairman of Area IV on Energy and Electromagnetic Systems in the Department of Electrical Engineering and Computer Science at the Massachusetts Institute of Technology, Cambridge, Massachusetts. His research interest is in the field of electromagnetic wave theory and applications. He is the author of *Electromagnetic Wave Theory* (Wiley, 1986), coauthor of *Applied Electromagnetism* (Brook/Cole, 1983) and *Theory of Microwave Remote Sensing* (Wiley, 1985), and Editor of *Research Topics in Electromagnetic Wave Theory* (Wiley, 1981), and the Wiley Series in Remote Sensing.

Ying-ching Eric Yang was born in Taiwan in 1959. He received his B.S.E.E. degree from National Taiwan University, Taipei in 1981 and the M.S. degree in electrical engineering from the Massachusetts Institute of Technology, Cambridge in 1985 and is currently working toward his Ph.D. degree. From 1981 to 1983 he served in the Chinese Navy as an instructor. Since 1983 he has been with the Department of Electrical Engineering and Computer Science and the Research Laboratory of Electronics of the Massachusetts Institute of Technology, where he worked as a Research Assistant and a Teaching Assistant. His research interest is in the time-domain and frequency-domain analysis of electromagnetic wave propagation in layered media. Mr. Yang is a member of the IEEE and Sigma Xi.